Carnegie Mellon University

CARNEGIE INSTITUTE OF TECHNOLOGY

THESIS

SUBMITTED IN PARTIAL FULFILLMENT OF THE REQUIREMENTS

FOR THE DEGREE OF Doctor of Philosophy

TITLE Model-based Control and Optimization of Grade Transitions in Polyethylene Solution Polymerization Processes

PRESENTED BY Jun Shi

ACCEPTED BY THE DEPARTMENT OF

Chemical Engineering

LORENZ BIEGLER	4/27/16
LORENZ BIEGLER, ADVISOR AND DEPARTMENT HEAD	DATE

APPROVED BY THE COLLEGE COUNCIL

VIJAYAKUMAR BHAGAVATULA	4/27/16
DEAN	DATE

CARNEGIE MELLON UNIVERSITY

Model-based Control and Optimization of Grade Transitions in Polyethylene Solution Polymerization Processes

A DISSERTATION

SUBMITTED TO THE GRADUATE SCHOOL

IN PARTIAL FULFILLMENT OF THE REQUIREMENTS

for the degree of

DOCTOR OF PHILOSOPHY

in

CHEMICAL ENGINEERING

by

JUN SHI

B.S., CONTROL SCIENCE AND ENGINEERING, ZHEJIANG UNIVERSITY

Pittsburgh, Pennsylvania

April, 2016

Acknowledgments

I am extremely grateful for all the opportunities that allow me to pursue my Ph.D. study and write this dissertation at Carnegie Mellon University. I would like to express my deepest gratitude to my advisor Prof. Lorenz T. Biegler, who has been a great mentor for me in academic and many other aspects. His enthusiasm and devotion towards research have greatly inspired me, and his patience and vast knowledge have tremendously helped me on my research and led me to the right direction. This work would have never been possible without him.

I would also like to express my sincere thanks to Dr. Intan Hamdan and Dr. John Wassick from the Dow Chemical Company for their valuable advice and strong support. The collaboration with them in the past several years is a great learning opportunity as well as an unforgettable experience.

I would like to express my special thanks to my committee members Prof. Erik Ydstie, Prof. Nikolas Sahinidis, Prof. Shlomo Ta'asan and Dr. Intan Hamdan, for their careful reading of my thesis and valuable comments on the dissertation.

I would also like to thank Prof. Ignacio Grossmann, Prof. Lorenz T. Biegler, Prof. Erik Ydstie, Prof. Nikolas Sahinidis and all the faculty in Center for Advanced Process Decision-making for providing students great resources and environment for research and for being great role models.

My thanks go to the Dow Chemical Company for the financial support as well as

the internship opportunities in the past few summers. Discussions with friendly, experienced engineers from the Core R&D group, the Performance Plastics Tech Center and the Polyethylene R&D at Dow have greatly inspired and motivated me. I have learned invaluable lessons from them during our collaboration.

Last but not least, I would like to thank my parents for their unconditional love. They always encourage me to explore the world and to chase my dream. Weekly remote video calls with them have been the biggest support for me in the past five years. I would also like to thank my friends for always being there for me and for teaching me many things. They have enlightened my life and made it an enjoyable journey.

Abstract

This thesis study focuses on the development of model-based control and optimization for optimal grade transitions in polyethylene solution polymerization processes. To meet the operational need of this particular process and to reduce transition time and off-grade production for economic benefit, four major topics are taken into account: 1) model development, 2) optimization formulations and solution strategies, 3) handling uncertainties, and 4) online implementation. These four parts cover two layers, the real time optimization layer and the advanced control layer, in the decision-making hierarchy of chemical processes. Both of them require detailed mathematical models that are representative of the process and efficient dynamic optimization strategies.

First, a detailed mathematical model is developed to capture the dynamic behavior of the process. This includes time delay models for vapor and liquid recycle streams as well as a reduced, yet accurate, vapor-liquid equilibrium (VLE) model derived from rigorous VLE calculations. Next, two optimization formulations, single stage and multistage, are developed to deal with single-value target and specification bands of product properties, respectively. The results show significant reduction in grade transition time and off-spec production. However, the performance can deteriorate in the presence of uncertainties, disturbances and model mismatch, which calls for robust optimization strategies. In our work, a flowchart is proposed and back-off constraints calculated from Monte Carlo simulations are

incorporated in the original optimization problem to generate optimal control policies that can be applied at different uncertainty levels. As an extension of this work, nonlinear model predictive control and state estimation are then considered. An online implementation framework is built up for grade transitions in such processes and can be further extended to other similar processes.

For dynamic optimization, simultaneous collocation method is applied to discretize the differential-algebraic equations, and the resulting nonlinear programming (NLP) problems are solved using NLP solvers. Because of the characteristics of the problem, singular control problems are considered and the influence of regularization is discussed for both offline dynamic optimization and optimization under uncertainty.

Contents

List of Figures

List of Tables

Chapter 1

Introduction

In the past several decades, substantial growth of model-based control and optimization applications has been observed in a number of different application areas. In the chemical industry, systematic optimization is essential to maintain competitive and successful applications, involving process design and synthesis, process operations and process control. With the advanced optimization algorithms and efficient computational implementation of these optimization methods, engineers and scientists are able to improve the process design and operations to achieve better product quality, lower cost and higher productivity.

Challenges that arise in real-world problems drive the need for better optimization formulations and more efficient algorithms. To solve the right problem with the right formulation and the right tool is the underlying topic of this thesis and the key to more widespread applications in many disciplines.

In this introductory chapter, a brief overview of decision-making hierarchy and model-based control and optimization is presented, which helps better illustrate the scope of our work. The motivating grade transition problem and its current challenges are then summarized to set the stage for the development of optimization formulations and control strategies in the subsequent chapters.

1.1 Hierarchical Process Operations

As shown in Figure 1.1, the decision-making hierarchy of chemical processes is typically represented as a pyramid-like structure. Usually, there are five layers involved which actively interact with neighboring layers: planning, scheduling, (dynamic) real-time optimization (RTO), advanced control such as model predictive control (MPC), and basic regulatory control. From the top to the bottom layer, the decision frequency increases while the problem scope narrows.

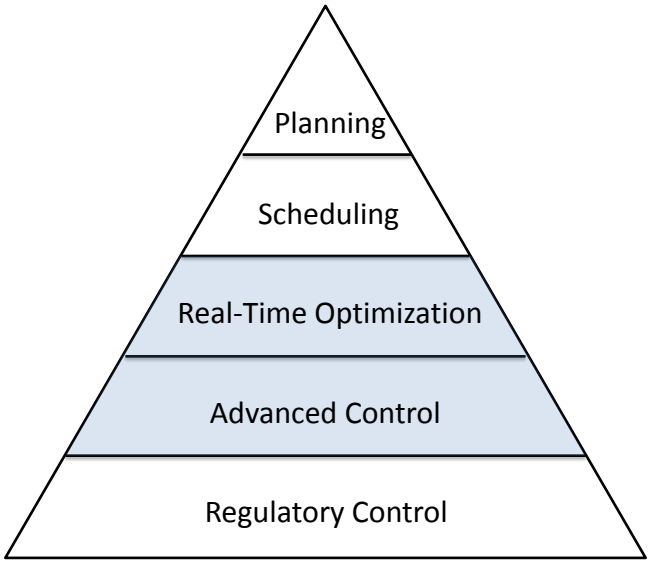

Figure 1.1: Decision-making hierarchy of chemical processes

At the top, planning and scheduling target at enterprise-wide plans and manufacturing sequences. The decisions made in these two layers are long-term ones with time scale varying from years to weeks.

The three layers at the bottom address operational decisions for one process unit or a set of process units at a higher frequency. Given the production plan made in the top two layers, real-time optimization generates and updates optimal operation conditions. RTO is the bridge between the top scheduling plans and the bottom process dynamics; it is carried out constantly to respond to changes in production

plan and to interact with the dynamic process below. Real-time optimization was first introduced to describe steady-state behavior in continuous processes and later extended to dynamic real-time optimization (DRTO) which includes process dynamics such that 1) transit behaviors and batch processes can be considered and optimized and 2) economic performance can be better pursued.

The operation conditions or setpoints calculated from RTO layer are then fed to the control system. The advanced control layer generates control actions that address maintenance of optimal process operation and rejection of disturbances. The most commonly used advanced control algorithm is Model Predictive Control (MPC) which exploits explicit process models to update controls in real time [53]. Depending on the nature of the process, either a linearized or a nonlinear model is used. The former one is typically termed as MPC, while the latter one as Nonlinear Model Predictive Control (NMPC) [25, 45, 54, 56]. For processes which exhibit strong nonlinearity in the operation, NMPC is of great interest due to its accuracy and applicability in a wider range of operating conditions.

Regulatory control layer makes the most frequent decisions mainly based on feedback mechanism [1]. Traditional PID controllers are usually built in this layer.

1.2 Model-Based Optimization and Control

The distinguishing feature of model-based optimization is the equation-oriented representation of the process of interest. Different from trial and error through case studies, model-based optimization enables us to find optimal process design, operations and plans based on the exploitation of explicit mathematical model structures. The optimization task is often translated to a mathematical programming problem, from which optimal solutions can be obtained from a mathematical point of view with the help of efficient optimization algorithms.

Model-based optimization is widely used in the decision-making hierarchy. However, the nature of the optimization problem that arises in different layers may be different, which drives the need for different model representations and different optimization algorithms. In the top two layers, discrete decisions such as whether to invest, which product to produce and which product delivery route to take are modeled. Therefore, optimization problems in these two layers are often mixed integer linear or nonlinear problems. As mentioned in the previous section, the RTO layer considers either a steady state model or a dynamic model that is representative of the actual process. This model usually involves nonlinear equations due to the nonlinearity of most of the chemical processes, and differential algebraic equations (DAEs) are taken into account when dynamic behavior is modeled [14, 15]. As a result, dynamic optimization algorithms is usually required in this layer for DRTO. For the advanced control layer, MPC is typically applied. This is a commonly used optimization-based control scheme, which also requires mathematical model representations and sometimes dynamic optimization strategies.

1.3 LLDPE and Loop Reactors

Polyethylene is the most widely used thermoplastic polymer today. Among the large family of polyethylene products, linear low-density polyethylene (LLDPE) has penetrated almost all traditional polyethylene markets. LLDPE is made by copolymerization of ethylene with longer-chain olefins; single-site catalysts are preferred, as they tend to provide a narrower distribution of molecular weight.

Solution polymerization in a continuous plant is a typical process for LLDPE production. Two common reactor configurations for solution polymerization are stirred-tank reactors and loop reactors. In particular, the loop reactor mainly consists of a non-adiabatic tubular system in a closed loop, with at least one heat exchanger for removing the heat generated by polymerization reactions and a pump to circulate

the reaction mixture through the pipe. Multiple feed positions are located along the loop for inlet monomer, comonomer and catalyst along with a product outlet [35]. The reactor is operated liquid filled, with temperature and pressure controlled to maintain the reaction mixture in liquid phase. The loop reactor is more effective than a stirred tank as it directly influences heat transfer conditions. Moreover, its effectiveness, described in Zacca and Ray [78], is due to operation at high circulation rates which allows operations under high polymer concentrations and a high length/diameter ratio which improves heat transfer conditions.

Modeling and simulation studies of loop reactors include Zacca and Ray [78], where the reactor is modeled as two interconnected tubular reactors, and Reginato *et al.* [59], which develops a nonideal CSTR model. In Touloupides *et al.* [68], loop reactors are modeled as an ideal CSTR followed by a semi-continuous product removal unit. As discussed in Zacca and Ray [78], the dynamic behavior of loop reactors can be characterized by its volumetric recycle ratio. At high recycle ratios, the loop reactor behaves like an ideal CSTR. This reactor type greatly simplifies the construction of a detailed dynamic model without incorporating additional information on reactor geometry, which is often proprietary.

1.4 Grade Transitions

Various grades of LLDPE tailored to different applications are defined by the specifications of product properties such as melt index (MI) and density. Typically, several grades are produced in the same production line. Due to high inventory cost and volatile market demand, frequent grade transitions are needed. Those grade transitions are considered to be challenging from an operational point of view because both process economics and safety issues should be taken into consideration. In certain instances, complex transitions rely heavily on operator/expert experience. Given the large market of LLDPE and the current experience-based transi-

tions, there is a need, and also room to improve transitions and change operating conditions in a more efficient way so that the transition time as well as off-grade production could be minimized.

Several studies have been performed to seek better transition policies. A comparison of the performance of experience-based transition strategies is presented [16] and a semi-continuous grade transition strategy aimed at preventing melting and agglomeration of particles in fluidized bed polyethylene reactors is developed and compared with other strategies [55].

Through computer simulations, researchers are able to compare a variety of transition policies and to select the best one. However, simulations alone are insufficient to create new policies; this motivates continuing studies on dynamic optimization of grade transitions. Dynamic optimization of grade transitions is an important topic and attracts attention of many researchers [8, 10, 22, 73]. The potential value of optimization includes great reduction in transition time, increased flexibility in the product wheel and guided complex transitions. Wang *et al.* [73] proposed an optimal grade transition control system by integrating nonlinear model predictive controller and offline dynamic optimizer using sequential dynamic optimization. Mixed integer dynamic optimization is applied to a gas-phase copolymerization fluidized bed reactor [11], and optimal control configuration and transition policies are achieved.

Among all the methods proposed, simultaneous dynamic optimization (or direct transcription approach) shows particular advantages in solving such problems. A successful application of simultaneous dynamic optimization on transition problems is discussed in Cervantes *et al.* [10], where optimal control strategies are obtained for grade transitions in large-scale LDPE plant models using orthogonal collocation on finite elements and an interior point method. Therefore, a simultaneous dynamic optimization strategy will be applied in this study to solve optimal transition problems of LLDPE solution polymerization.

1.5 Research Statement and Thesis Outline

The goal of the project is to build a model-based control and optimization framework for optimal grade transitions in polyethylene solution polymerization processes. To achieve this goal, there are four key topics we need to consider:

1. Model development
2. Optimization formulation and solution strategies
3. Optimization under uncertainty
4. Online implementation

A detailed model that is representative of the process is a solid base for all the subsequent tasks. Once the model is ready, we focus on the RTO and the NMPC layers in the decision-making hierarchy. The motivation, the background, the methodology as well as the results of each topic will be discussed in the remainder of the thesis.

Chapter 2 gives a brief overview of the optimization algorithms for dynamic optimization. We focus on simultaneous dynamic optimization in particular and will talk about singular control problems as well. These two topics lay the foundation of all the work presented here. The concept and methodology are widely used through the entire thesis; the simultaneous dynamic optimization approach enables efficient solution to the large-scale optimization problem while the singular control nature of the problem brings up the discussion on regularization.

Starting from Chapter 3, we focus on an industrial application of polyethylene solution polymerization processes. First, we discuss the model development in this chapter; a brief description of the process and a detailed explanation of the model are presented.

Then in Chapter 4 dedicated to the real-time optimization layer, the simultaneous dynamic optimization method is applied to two distinct optimization formulations: one is for single-value product property targets while the other goes one step further to deal with specification bands. Several case studies are presented to explain the optimal transition policy and to illustrate the influence of regularization.

Chapter 5 aims at obtaining robust optimal solutions in the presence of uncertainty. The motivation of considering uncertainty, as well as the background information on related research topics, will be introduced at the beginning of the chapter. Next, we formulate the back-off problem and demonstrate its effectiveness using a set of case studies.

Chapter 6 begins with a review of the commonly used nonlinear model predictive control and moving horizon estimation, and then proceeds to a modified version which is tailored to this particular grade transition problem. Two cases studies are presented to show the online control performance with either full state feedback or partial state measurement. Moreover, the dividing line between RTO and advance control is removed by applying economic NMPC to the grade transition problem.

Chapter 7 concludes the dissertation, discusses the contributions of our work, and points out some open questions and future research directions.

Chapter 2

Optimization Methodology

In the previous introduction, we briefly discussed the two aspects of the thesis: the right tool from a mathematical programming point of view and the right problem formulation at the engineering level. Efficient solution strategies for dynamic optimization is the enabling tool for successful execution of model-based optimization tasks in both real-time optimization and model predictive control layer. Problems that arise in the area of real-time optimization (or offline optimization) include recipe optimization of batch processes, grade transition in continuous processes and parameter estimation, while online implementation in the advanced control layer usually involves model predictive control, state estimation and online process identification. In this chapter, we first present the dynamic optimization methods that apply to all these problems and introduce the commonly used notations as well as basic formulations, before we delve into specific problems of grade transitions in the subsequent chapters.

2.1 Solution Approaches for Dynamic Optimization

Consider the general-purpose dynamic optimization problem given by:

$$\begin{aligned} \min \quad & F(z(t_f)) \\ s.t. \quad & \dot{z} = f(z(t), y(t), u(t), p), z(0) = z_0, \\ & g(z(t), y(t), u(t), p) = 0, \\ & h(z(t), y(t), u(t), p) \leq 0, \\ & z_L \leq z(t) \leq z_U, y_L \leq y(t) \leq y_U, u_L \leq u(t) \leq u_U, p_L \leq p \leq p_U \end{aligned} \tag{2.1}$$

with the differential-algebraic equations (DAEs) model. Here $z(t) \in \mathbb{R}^{n_z}$ are differential variables, $y(t) \in \mathbb{R}^{n_y}$ are algebraic variables, $u(t) \in \mathbb{R}^{n_u}$ are control variables, and p are variables that are independent of time t. The problem is defined in the continuous time domain from 0 to t_f. $F(\cdot)$ is the objective function in the Mayer form, which considers the final time objective as a function of differential states. $f(\cdot)$ represent process dynamics in ordinary differential equations, and $g(\cdot)$ describe the rest of process model using algebraic equations. Both of them come from first-principles or data-driven model of the process. $h(\cdot)$ and variable bounds arise from optimization constraints such as feasible control movement, process safety constraints, product property requirement, etc. Both end-point constraints and the path constraints can be represented in the presented form.

Numerical solution methods for dynamic optimization are usually classified in two categories: 1) the sequential approach and multiple shooting with parameterized control and embedded DAE solvers [7, 21, 62, 70, 70], and 2) the simultaneous approach with fully discretized states and controls [14].

2.1.1 Sequential Approach and Multiple Shooting

The basic idea of sequential approach is to separate the DAE problem from the optimization task, with sensitivity calculation linking them together. This involves repeated execution of three functional blocks: the DAE solver, the sensitivity calculation and the NLP solver. The integration of DAEs are performed in the first block. And then in the second block, either direct sensitivity or adjoint sensitivity is calculated. The reduced size NLP problem is solved in the third block based on the gradient information provided from sensitivity calculation. After each iteration, the NLP solver generates new optimal decision profiles, send them to the DAE solver for integration and a new iteration starts.

Multiple shooting [7, 40] is developed to avoid the instability problem that arises in the sequential approach. In this approach, the time domain is discretized into several smaller time periods and the integration of the DAE model is performed in each period. In this way, not only the control variables but also the initial conditions of the states in each period are considered in the sensitivity calculation, and thus more state variable information can be utilized by the NLP solver.

Sequential approach and multiple shooting are classified in the same category as both of them require embedded DAE solvers and repeated solutions of the DAE system. Because of this, both approaches rely heavily on the efficiency and reliability of the DAE solver. Moreover, the sequential nature of the approach destroys the original sparsity of the dynamic model and makes the computation more expensive.

2.1.2 Simultaneous Dynamic Optimization

The simultaneous collocation method discretizes the continuous time horizon into a finite element mesh, and then the differential-algebraic equation optimization problems are converted into nonlinear programming problems [34]. Here state

and control profiles are represented by a family of polynomials on finite elements. Typically the control decisions $u(t)$ are represented by piecewise constant or piecewise linear profiles, and the differential and algebraic state variables $z(t)$ and $y(t)$, respectively can be represented by the Runge-Kutta basis representation:

$$z(t) = z_{i-1} + h_i \sum_{j=1}^{K} \Omega_j(\tau) \dot{z}_{i,j} \tag{2.2a}$$

$$y(t) = \sum_{j=1}^{K} l_j(\tau) y_{i,j} \tag{2.2b}$$

$$t = t_{i-1} + \tau h_i \tag{2.2c}$$

where i is the index of the element and j is the index of the collocation points within the element; h_i is the length of the element, $\tau \in [0, 1]$ is the normalized time in the element, z_{i-1} is the state value at the beginning of the element, $y_{i,j}$ is the state variable $y(t)$ and $\dot{z}_{i,j}$ is the first derivative of state variable $z(t)$ with respect to time at collocation point j, and $\Omega_j(\tau)$ is a polynomial of order K.

$$\Omega_j(\tau) = \int_0^{\tau} l_j(\tau') dt' \tag{2.3}$$

Here, $l_j(\tau)$ is Lagrange interpolation polynomial basis function. Continuity of the state profiles across element boundaries is enforced by a set of continuity equations, as shown in (2.4). Similar to (2.2), by setting $\tau = 1$, the state value at the end of the element is calculated and passed to the next element.

$$z_i = z_{i-1} + h_i \sum_{j=1}^{K} \Omega_j(1) \dot{z}_{i,j} \tag{2.4}$$

Substituting (2.2) for the state and control profiles into the differential-algebraic equations and adding (2.4) leads to a fully discretized dynamic optimization problem which can be solved by nonlinear programming (NLP) solvers, such as CONOPT [18] and IPOPT [72].

The NLP problem converted from the dynamic optimization problem (2.1) is stated as:

$$
\begin{aligned}
\min \quad & F(z_{i,j}) \\
s.t. \quad & z_{i,j} = z_{i-1} + h_i \sum_{j=1}^{K} \Omega_j(\tau_j) \dot{z}_{i,j}, \\
& z_i = z_{i-1} + h_i \sum_{j=1}^{K} \Omega_j(1) \dot{z}_{i,j}, \\
& \dot{z}_{i,j} = f(z_{i,j}, y_{i,j}, u_{i,j}, p), z_{1,0} = z_0, \\
& g(z_{i,j}, y_{i,j}, u_{i,j}, p) = 0, \\
& h(z_{i,j}, y_{i,j}, u_{i,j}, p) \leq 0, \\
& z_L \leq z_{i,j} \leq z_U, y_L \leq y_{i,j} \leq y_U, \\
& u_L \leq u_{i,j} \leq u_U, p_L \leq p \leq p_U.
\end{aligned}
\tag{2.5}
$$

More detailed information on simultaneous strategies can be found in the overview by Biegler [3].

2.2 Nonlinear Programming Methods

The NLP solver is a must no matter you choose sequential approach, multiple shooting or simultaneous approach to solve the dynamic optimization problem. It is the key component in all the dynamic optimization approaches because it conducts optimization searches and determines the optimal decision profiles and its efficiency and reliability highly influence the performance. Newton type solvers are generally preferred due to their fast convergence properties [49]. Three nonlinear programming algorithms are usually adopted in the current NLP solvers.

The sequential quadratic programming (SQP) method solves a sequence of quadratic programs (QP) to guide the search. To construct each QP, the variable value and derivative information at each iteration are used. SQP solvers are favored by the sequential method for dynamic optimization for the following two reasons. First, the size of the NLP problem is relatively small in the sequential approach. Also,

second-order derivatives are very expensive to compute via sensitivity analysis, but SQP methods usually perform well with approximated derivatives using BFGS.

Another method is the generalized reduced gradient (GRG) method. One key feature of this GRG method is that it partitions the variables in an NLP into three types: basic, nonbasic, and superbasic variables. Basic variables are used to solve equality constraints, nonbasic variables are fixed at either their upper or lower bounds, and superbasic variables drive the optimization search. Among all the NLP solvers, CONOPT is a representative solver exploiting this method.

The interior point method is preferred when dealing with large-scale problems with many degrees of freedom, and it is often used to solve NLP problems resulting from the simultaneous collocation method. This method reformulates the inequality constraints as barrier terms to the objective function, and solves a series of NLP problems with decreasing barrier parameters to recover the optimal solution of the original problem. One good example of this type of solvers is IPOPT.

2.3 Singular Control Problems

Singular control problem often arises in process engineering when the control appears linearly in the differential equations and in the performance index. Accurate control structures and junctions between optimal non-singular and singular arcs are required to generate optimal control profiles. Moreover, the singular arcs can not be determined directly from the Euler-Lagrange equations. The ill-conditioned DAEs result in oscillatory control profiles and require repeated time differentiations to recover the control.

A number of techniques have been proposed to address the singular control problem. One approach as proposed in [31] is adding regularization term in the objective function. The regularization term is a time-integral of the control variables

u with a adjustable weight, which needs to be determined carefully such that the optimal control profiles do not deteriorate and the actual objective function is adequately emphasized. Jacobson *et al.* formulate the original singular control problem as a sequence of non-singular problems with a decreasing barrier parameter. But numerical instabilities may occur when the barrier parameter is too small. On the other hand, the actual objective or the original performance index is not addressed if the barrier parameter is too large. Another heuristic approach [4] applies a coarser discretization grid on the control variables. In the simultaneous collocation approach, piecewise constant control can be enforced to realize this.

In addition to the regularization approach and the coarse grid, indirect and direct approaches are two common strategies designed for singular control problems. The key idea of indirect approach is the pre-determined solution structure and explicit expression for the singular control. However, determining the right structure and expression for the singular control is difficult. Contrary to the indirect approach, direct approaches do not require prior knowledge of the control structure. The detection of control switching structure is based on the coarse resolution of the control profile, and then a multistage problem is formulated and solved using a sequential NLP approach.

Recently, Chen and Biegler [12] proposed a nested direct transcription optimization approach which leads to solutions that satisfy the necessary optimality conditions for singular optimal control problems. This approach is enabled by a simultaneous approach with moving finite elements [13].

In the dissertation, regularization and piecewise constant profiles are adopted in the optimal grade transition problem. A detailed procedure of the determination of weighting factors will be further discussed in the subsequent chapters.

Chapter 3

Model Development of Polyethylene Solution Polymerization Processes

In this chapter, we focus on the model development for the motivating industrial polymerization process as described in the introduction. We first give a brief description of the process, including the process flowsheet and the reaction mechanism, and then explain all the components of the model in detail, which include: (1) mass and energy balance equations, (2) the moment model to predict product properties, (3) a simple yet accurate vapor-liquid equilibrium (VLE) model derived from rigorous calculations, and (4) a variable time delay model for the rest of the flowsheet. The resulting model is capable of capturing the detailed dynamics of the system.

3.1 Process Overview

3.1.1 Process Flowsheet

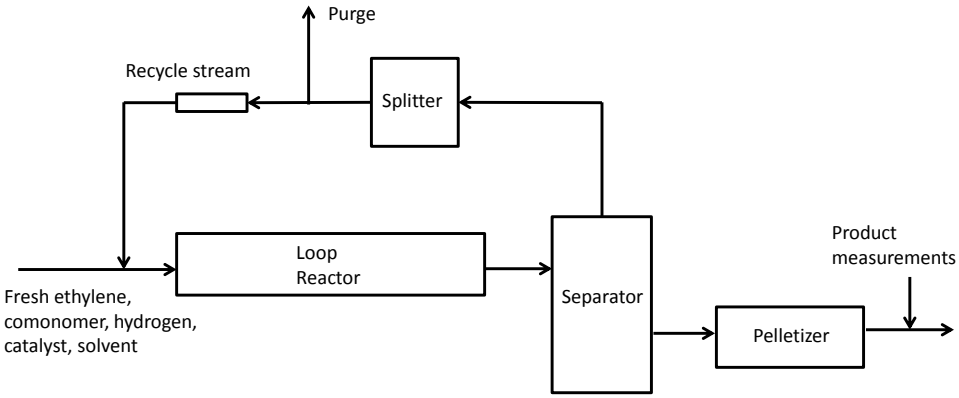

Figure 3.1: Flowsheet of Solution Polymerization Process

The flowsheet of this entire LLDPE process is shown in Fig. 3.1. LLDPE is produced using solution polymerization, where the loop reactor operates at high recycle ratio and is modeled as an ideal CSTR, based on the observation of Zacca and Ray's work [78]. This assumption also avoids specification of additional information on reactor geometry and equipment information required for loop reactors, which is often proprietary. In this study, both raw material and recycle flows are combined as inlet reactor flow. Ethylene, comonomer, catalyst, hydrogen, solvent and impurities are continuously injected into the jacketed reactor, and ethylene is partially polymerized to produce products of different grades. Cooling media flow through the reactor jacket to control the reactor temperature to an acceptable range, and to ensure all components remain in liquid phase while maintaining efficient reaction rates. The reactor is followed by a separator which separates polymers from other components and a splitter which recycles both liquid and vapor streams.

From a process control perspective, available manipulated variables are ethylene flowrate, comonomer flowrate, hydrogen flowrate, catalyst flowrate and inlet cool-

ing media temperature while the controlled variables are ethylene conversion, reactor temperature, MI and product density. Perfect mixing is assumed in the reactor; thus, there is no position dependence in the reactor model.

3.1.2 Reaction Mechanism

The liquid phase olefin polymerization is represented by the following reactions [78]. For our process, we assume that catalyst activation is very fast compared to other reactions; once the catalyst is fed into the reactor all sites of the catalyst become activated. Also, as single-site catalyst (metallocene) is used in this study, no site transformation is considered. The selected kinetic reactions can be seen in Table 3.1, with P_0, the empty site; M, monomer and comonomer denoted by different subscripts i and j; $P_{n,i}$, growing polymer of chain length n and end-group M_i; $D_{n,i}$, dead polymer of chain length n and end-group M_i; C_d, dead catalyst site; and A, S, T, X for cocatalyst, solvent, transfer agent and poison, respectively.

Chain initiation	$P_0 + M_i \Rightarrow P_{1,i}$	rate constant k_p
Chain propagation	$P_{n,i} + M_j \Rightarrow P_{n+1,j}$	rate constant k_{pij}
Chain transfer		
1. to hydrogen	$P_{n,i} + H_2 \Rightarrow P_0 + D_{n,i}$	rate constant k_{cH}
2. to cocatalyst	$P_{n,i} + A \Rightarrow P_0 + D_{n,i}$	rate constant k_{cA}
3. to solvent	$P_{n,i} + S \Rightarrow P_0 + D_{n,i}$	rate constant k_{cS}
4. to transfer agent	$P_{n,i} + T \Rightarrow P_0 + D_{n,i}$	rate constant k_{cT}
5. to monomer	$P_{n,i} + M_j \Rightarrow P_{1,j} + D_{n,i}$	rate constant k_{cm}
6. spontaneous	$P_{n,i} \Rightarrow P_0 + D_{n,i}$	rate constant k_{csp}
Chain deactivation		
1. by poison	$P_{n,i} + X \Rightarrow Cd + D_{n,i}$	rate constant k_{dx}
	$P_0 + X \Rightarrow C_d$	rate constant k_{dx0}
2. spontaneous	$P_{n,i} \Rightarrow C_d + D_{n,i}$	rate constant k_{dsp}
	$P_0 \Rightarrow C_d$	rate constant k_{dsp0}

Table 3.1: LLDPE polymerization reactions considered in this study

3.2 Model Development

3.2.1 First-principles Model Equations

For the copolymerization process considered in the study, there are four propagation rate constants k_{p11}, k_{p12}, k_{p21} and k_{p22} with the first subscript representing the end-group in growing polymer, and the second representing the monomer adding to the polymer chain; the values 1 and 2 represent ethylene and comonomer, respectively. The propagation rates for different end-groups and different monomers are not identical. Two reactivity ratios are defined as $r_1 = k_{p11}/k_{p12}$ and $r_2 = k_{p22}/k_{p21}$. These reactivity ratios are reported [27]. The Arrhenius law is used to describe the dependence of reaction rate on temperature. All of the remaining rate constants and activation energies can be found in literature [78]. A table of kinetic parameters used in this study is in Table 3.2.

Reaction		k_0	Unit	E_a (kcal/gmol)
Chain initiation	k_p	4.84×10^8	L/gmol/s	12.0
Propagation	k_{p11},k_{p21}	4.84×10^8	L/gmol/s	12.0
Chain transfer				
to hydrogen	k_{cH}	4.4×10^6	L/gmol/s	12.0
spontaneous	k_{csp}	3.85×10^2	L/gmol/s	12.0
to monomers	k_{cm}	6.16×10^3	L/gmol/s	12.0
Site deactivation				
spontaneous	k_{dsp}	7.92×10^3	L/s	12.0

Table 3.2: Kinetic rate constants: $k = k_0 e^{-E_a/RT}$, $r_1 = 10$, $r_1 \times r_2 = 1$

Five dynamic mass balances are derived for ethylene, comonomer, empty catalyst site, hydrogen, and solvent and presented in Eq.(3.1). Fresh and recycled ethylene are fed into the reactor at rate F_1 and F_{1r} with concentrations M_1^0 and M_{1r}, respectively and ethylene is consumed by initialization, propagation and chain transfer reactions. Similarly the mass balance equation of comonomer is derived with fresh comonomer flowrate F_2, concentration M_2^0 and recycled comonomer flowrate F_{2r} with concentration M_{2r}. Activated empty catalyst site P_0 is introduced into the

reactor at rate F_c, occupied by chain propagation reactions and deactivated by poisoning and spontaneous deactivation. The chain transfer reactions release the occupied site and generate activated empty sites. In addition, mass balances of hydrogen and solvent are described with additional differential equations. Here fresh hydrogen enters the reactor at rate F_H and concentration H_2^0, together with recycled hydrogen flow at rate F_{Hr} and concentration H_{2r}. A similar equation is derived for solvent.

$$\begin{aligned}
\dot{M}_1 &= \frac{F_1 M_1^0 + F_{1r} M_{1r} - F_{out} M_1}{V} \\
&\quad - k_p M_1 P_0 - k_{p11} M_1 \sum_{n=1}^{\infty} P_{n,1} - k_{p21} M_1 \sum_{n=1}^{\infty} P_{n,2} - k_{cm} M_1 (\sum_{n=1}^{\infty} P_{n,1} + \sum_{n=1}^{\infty} P_{n,2}) \quad (3.1a) \\
\dot{M}_2 &= \frac{F_2 M_2^0 + F_{2r} M_{2r} - F_{out} M_2}{V} \\
&\quad - k_p M_2 P_0 - k_{p22} M_2 \sum_{n=1}^{\infty} P_{n,2} - k_{p12} M_2 \sum_{n=1}^{\infty} P_{n,1} - k_{cm} M_2 (\sum_{n=1}^{\infty} P_{n,1} + \sum_{n=1}^{\infty} P_{n,2}) \quad (3.1b) \\
\dot{P}_0 &= \frac{F_c P_0^0 - F_{out} P_0}{V} - k_p M_1 P_0 - k_p M_2 P_0 - k_{dx0} X P_0 - k_{dsp0} P_0 \\
&\quad + (k_{cH} H_2 + k_{cA} A + k_{cS} S + k_{cT} T + k_{csp}) (\sum_{n=1}^{\infty} P_{n,1} + \sum_{n=1}^{\infty} P_{n,2}) \quad (3.1c) \\
\dot{H}_2 &= \frac{F_H H_2^0 + F_{Hr} H_{2r} - F_{out} H_2}{V} - k_{cH} H_2 (\sum_{n=1}^{\infty} P_{n,1} + \sum_{n=1}^{\infty} P_{n,2}) \quad (3.1d) \\
\dot{S} &= \frac{F_S S^0 + F_{Sr} S_r - F_{out} S}{V} - k_{cS} S (\sum_{n=1}^{\infty} P_{n,1} + \sum_{n=1}^{\infty} P_{n,2}) \quad (3.1e)
\end{aligned}$$

In addition to the mass balance equations, the population balance equations for polymer chains can be expressed as Eq.(3.2). As seen from the equations, each individual polymeric species, live/dead polymer chain with a certain length and a certain end-group, is described by an ordinary differential equation. When the

chain length grows, the number of population balance equations becomes large.

$$\begin{aligned}\dot{P}_{1,i} =& -\frac{F_{out}P_{1,i}}{V} + k_p M_i P_0 - \sum_{j=1,2} k_{pij} M_j P_{1,i} - (k_{cH}H_2 + k_{cA}A + k_{cS}S + k_{cT}T + k_{csp})P_{1,i} \\ & - (k_{dsp} + k_{dx}X)P_{1,i} - k_{cm}(M_1 + M_2)P_{1,i} + k_{cm}M_1 \sum_{n=1}^{\infty}(P_{n,i} + P_{n,j}), \quad i = 1,2 \end{aligned} \tag{3.2a}$$

$$\begin{aligned}\dot{P}_{n,i} =& -\frac{F_{out}P_{n,i}}{V} + \sum_{j=1,2} k_{pji} M_i P_{n-1,j} - \sum_{j=1,2} k_{pij} M_j P_{n,i} - (k_{dsp} + k_{dx}X)P_{n,i} \\ & - (k_{cH}H_2 + k_{cA}A + k_{cS}S + k_{cT}T + k_{csp})P_{n,i} - k_{cm}(M_1 + M_2)P_{1,i}, \quad n \geq 2,\ i = 1,2 \end{aligned} \tag{3.2b}$$

$$\begin{aligned}\dot{D}_{n,i} =& -\frac{F_{out}D_{n,i}}{V} + (k_{cH}H_2 + k_{cA}A + k_{cS}S + k_{cT}T + k_{csp})P_{n,i} + k_{cm}(M_1 + M_2)P_{n,i} \\ & + (k_{dsp} + k_{dx}X)P_{n,i}, \quad n \geq 1,\ i = 1,2 \end{aligned} \tag{3.2c}$$

Heat balance equations are included for reactor temperature and jacket temperature as shown in (3.3). Reactor feed enters the reactor at temperature T^0, while the outlet leaves at temperature T. The solution inside the reactor, which has a solution density ρ_s and heat capacity C_{ps}, is heated mainly by heat generated from the chain propagation reactions, and cooled by cooling water in the jacket. U denotes the heat transfer coefficient, A the heat transfer area and ΔH the reaction heat. The temperature change in the jacket is described in Eq.(3.3b) with inlet temperature of cooling media T_j^0, the jacket volume V_j, the density of cooling media ρ_j and the heat capacity C_{pj}.

$$\begin{aligned}\dot{T} =& \frac{F_{in}T^0 - F_{out}T}{V} - \frac{UA(T - T_j)}{\rho_s C_{ps} V} \\ & + \frac{\Delta H(k_{p11}M_1 \sum_{n=1}^{\infty} P_{n,1} + k_{p12}M_2 \sum_{n=1}^{\infty} P_{n,1} + k_{p21}M_1 \sum_{n=1}^{\infty} P_{n,2} + k_{p22}M_2 \sum_{n=1}^{\infty} P_{n,2})}{\rho_s C_{ps}} \end{aligned} \tag{3.3a}$$

$$\dot{T}_j = \frac{F_j(T_j^0 - T_j)}{V_j} + \frac{UA(T - T_j)}{\rho_j C_{pj} V_j} \tag{3.3b}$$

3.2.2 Moment Model

The above population balance introduces an equation for each species and for each polymer chain length. It is capable of tracking the molecular weight distribution (MWD), but the size of the population balance model increases and the model becomes computationally intractable and inefficient as the chain length gets larger. Instead, the method of moments provides an efficient way to solve polymerization systems by aggregating polymers of various chain lengths with different weights.

The kth moment of growing polymer with end-group M_i is defined as

$$\mu_{k,i} = \sum_{n=1}^{\infty} n^k P_{n,i} \tag{3.4}$$

and the kth moment of bulk (live and dead) polymer is

$$\lambda_{k,i} = \sum_{n=1}^{\infty} n^k (P_{n,i} + D_{n,i}) \tag{3.5}$$

where $P_{n,i}$ denotes the population of live polymer chains with length n and end-group M_i and $D_{n,i}$ is the population of dead polymer chains with length n and end-group M_i. Average distributional properties can be calculated from those moments. As the product properties considered in the study, MI and density, are correlated with these molecular weight averages, dynamic molecular weight moment equations are derived for the zeroth, first and second moments from polymer population balance equations.

To simplify the following moment equations, we define a lumped term for chain transfer reactions as in Eq. (3.6).

$$KC = k_{cH}H_2 + k_{cA}A + k_{cS}S + k_{cT}T + k_{csp} + k_{cm}(M_1 + M_2) + k_{dsp} + k_{dx}X \quad (3.6)$$

Live Polymer Moments

0^{th} moments

$$\dot{\mu}_{01} = -\frac{F_{out}\mu_{01}}{V} + k_p M_1 P_0 + k_{P21} M_1 \mu_{02} - KC\mu_{01} - k_{p12} M_2 \mu_{01} + k_{cm} M_1(\mu_{01} + \mu_{02}) \quad (3.7a)$$

$$\dot{\mu}_{02} = -\frac{F_{out}\mu_{02}}{V} + k_p M_2 P_0 + k_{P12} M_2 \mu_{01} - KC\mu_{02} - k_{p21} M_1 \mu_{02} + k_{cm} M_2(\mu_{01} + \mu_{02}) \quad (3.7b)$$

1^{st} moments

$$\begin{aligned}\dot{\mu}_{11} = &-\frac{F_{out}\mu_{11}}{V} + k_{p11} M_1 \mu_{01} + k_{p21} M_1(\mu_{02} + \mu_{12}) \\ &- KC\mu_{11} + k_{p1} M_1 P_0 - k_{p12} M_2 \mu_{11} + k_{cm} M_1(\mu_{01} + \mu_{02}) \quad (3.7c)\\ \dot{\mu}_{12} = &-\frac{F_{out}\mu_{12}}{V} + k_{p22} M_2 \mu_{02} + k_{p12} M_2(\mu_{01} + \mu_{11}) \\ &- KC\mu_{12} + k_{p2} M_2 P_0 - k_{p21} M_1 \mu_{12} + k_{cm} M_2(\mu_{01} + \mu_{02}) \quad (3.7d)\end{aligned}$$

2^{nd} moments

$$\begin{aligned}\dot{\mu}_{21} = &-\frac{F_{out}\mu_{21}}{V} + k_{p11} M_1(2\mu_{11} + \mu_{01}) + k_{p21} M_1(\mu_{22} + 2\mu_{12} + \mu_{02}) \\ &- KC\mu_{21} - k_{p12} M_2 \mu_{21} + k_{p1} M_1 P_0 + k_{cm} M_1(\mu_{01} + \mu_{02}) \quad (3.7e)\\ \dot{\mu}_{22} = &-\frac{F_{out}\mu_{22}}{V} + k_{p22} M_2(2\mu_{12} + \mu_{02}) + k_{p12} M_2(\mu_{21} + 2\mu_{11} + \mu_{01}) \\ &- KC\mu_{22} - k_{p21} M_1 \mu_{22} + k_{p2} M_2 P_0 + k_{cm} M_2(\mu_{01} + \mu_{02}) \quad (3.7f)\end{aligned}$$

Bulk Polymer Moments

0^{th} moments

$$\dot{\lambda}_{01} = -\frac{F_{out}\lambda_{01}}{V} + k_p M_1 P_0 + k_{p21} M_1 \mu_{02} - k_{p12} M_2 \mu_{01} + k_{cm} M_1 (\mu_{01} + \mu_{02}) \tag{3.8a}$$

$$\dot{\lambda}_{02} = -\frac{F_{out}\lambda_{02}}{V} + k_p M_2 P_0 + k_{p12} M_2 \mu_{01} - k_{p21} M_1 \mu_{02} + k_{cm} M_2 (\mu_{01} + \mu_{02}) \tag{3.8b}$$

1^{st} moments

$$\dot{\lambda}_{11} = -\frac{F_{out}\lambda_{11}}{V} + k_{p11} M_1 \mu_{01} + k_{p21} M_1 (\mu_{02} + \mu_{12}) \tag{3.8c}$$

$$+ k_{p1} M_1 P_0 - k_{p12} M_2 \mu_{11} + k_{cm} M_1 (\mu_{01} + \mu_{02}) \tag{3.8d}$$

$$\dot{\lambda}_{12} = -\frac{F_{out}\lambda_{12}}{V} + k_{p22} M_2 \mu_{02} + k_{p12} M_2 (\mu_{01} + \mu_{11}) \tag{3.8e}$$

$$+ k_{p2} M_2 P_0 - k_{p21} M_1 \mu_{12} + k_{cm} M_2 (\mu_{01} + \mu_{02}) \tag{3.8f}$$

2^{nd} moments

$$\dot{\lambda}_{21} = -\frac{F_{out}\lambda_{21}}{V} + k_{p11} M_1 (2\mu_{11} + \mu_{01}) + k_{p21} M_1 (\mu_{22} + 2\mu_{12} + \mu_{02})$$

$$- k_{p12} M_2 \mu_{21} + k_{p1} M_1 P_0 + k_{cm} M_1 (\mu_{01} + \mu_{02}) \tag{3.8g}$$

$$\dot{\lambda}_{22} = -\frac{F_{out}\lambda_{22}}{V} + k_{p22} M_2 (2\mu_{12} + \mu_{02}) + k_{p12} M_2 (\mu_{21} + 2\mu_{11} + \mu_{01})$$

$$- k_{p21} M_1 \mu_{22} + k_{p2} M_2 P_0 + k_{cm} M_2 (\mu_{01} + \mu_{02}) \tag{3.8h}$$

The number average molecular weight M_n and the weight average molecular weight M_w can be calculated from the following moments: $M_n = \overline{MW}\frac{\lambda_{11} + \lambda_{12}}{\lambda_{01} + \lambda_{02}}$ and $M_w = \overline{MW}\frac{\lambda_{21} + \lambda_{22}}{\lambda_{11} + \lambda_{12}}$, where $\overline{MW}$ is the molecular weight of the repeating units. In the process considered in our study, $\overline{MW}$ can be computed as a weighted average

of the molecular weights of monomer and comonomer, MW_1 and MW_2.

$$\overline{MW} = (1-\omega)MW_1 + \omega MW_2 \tag{3.9a}$$

$$\omega = \frac{\mu_{12}}{\mu_{12} + \mu_{11}} \tag{3.9b}$$

The melt index (MI) correlation and its parameters can be found in relevant work [19, 20, 36, 37, 63].

$$MI = a_1 M_w^{a_2} \tag{3.10}$$

where $a_1 = 3 \times 10^{19}$, $a_2 = -3.92$.

A simple data fit leads to the density correlation with branch content from the data[51].

$$\rho = b_1 log(100\omega) + b_2 \tag{3.11}$$

where $b_1 = -0.023$, $b_2 = 0.9192$ and 100ω is the percentage of branch content of the comonomer.

3.2.3 Surrogate VLE Model

A key component of the model is vapor-liquid equilibrium of the polymer solution, which is used to estimate bubble point pressure. Since the whole process takes place in liquid phase, bubble point pressure of the mixture should be maintained below operating pressure at all time. For polyethylene system, the most accepted vapor-liquid equilibrium models are Equation-of-State (EOS) models; these include the Sanchez-Lacombe model based on the lattice theory, Polymer SRK, which extends the SRK equation of state, and PC-SAFT, based on perturbation theory of fluids. The EOS model has the following advantages compared to activity

coefficient models: 1) it is consistent in the critical region; 2) it can represent both vapor and liquid phases; 3) and its parameters extrapolate well with temperature. However, developing and solving such an EOS model is difficult due to its complexity.

The need for a simple, yet accurate thermodynamic model gives rise to the idea of surrogate thermodynamic model, derived from an EOS model. One choice of surrogate model is the well-known Kriging model [23, 42]. It consists of two parts, i) the regression model $f_k^s(x) \in \mathbb{R}^{n_x} \rightarrow \mathbb{R}^{n_s}$, with $k = 1, \ldots, n_p$ with regression parameter vector η^* and ii) the correlation model $R^s(\theta, x) \in \mathbb{R}^{n_x} \rightarrow \mathbb{R}^{n_d}$ with correlation parameter vector ζ^* shown in (3.12). Here $x \in \mathbb{R}^{n_x}$ is the input vector of the model, $s \in \mathbb{R}^{n_s}$ is the vector calculated from x, n_p is the number of regression terms and n_d is the number of training data points.

$$s(x) = \sum_{k=1}^{n_p} \eta_k^* f_k(x) + \sum_{i=1}^{n_d} \zeta_i^* R_i^s(\theta, x) \tag{3.12}$$

The mathematical form of the regression model is chosen as quadratic combinations of input variables as shown in (3.13) while the correlation model has a Gaussian expression as shown in (3.14). $w_i \in \mathbb{R}^{n_x}$ is the input vector of the ith training data with $i = 1, 2, \ldots, n_d$. The correlation model is asymptotically zero when the distance between training point w_i and x is large. This phenomenon is anisotropic, where coefficients θ_j control the decay rates, which are distinct in the n_x directions.

Regression model

$$
\begin{aligned}
& n_p = \frac{1}{2}(n+1)(n+2) \\
& f_1^s(x) = 1 \\
& f_2^s(x) = x_1, \ldots, f_{n+1}^s(x) = x_n \\
& f_{n+2}^s(x) = x_1^2, \ldots, f_{2n+1}^s(x) = x_1 x_n \\
& f_{2n+2}^s(x) = x_2^2, \ldots, f_{3n}^s(x) = x_2 x_n \\
& \ldots \\
& f_p^s(x) = x_n^2
\end{aligned}
\tag{3.13}
$$

Correlation model

$$
R_i^s(\theta, x) = \prod_{j=1}^{n} exp(-\theta_j (w_{ij} - x_j)^2) \tag{3.14}
$$

In this study, 250 training points are designed by the Latin Hypercube Sampling method in the region of interest, shown in Table 3.3. A surrogate Kriging model representing the relationship between the mass fraction of the components, temperature of the mixture and the bubble point pressure, is built based on those training data points generated from ASPEN. DACE, a MATLAB toolbox [42], is used to build the Kriging model.

Independent Variables in the Surrogate Model	Range of Interest
Reactor Temperature	80-220 ^oC
Mass Fraction of Ethylene	0-0.1
Mass Fraction of Comonomer	0-0.3
Mass Fraction of Hydrogen	0-0.001
Mass Fraction of Polymer	0-0.4

Table 3.3: Ranges of independent variables in the surrogate model

To test the resulting model's performance, 10 different compositions are considered to construct a test data set. For each composition, around 10 data points are generated using the ASPEN EOS model with increasing temperature, as seen in Table 3.4.

Fig. 3.2 provides a comparison of bubble point pressures from the Kriging model

Test Scenario	Ethylene mass frac.	Comonomer mass frac.	Solvent mass frac.	Hydrogen mass frac.	Polymer mass frac.	Temperature ^oC
1	0.050	0.029	0.620946	0.000054	0.3	100-220
2	0.000	0.029	0.670950	0.000050	0.3	100-270
3	0.000	0.029	0.670800	0.000200	0.3	100-260
4	0.100	0.029	0.571000	0.000000	0.3	100-170
5	0.100	0.029	0.570900	0.000100	0.3	100-170
6	0.100	0.029	0.570800	0.000200	0.3	100-170
7	0.075	0.029	0.595946	0.000054	0.3	100-200
8	0.025	0.029	0.645946	0.000054	0.3	100-250
9	0.050	0.029	0.620975	0.000025	0.3	100-220
10	0.050	0.029	0.620925	0.000075	0.3	100-230

Table 3.4: Test data for the surrogate VLE model

prediction and ASPEN model simulation for 126 test (validation) points, and demonstrates the accuracy of the surrogate model in the region of interest. Note the bubble point pressure prediction of the Kriging model is slightly higher than that from the ASPEN model, which allows a safety margin in the pressure specification. Along the reactor, we need to guarantee that the bubble point pressure is below operating pressure at two positions, one inside the reactor and the other for the feed mixture. We use two surrogate thermodynamic models for those two positions.

3.2.4 Recycle Time Delay Model

As shown in Fig. 3.1, separator units and recycle loops are included to reuse unreacted materials. The effect of recycle streams on grade transitions is not negligible and must be considered because there is no direct control of recycle flowrate in the real plant; this is determined solely by the outlet flowrate and its composition. Also, recycle loops introduce several *variable time delays* into the system. As a result, the grade transition policy depends on the current reactor conditions as well as previous outlet flows.

There are several ways to model recycle streams and time delays, including representing the variable time delay as a transportation delay in a pipe. Here, we divide

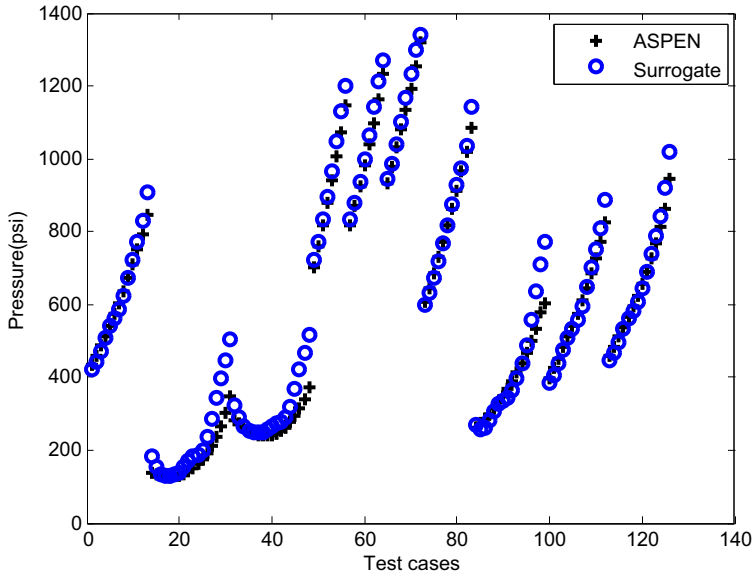

Figure 3.2: Comparison between ASPEN model and Kriging model

a pipe with total length L into N small, well-mixed segments. The resulting mass balance equation for the kth component in the ith segment is given by Eq.(3.15), where $C_i^k(t)$ is the concentration of species k in the ith segment at time t, F is the flowrate, ΔL is the length of each small pipe segment and A is the cross-section.

$$\begin{aligned} &\dot{C}_i^k(t) = (C_{i-1}^k(t) - C_i^k(t))\frac{F(t)}{A\Delta L},\ \Delta L = \frac{L}{N} \\ &k \in \{\text{ethylene, comonomer, hydrogen, solvent}\},\ i = 1, 2, \ldots, N \end{aligned} \tag{3.15}$$

The time delays in the vapor (unreacted ethylene and hydrogen) and liquid (solvent and unreacted comonomer) recycle loops are 1.05 hours and 1.5 hours, respectively. To determine an appropriate N, we performed a number of step response simulations and compared the resulting profiles for different values; N is determined when there is no further improvement in approximation accuracy. Dynamic profiles of output variables, MI and ρ are compared in Fig. 3.3 and Fig. 3.4 for various values of N. With increased N, the approximation accuracy improves and the model is capable of capturing oscillatory behaviors of MI, as can be seen in the

profiles of $N = 50$ and $N = 200$. However, the magnitude of those oscillations is relatively small compared to the overall trend of MI. Considering the increased computational demand caused by the large value of N and its negligible effect in the optimization problem, we set $N = 10$ in both recycle loops, as this balances accurate discretization with smaller problem size.

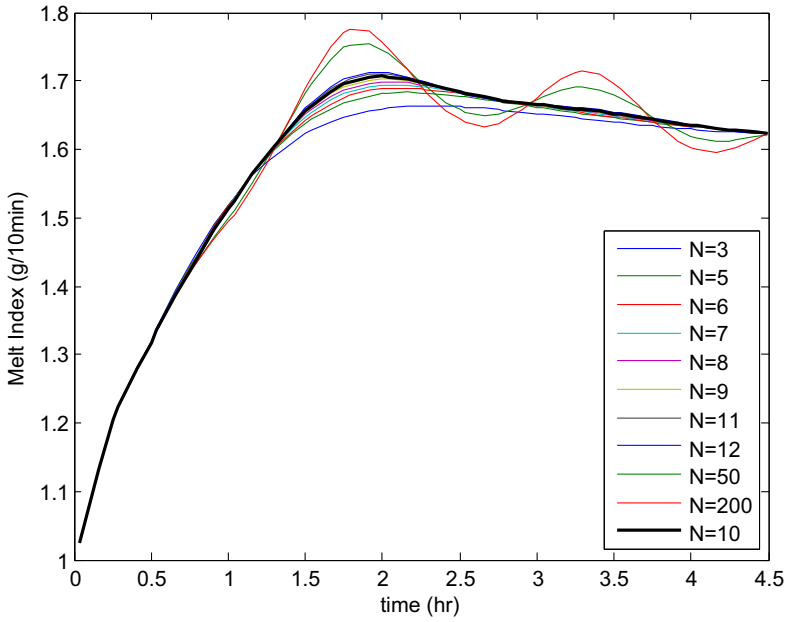

Figure 3.3: MI profiles with different number of segments used to approximate recycle delays

3.2.5 Process Constraints

In addition to the mass and heat balance equations, property correlations, the surrogate VLE model and the variable time delay model, we identify process constraints, which cover the following three aspects:

- Feasible operation: constraints on manipulated variables

  Maximum and minimum of feed flowrate and temperature of inlet cool-

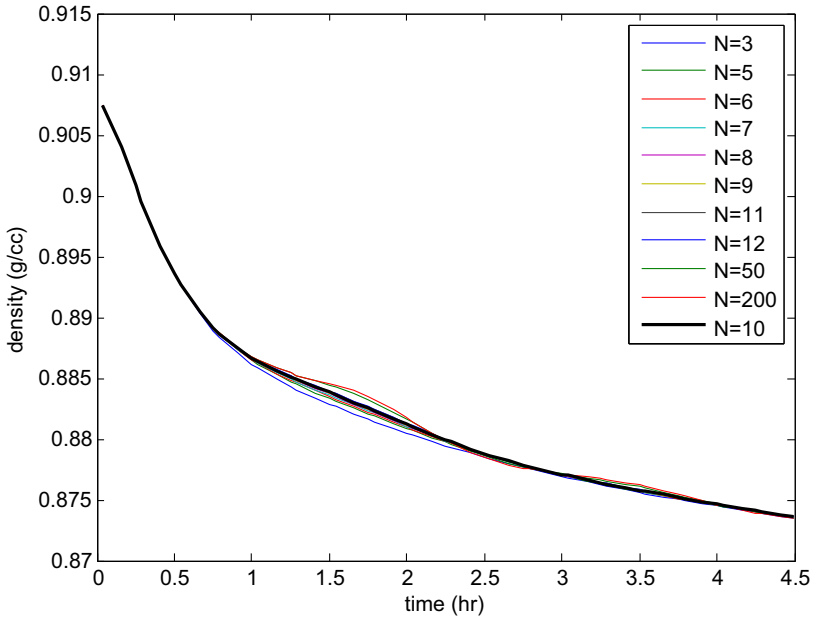

Figure 3.4: Density profiles with different number of segments used to approximate recycle delays

ing water:

$$F_{min} \leq F \leq F_{max}, \quad F \in \{F_1, F_2, F_c, F_H\} \tag{3.16a}$$

$$T^0_{j,min} \leq T^0_j \leq T^0_{j,max} \tag{3.16b}$$

- Acceptable performance: constraints on output variables

  Reactor temperature should be in a certain range:

$$T_{min} \leq T \leq T_{max} \tag{3.17}$$

MI and density should be kept within a certain range to get rid of overshooting and undershooting

$$MI_{min} \leq MI \leq MI_{max} \tag{3.18a}$$

$$\rho_{min} \leq \rho \leq \rho_{max} \tag{3.18b}$$

Production rate is maintained within a certain range near maximum capacity:

$$P_{min} \leq P \leq P_{max} \tag{3.19}$$

Critical concentration of reaction is addressed during both steady state operations and grade transitions:

$$\theta \geq \theta_{min},\ \theta \text{ is the conversion rate of ethylene} \tag{3.20}$$

- Safety considerations and process requirements

  Bubble point pressure should be controlled below operating pressure:

$$\text{Inside the reactor: } P_b \leq P_{b,max} \tag{3.21a}$$
$$\text{At the feed point: } P_{f,b} \leq P_{f,b,max} \tag{3.21b}$$

3.3 Concluding Remarks

This chapter presents a rigorous mathematical model developed for the entire flowsheet of the solution polymerization process in a loop reactor. This includes time delay models for vapor and liquid recycle streams as well as a data-driven surrogate vapor-liquid equilibrium model for monitoring the bubble point pressure. In addition, the moment model is built to bridge the gap between numerous polymer chains in the reactor and physical properties of the product.

One highlight of this work is the data-driven surrogate VLE model. Maintaining the bubble point pressure of the mixture inside the reactor and in the feed under operating pressure is of great importance in solution polymerization processes. This is enforced in our model through non-ideal VLE constraints at all points in time.

Another point we should mention is the scope of this model. Not only the individual reactor but also the recycle stream and its transport delay are considered in the model using a variable time delay model. This drives the need for longer time horizons for the grade transition, but provides more realistic solutions that match the actual process operation.

In total, the model contains 59 differential equations and 114 algebraic equations.

To prepare the model for later optimization problems, simultaneous collocation approach, which allows for detailed representation of state and control profiles, is applied to discretize the model. Applying 3-point collocation on 48 finite elements leads to a large-scale nonlinear programming problem with 157,935 variables and 159,683 constraints. More detailed optimization formulation and computational aspects will be discussed in the subsequent chapters.

Chapter 4

Optimization of Grade Transitions

Optimization of grade transitions in continuous processes is a heated topic in the past several decades. The potential value of model-based optimization of grade transitions includes great reduction in transition time as well as the off-grade production, increased flexibility in the production wheel and guided complex transitions. In this chapter, two distinct optimization formulations are considered: one is for single-value product property targets and the other goes one step further to deal with specification bands. With the detailed model developed in the last chapter and the simultaneous dynamic optimization strategy described in Chapter 2, the corresponding NLP problems for both formulations are solved for two grade transitions and the influence of regularization in the objective function is analyzed.

4.1 Single-stage Optimization Formulation

With the aim of minimizing off-grade products and transition time, we set a weighted integral error function as the objective function to minimize the transition time; this implies minimum waste of material and minimum utility consumption.

The objective function can be formulated as below:

$$min \int_{t_0}^{t_f} \parallel y(t) - y^* \parallel_Q^2 + \frac{1}{\gamma} \parallel u(t) - u^* \parallel_R^2 dt \tag{4.1}$$

where t_f is time horizon, y is a vector of algebraic state variables, which contains MI, product melt index, and ρ, product density, and u represents a vector of manipulated variables. The superscript * marks the setpoint of final grade product properties and steady-state operation conditions of manipulated variables. γ, Q and R in Eq.(4.1) are weighting factors described in Eq.(5.14) and Eq.(5.15).

$$Q = \begin{pmatrix} w_{MI}/(MI_0 - MI^*)^2 & 0 \\ 0 & w_\rho/(\rho_0 - \rho^*)^2 \end{pmatrix} \tag{4.2}$$

$$R = diag(1/(u_j^0 - u_j^*)^2) \tag{4.3}$$

The initial condition is the steady state production of a certain grade before transition, while the setpoint and reference inputs are the steady state outputs of the desired grade after transition. Constraints such as available operating ranges of manipulated variable and acceptable range of temperature are also incorporated in the dynamic optimization problem, as discussed in the previous section. The surrogate Vapor-Liquid Equilibrium (VLE) equations derived from (3.12) are used to calculate the bubble point pressure. In order to maintain the reactor and its feed in liquid phase, bubble point pressures should not exceed operating pressures at these locations.

The single-stage optimization problem is stated as follows:

$$
\begin{aligned}
min \quad & \int_{t_0}^{t_f} \parallel y(t) - y^* \parallel_Q^2 + \frac{1}{\gamma} \parallel u(t) - u^* \parallel_R^2 dt \\
s.t. \quad & \textit{Reactor model } (3.1), (3.3) \\
& \textit{Moment model } (3.7) - (3.8) \\
& \textit{Product property correlations } (3.9) - (3.11) \\
& \textit{Surrogate VLE model } (3.12) - (3.14) \\
& \textit{Recycle variable time delay model } (3.15) \\
& \textit{Process constraints } (3.16) - (3.21)
\end{aligned} \tag{4.4}
$$

The weighting factor γ and scaling matrices Q and R greatly influence the solution performance and need to be determined appropriately. In the objective function, the first term addresses the gap between current property predictions and their targets, while the second ensures that it reaches the target steady state smoothly. When this regularization term is removed, the problem becomes an ill-conditioned, singular control problem, the optimal solution is very sensitive to numerical error, and this leads to highly oscillatory profiles. As the regularization weight $1/\gamma$ increases, smoother control profiles can be observed at the expense of transition time.

To systematically determine the weighting factors, we consider the impact of Q, R and γ in two parts: i) scaling matrices Q and R based on the units and the magnitude of the variables, and ii) the regularization γ for the control terms. The selection of weights can be summarized in the following two steps, and will be further illustrated in the case studies in Section 4.

1. Q is determined to give the elements of the output vector, y (MI and ρ), equal weight. Similarly, R is chosen for the control variables, and it depends on the operating conditions of grade A and B.

2. To balance oscillatory profiles without significant loss of optimality, we plot the optimal performance with respect to γ and find the smallest value of γ where the performance remains unchanged.

4.2 Multistage Optimization Formulation

From a practical point of view, the specification of any polyethylene grade is a specified band centered at a target value with an acceptable deviation. For example, instead of a target density ρ, a grade may have a typical specification band of density $\rho \pm \Delta\rho$. This slight change from single-value target to specification band may lead to large adjustments in control policies as well as large differences in off-grade production calculation. This requires a modified dynamic optimization formulation for grade transitions. Prata *et al.* (2008) [52] considered the specification band in the integrated scheduling and dynamic optimization problem. The objective function in their work minimizes the weighted summation of total production time, raw material consumption and the amount of off-spec material produced during a transitional stage. Nystrom *et al.* (2005) [50] considered specification bands and different production modes, such as processing modes and transitional modes. The dynamic model is treated differently in different time intervals, either as a transition stage or a production stage. But their main focus is on production sequencing problem with several orders. In the work of Gisnas *et al.*[26], the specification bands are considered as a grade belt explicitly. Two objectives to minimize the transition time needed to reach the target grade band and the amount of off-grade material are compared.

In our study, we take a closer look at the impact of specification band on grade transition policies. Moreover, it is more realistic to compute off-grade production during transitions based on specification bands. Therefore, we propose a multistage optimization formulation that extends previous studies. As shown in Fig. 4.1, we divide the entire transition period into three stages: 1) Grade A in-spec, 2) off-grade and 3) Grade B in-spec. The same dynamic model is used in all stages, although different input values and constraints are required for each stage. In Stage 1 and Stage 3, lower and upper bounds of product qualities of Grade A and Grade B, re-

spectively, are invoked to ensure in-spec production in those two stages. The goal of the grade transition is to minimize a combination of the off-spec production time in Stage 2 from t_1 to t_2 and the transition time from the beginning of Stage 1, t_0, to the end of Stage 2, t_2.

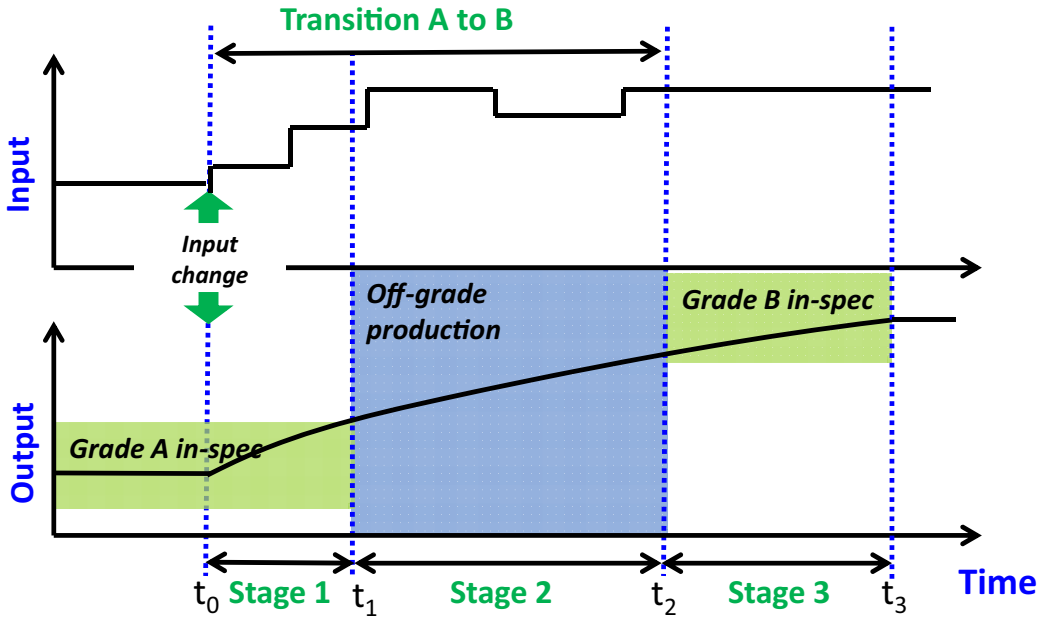

Figure 4.1: Grade transitions when specification bands are considered

Based on the analysis of the influence of specification band and the concept of multistage, we modify Eq.(4.4) to obtain the multistage optimization problem as follows.

$$
\begin{aligned}
min \quad & \alpha_t(t_2 - t_1) + \beta_t(t_1 - t_0) + \int_{t_0}^{t_f} ||y(t) - y^*||_Q^2 + \frac{1}{\gamma} ||u(t) - u^*||_R^2 \, dt \\
s.t. \quad & \textit{Reactor model } (3.1), (3.3) \\
& \textit{Moment model } (3.7) - (3.8) \\
& \textit{Product property correlations } (3.9) - (3.11) \\
& \textit{Surrogate VLE model } (3.12) - (3.14) \\
& \textit{Recycle variable time delay model } (3.15) \\
& \textit{Process constraints } (3.16) - (3.21) \\
& \textit{Property specifications in the first and the last stages} \\
& \quad MI_{A,min} \leq MI \leq MI_{A,max}, \;\; \rho_{A,min} \leq \rho \leq \rho_{A,max}, \;\; t \in [t_0, t_1] \\
& \quad MI_{B,min} \leq MI \leq MI_{B,max}, \;\; \rho_{B,min} \leq \rho \leq \rho_{B,max}, \;\; t \in [t_2, t_f]
\end{aligned}
\tag{4.5}
$$

In problem (4.5) $y(t)$ denotes output (algebraic) variables, $u(t)$ are manipulated variables and t is time. In the objective function, the terms represent the time period of producing off-spec product $(t_2 - t_1)$, initiation to the first transition $(t_1 - t_0)$ and a regularization term that promotes a smooth solution to the target steady state of the second grade, respectively. α_t, β_t, γ, Q and R are weighting factors and matrices which need to be tuned to balance these objectives, similar to the weighting factors in the single stage formulation. Following the results for γ, Q and R in single-stage formulation, we tune the weights to balance highly oscillatory (noisy) profiles without significant loss of optimality. A summary of the tuning procedure is presented in the following two steps, and details of this tuning are described in the next section.

1. Q and R are scaling matrices and fixed as in the single-stage objective function. α_t is chosen to balance $\|y(t) - y^*\|_Q^2$ and β_t is set to keep $(t_1 - t_0)$ small.

2. The regularization weight γ is needed to promote smooth solutions to the target. Similar to the tuning for single-stage objective, we plot the transition

time with respect to γ and find the smallest value of γ where the transition time remains fairly flat.

The multistage formulation can be easily extended to consider a direct minimization of off-spec material. Here we illustrate the idea by introducing a term for off-spec production in the objective.

$$\alpha_p \int_{t_1}^{t_2} P(t)dt + \beta_t(t_1 - t_0) + \int_{t_0}^{t_f} ||y(t) - y^*||_Q^2 + \frac{1}{\gamma} ||u(t) - u^*||_R^2 \, dt \tag{4.6}$$

where $P(t)$ is production rate at time t, and off-spec product is made in period $[t_1, t_2]$. Similar to the case with minimum transition time, the weights α_p, β_t and γ can be tuned systematically with fixed Q and R.

4.3 Case Study

In order to illustrate and test the idea of single-stage and multistage formulation, we optimize two transitions between two grades. The target density and melt index as well as steady state operating conditions are shown in Table 4.1.

		Meaning	Grade A	Grade B
Outputs	**MI**	*Melt index (g/10min)*	1.0	12.0
	Density	*Density (g/cm^3)*	0.908	0.864
	$\boldsymbol{\theta}$	*Ethylene conversion rate*	0.825	0.833
Scaled Manipulated Variables	$\mathbf{T_j^0}$	*Inlet cooling water temperature*	0.62	0.66
	$\mathbf{F_1}$	*Ethylene inlet flow*	0.98	0.70
	$\mathbf{F_2}$	*Comonomer inlet flow*	0.18	0.97
	$\mathbf{F_H}$	*Hydrogen inlet flow*	0.50	0.93
	$\mathbf{F_c}$	*Feed catalyst*	0.97	0.88

Table 4.1: Steady states of two grades in this study

The product density is highly dependent on the comonomer incorporation. It is easier for molecules with fewer short chain branches to fold, which leads to higher density. As we can see from the table, Grade A with a high density needs a small

amount of comonomer feed. When transitions from Grade A to Grade B are performed, there is a small initial amount of comonomer inside the reactor and the recycle loop. Increasing the comonomer feed flowrate helps the whole system achieve the Grade B target. However, transitions are expected to be slower when the density of our target grade is higher (Grade B $\rightarrow$ Grade A). The reason is that a large amount of comonomer exists in the reactor and the recycle loop at the beginning of the transition, and it takes more time for the process to digest and to remove comonomers from the reactor and recycle. To demonstrate the difference between these two cases, we perform two transitions in opposite directions. In each case, both single-stage and multistage problems are solved and the resulting profiles are compared.

Time (hour)	Description	Number of finite element (nfe)	Element length (hour)
$[0, 5]$	steady state simulation	10	0.5
$(5, 25]$	grade transition on fine grid	40	0.5
$(25, 35]$	continued grade transition	2	5
$(35, 65]$	continued grade transition	2	15
$(65, 125]$	continued grade transition	2	30
$(125, 225]$	continued grade transition	2	50

Table 4.2: Initial setting of the entire horizon and element lengths

As discussed in the model development section, the grade transition problem in the case study considers not only the individual reactor, but also the dynamic optimization of the entire plant with liquid and vapor recycles. This requires longer time horizons for the grade transition. In the following case studies, the first 5 hours of the horizon are used as steady state simulation for the current grade, and the transition is set to start at $t_0 = 5$ hours. Most of the transitions in control and output responses happen within 20 hours. For this period, we have verified that a discretization with 40 elements is accurate. After the first 25 hours (5-hour steady state production and 20-hour transition), a coarser discretization grid with 8 elements over 200 hours is considered to ensure the steady state. The initial setting

of the entire horizon and element lengths is summarized in Table 4.2. Moreover, this mesh was validated for sufficiently high accuracy with additional simulations of the DAE system.

	# of Var.	# of Con.	CPU (s)	Weights					
				α_p	α_t	β_t	γ	w_{MI}	w_ρ
single-stage	157598	158881	666.7	-	-	-	20	10	100
Min-time	157935	159683	169.0*	-	30	15	20	10	100
Min-off-spec	157935	159683	101.7*	0.1	-	15	20	10	100

Table 4.3: A→B: Optimization statistics for transition to low density. Multistage optimization problem is initialized with single stage solution. Min-time for the minimum transition time objective (4.5), and Min-off-spec for the minimum off-spec production objective (4.6).

	# of Var.	# of Con.	CPU (s)	Weights					
				α_p	α_t	β_t	γ	w_{MI}	w_ρ
single-stage	157598	158881	540.4	-	-	-	20	200	100
Min-time	157935	159683	269.0*	-	40	20	3.33	200	100
Min-off-spec	157935	159683	96.3*	0.01	-	20	3.33	200	100

Table 4.4: B→A: Optimization statistics for transition to high density. Multistage optimization problem is initialized with single stage solution. Min-time for the minimum transition time objective (4.5), and Min-off-spec for the minimum off-spec production objective (4.6).

Application of 3-point collocation on 48 finite elements over 220 hours, excluding the first 5-hour steady state simulation part, results in a nonlinear programming problem with more than 150,000 variables and equations, as stated in Table 4.3 and Table 4.4. The resulting NLP problems are solved with nonlinear optimization solver CONOPT in the General Algebraic Modeling System (GAMS) [9] (similar CPU times are also obtained with IPOPT). Also shown are the values of weighting factors in the objective function to balance transition time, off-grade and smooth profiles. A detailed discussion of the selection of the weighting factors is presented as follows.

4.3.1 Grade Transition to Low Density: A→B

Determination of weighting factors in the objective function

In both single-stage and multistage formulations, there are several weighting factors in the objective function that need to be tuned. To better understand the mechanism of tuning weighting factors, a step-by-step procedure is presented below with detailed analysis and illustrative graphs.

1. To select the scaling matrices Q and R we balance w_{MI} and w_ρ in (5.14) such that two curves can reach the target at the same time. Resulting dynamic behavior of MI and ρ indicates $w_{MI} = 10$ and $w_\rho = 100$.

2. For single-stage objective, we keep w_{MI} and w_ρ constant to choose the regularization weight γ. A plot of transition time with respect to γ is shown in Fig. 4.2 and the smallest value of γ where the objective remains fairly constant is found to balance oscillatory profiles without significant loss of optimality.

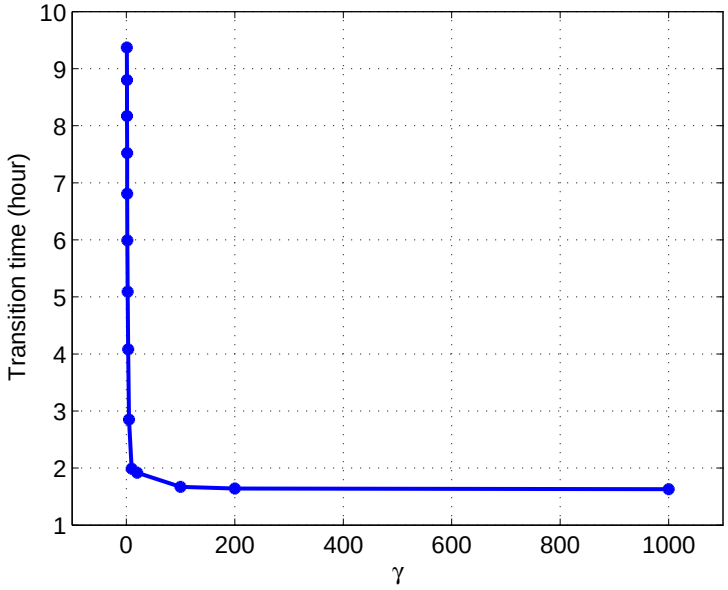

Figure 4.2: A→B: Influence of γ on transition time in single-stage problem

As γ decreases, more emphasis is placed on smooth control profiles instead of the actual objective and thus the transition time increases. When larger γ is used, transition time becomes shorter, and the reduction of transition time is negligible when γ increases from 200 to 1000. The single-stage optimal solutions with $\gamma = 1000, 200, 100, 20$ are shown in Fig. 4.4, Fig. 4.5 and Fig. 4.3.

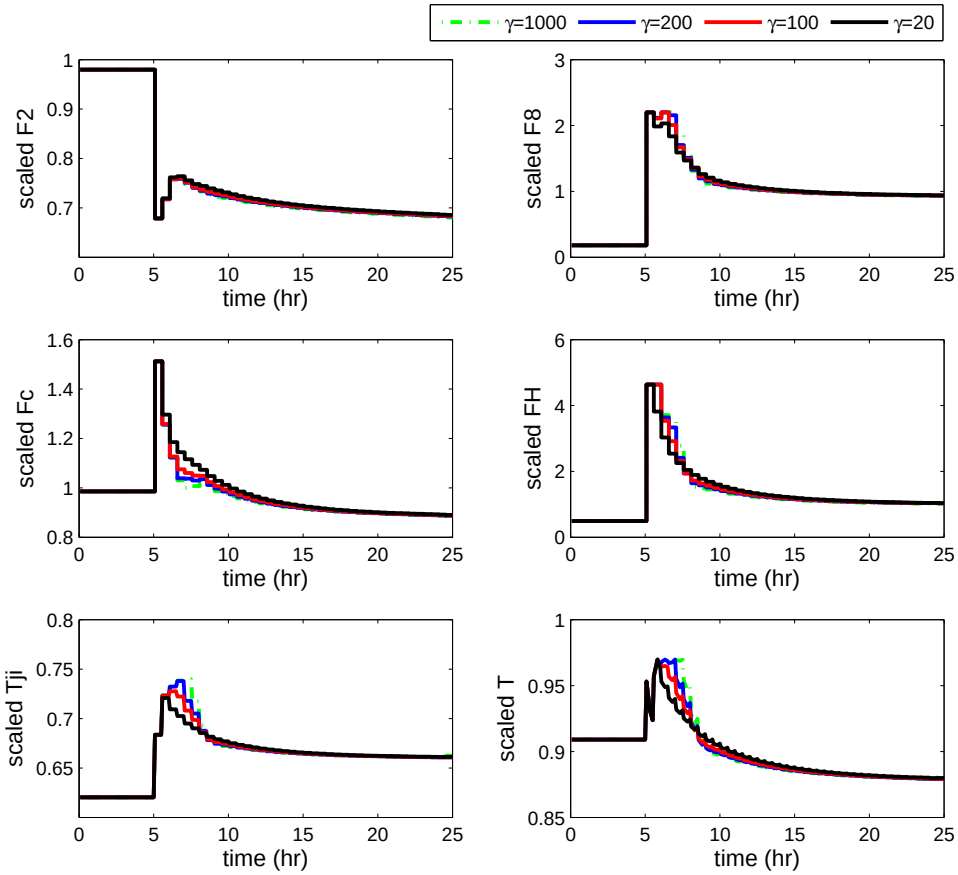

Figure 4.3: A→B: Single-stage optimal control and temperature profiles with varying γ

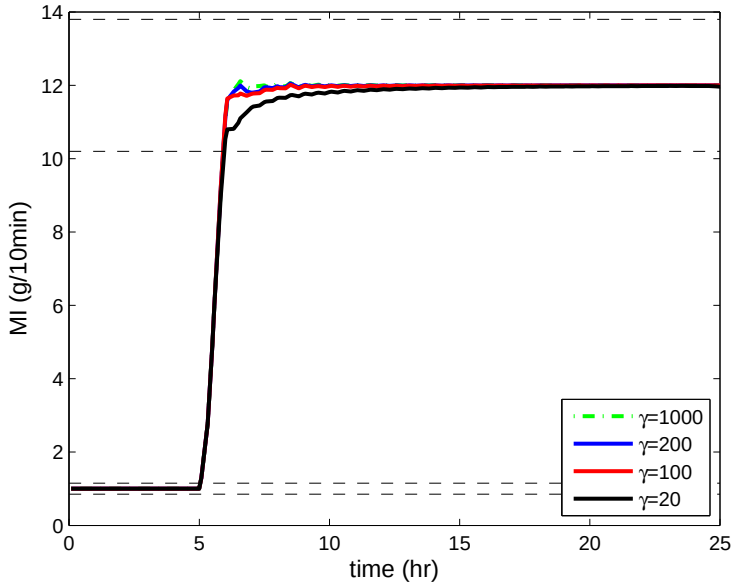

Figure 4.4: A→B: Single-stage optimal MI profiles with varying γ

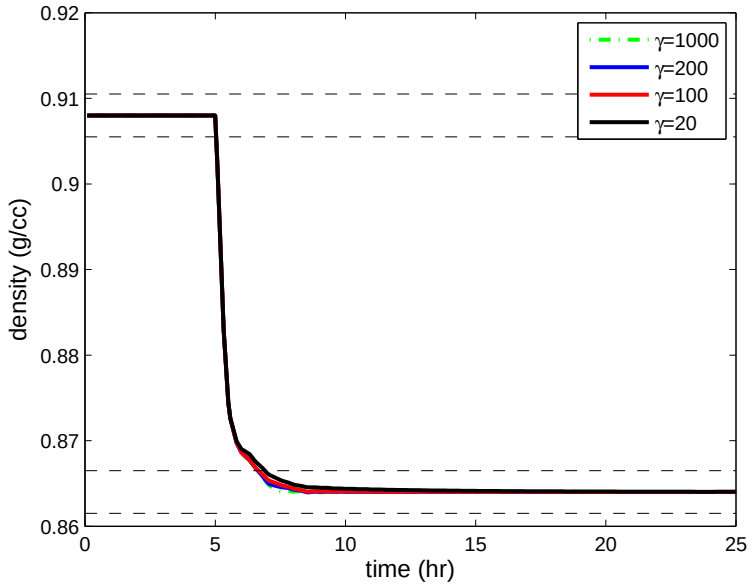

Figure 4.5: A→B: Single-stage optimal density profiles with varying γ

To balance oscillatory profiles and loss of optimality, $\gamma = 20$ is chosen based on the previous analysis.

3. For multistage formulation, we also vary γ, once α_t, β_t, Q and R have been fixed as scale factors. As seen in Table 4.3 the same values of Q and R are used here as in the single-stage case.

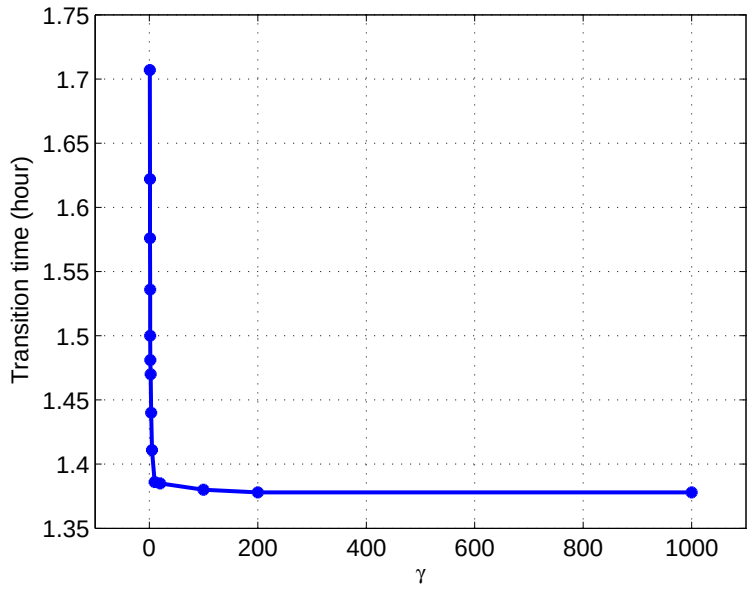

Figure 4.6: A→B: Influence of γ on transition time in multistage problem

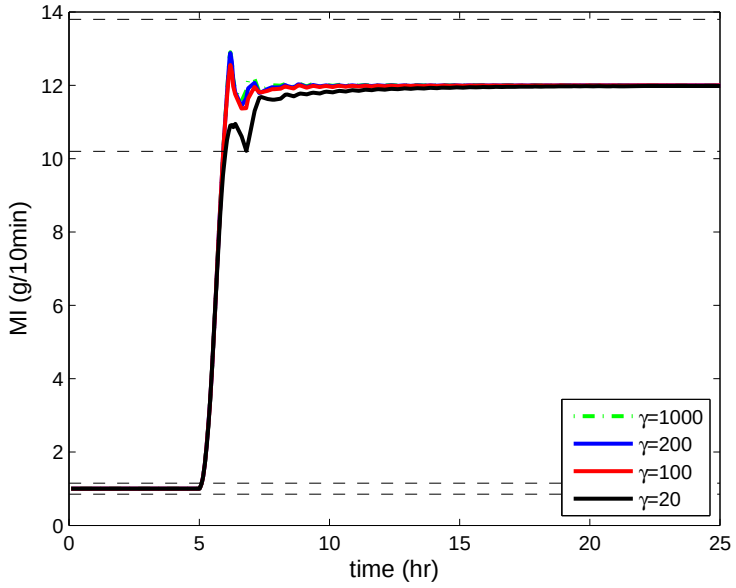

Figure 4.7: A→B: Multistage optimal MI profiles with varying γ

From Fig.4.6, the decrease of transition time with the increase of γ can be seen clearly. And the multistage solutions with $\gamma = 1000, 200, 100, 20$ are shown in Figures 4.7 to 4.9. To balance oscillatory profiles and optimality, γ is set to 20.

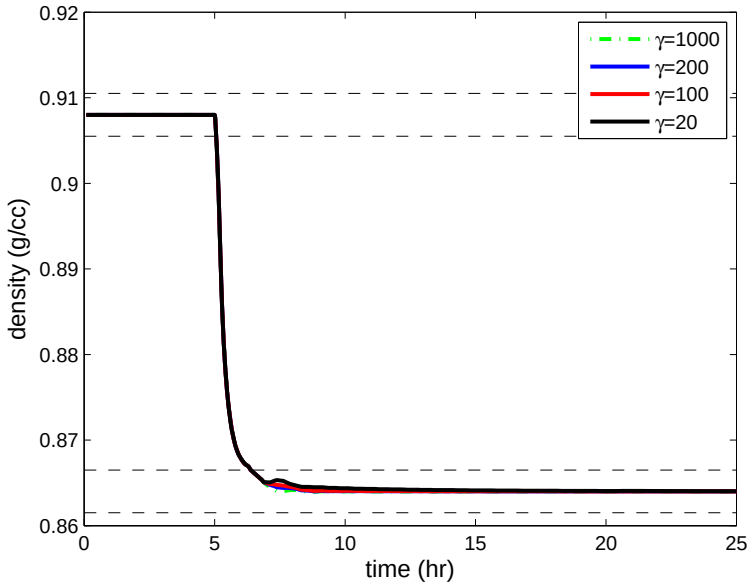

Figure 4.8: A→B: Multistage optimal density profiles with varying γ

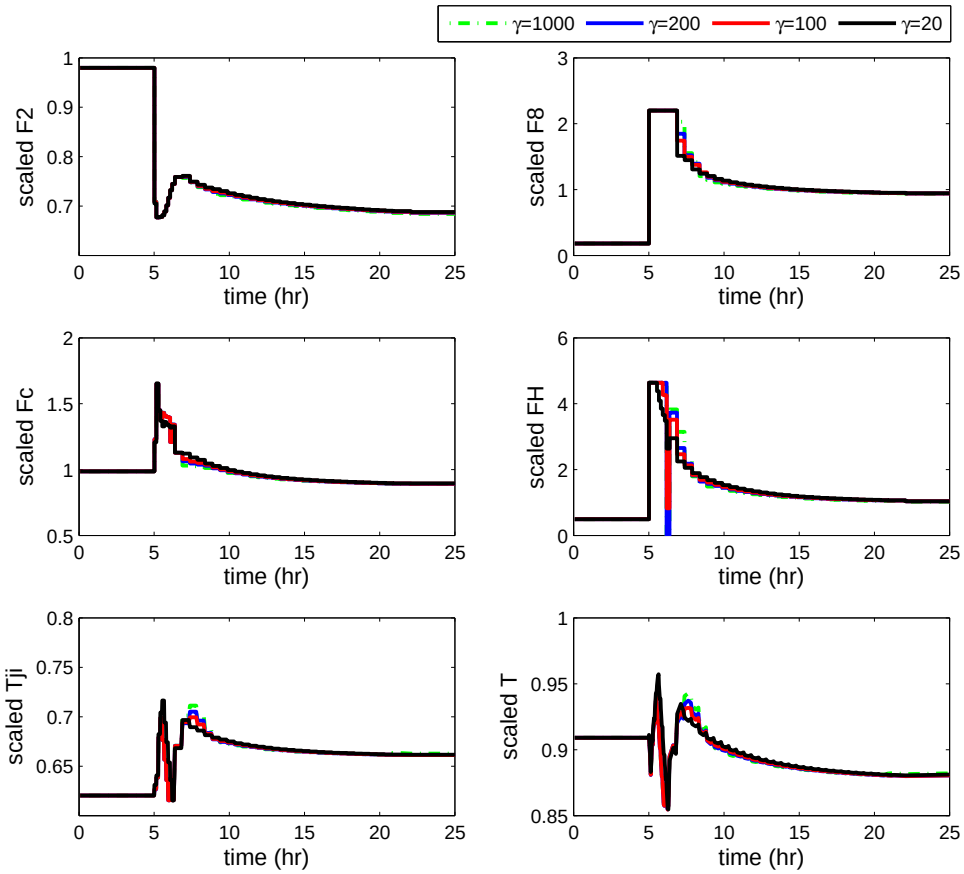

Figure 4.9: A→B: Multistage optimal control and temperature profiles with varying γ

Results and discussion

With the weighting factors chosen based on the tuning results, we compare four different grade transition policies for this particular transition: 1) step response, 2)single-stage formulation, 3)multistage with minimum transition time and 4) multistage with minimum off-spec production.

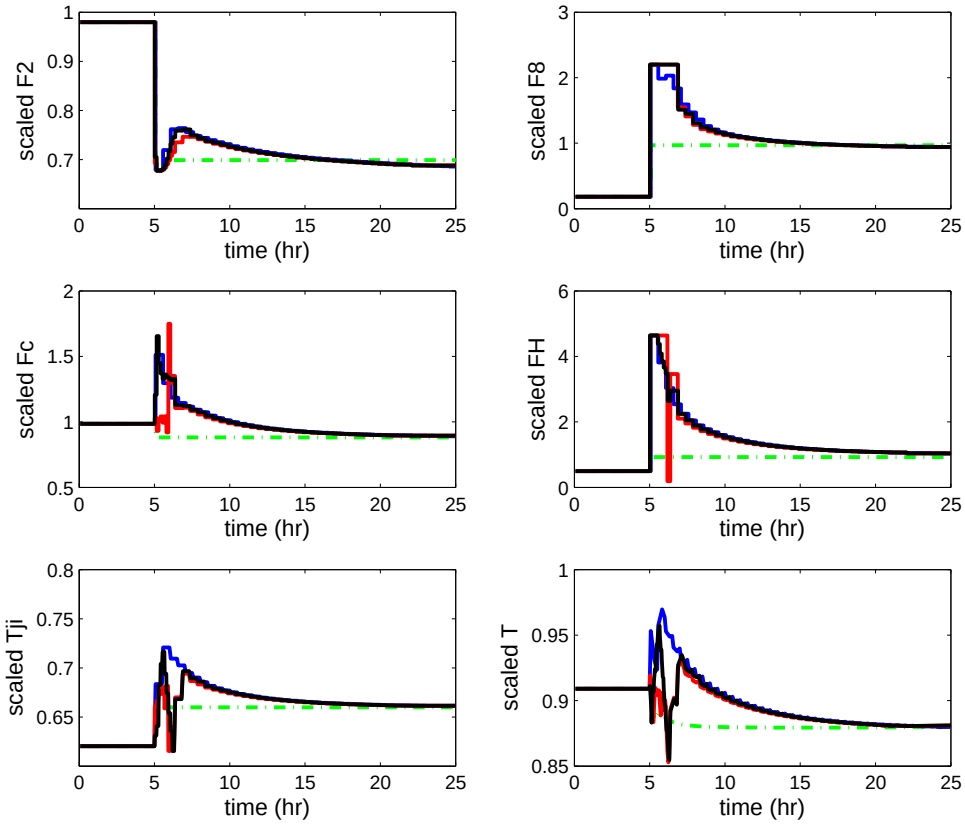

Figure 4.10: A→B: Optimization result of manipulated variables and reactor temperature with a green dashed-dotted curve for step response and solid blue curve for single-stage problem (4.4). The multistage solutions are represented by solid red curves for minimum off-spec production (4.6) and solid black curve for minimum transition time (4.5).

The resulting optimal control profiles, as well as the reactor temperature profile, for transition from a high density to low density are shown in Fig. 4.10, starting at t = 5. The multistage solution curves have different durations for each stage, and the control policy obtained from multistage formulation is more aggressive, leading to a shorter transition time. The optimal control trajectories also provide the following valuable guidelines for facilitating grade transitions under process constraints.

- A large amount of comonomer is injected into the reactor to increase the degree of incorporation of comonomer in polymer chains at the beginning. Then the comonomer feed flowrate decreases because an adequate amount of comonomer becomes available from the liquid recycle.
- More catalyst is needed in the first hour to speed up the reactions.
- The feed hydrogen flowrate increases to achieve shorter polymer chains, which leads to higher MI.

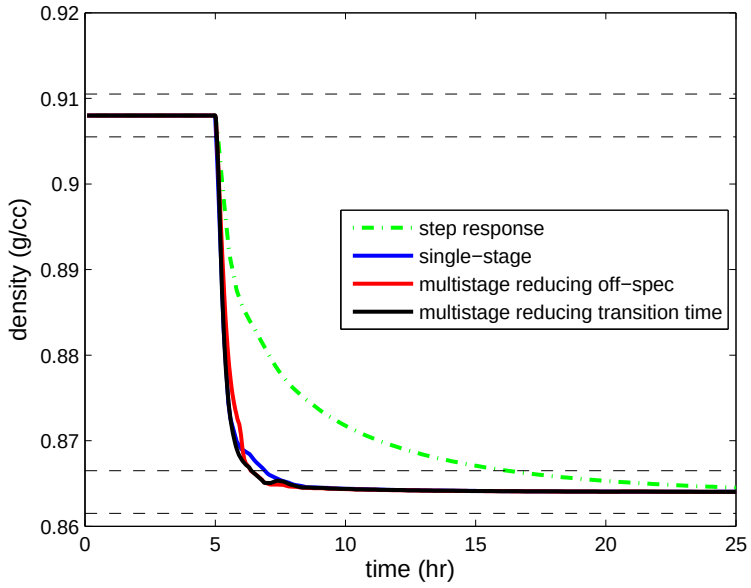

Figure 4.11: A→B: Comparison of density profiles

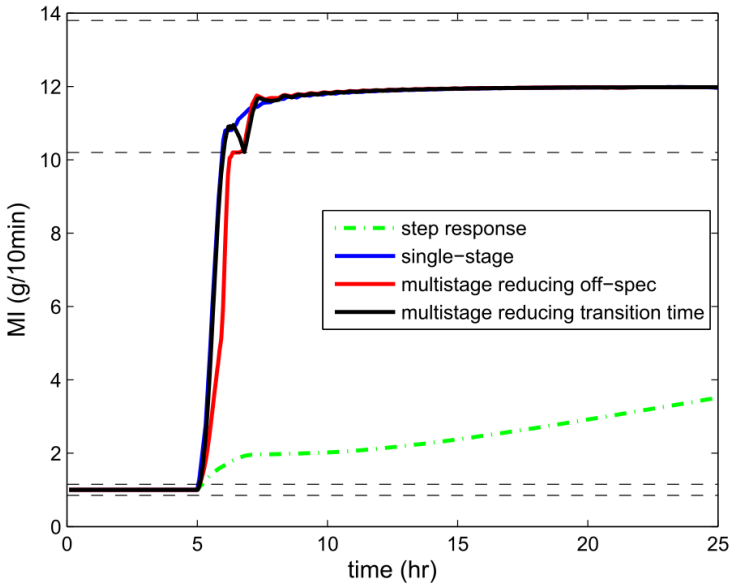

Figure 4.12: A→B: Comparison of MI profiles

The profiles of density and MI are shown in Fig. 4.11 and Fig. 4.12 with the product property specification bands marked by horizontal dotted lines. Note that multistage optimization provides much improved transition policies. As seen from the density profile, for example, the multistage solution quickly leaves the first specification band and performs a fast transition to the boundary of the second band. In this way, the duration of the second (out-of-spec) stage is minimized. Also, for the MI profile there are some oscillations in the multistage solution within the target specification band, but all the product within the band is in specification.

Transition A→B	Transition time (hr)	Stage 1 duration (hr)	Stage 2 duration (hr)	Off-spec production
Step response	>20	0.18	>20	>8.96
Single-stage	1.91	0.04	1.87	1.00
Min-off-spec	1.31	0.10	1.21	0.61
Min-time	1.28	0.10	1.18	0.65

Table 4.5: A→B: Comparison of step response, single-stage and multistage solutions for transition to low density. Off-spec production is scaled by single-stage solution.

In Fig. 4.11, Stage 3 of the multistage solution begins at $t_2 = 6.36$ hrs., while the single-stage solution reaches the boundary of the target band at $t_2 = 6.91$ hrs. On the other hand, Stage 2 begins at almost the same time for both solutions. Similarly, we can obtain the statistics for MI profiles in Fig. 4.12. The total transition times and the durations of Stage 2 are shown in Table 4.5.

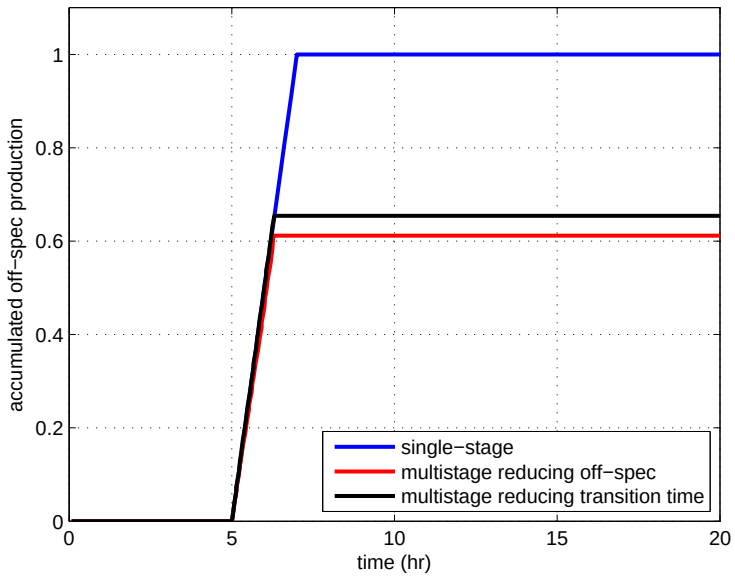

Figure 4.13: A→B: Comparison of accumulated off-spec production

For both single-stage and multistage formulations, minimum transition time is considered and the solutions suggest an increased production rate during transition. In contrast, the modified formulation (4.6) directly minimizes off-spec production and indicates a lower production rate during transition. Based on those solutions, we plot the accumulated off-spec production in Fig.4.13. Compared to the single-stage formulation, the multistage one achieves more than 30% reduction in both transition time and off-spec production. Note that the multistage formulations significantly outperform the single stage formulation, and are capable to directly reduce the amount of off-grade product as well as the transition time.

4.3.2 Grade Transition to High Density: B→A

Similar to the transition to low density, the transition to high density is optimized using single-stage and multistage formulations. Model information and optimization statistics are listed in Table 4.4.

Determination of weighting factors in the objective function

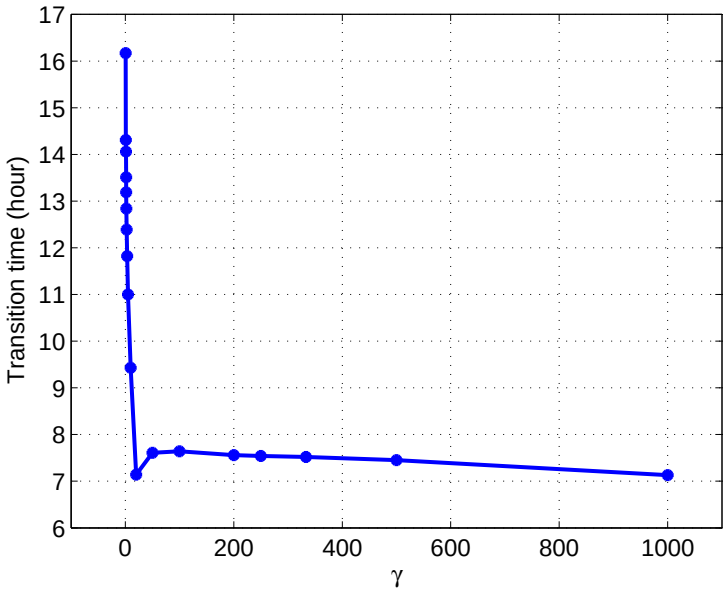

Figure 4.14: B→A: Influence of γ on transition time in single-stage problem

As discussed in the transition from A to B, the scaling matrices are determined first to balance the dynamics for the outputs, MI and ρ. Next, in the single-stage optimization problem, we vary the weight on the regularization term, γ, to balance oscillatory profiles and loss of optimality. The influence of varying γ on transition time is shown in Fig. 4.14, and $\gamma = 20$ is chosen because it leads to smoother control profiles without the loss of optimality, compared to the other cases with similar transition times.

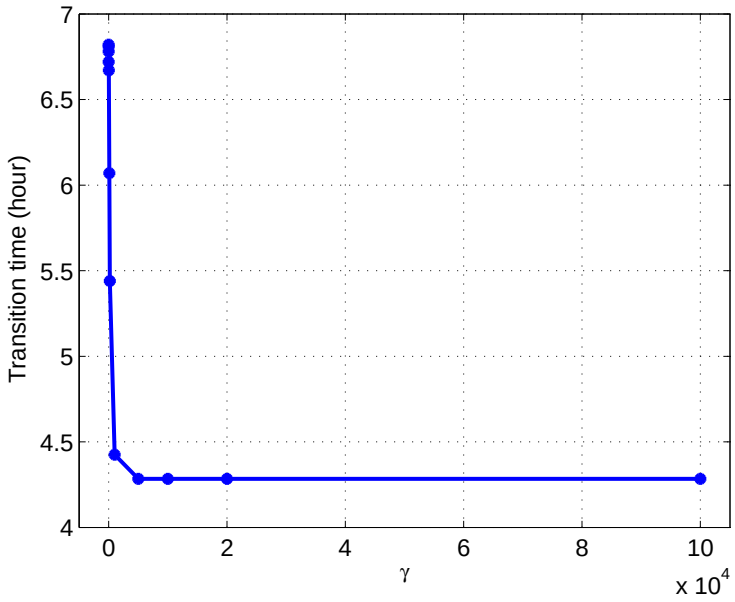

Figure 4.15: B→A: Influence of γ on transition time in multistage problem

In multistage optimization, we follow the same tuning procedure as discussed in the other case. We first fix α_t, β_t and α_p and then vary γ for the regularization term. Fig. 4.15 provides a guideline for selecting γ. One candidate solution is located around the kink at $\gamma = 5000$ and 4.3 hrs, and it yields highly oscillatory control profiles with short transition time. However, these oscillatory profiles may be hard to implement in the real plant. At the expense of transition time, we search along the curve and reach another solution at $\gamma = 3.33$ and 6.8 hrs., which leads to much smoother control profiles. A comparison between those two candidate solutions can be found in Fig. 4.16, Fig. 4.17 and Fig. 4.18.

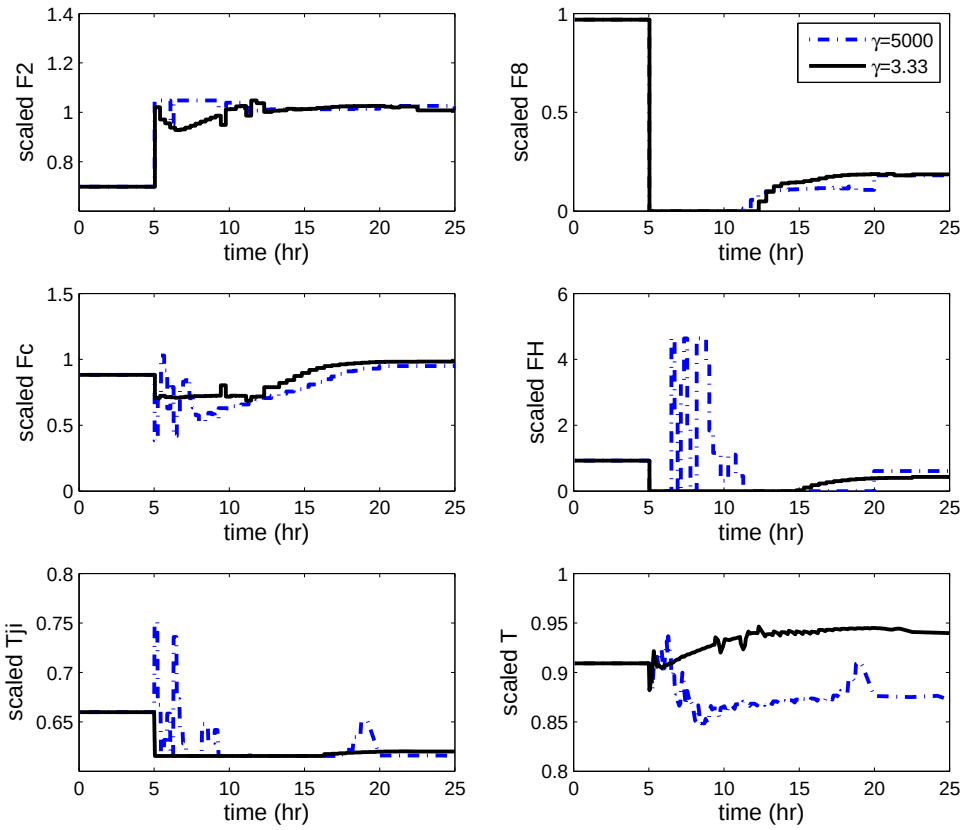

Figure 4.16: B→A: Optimization results of two candidate solutions

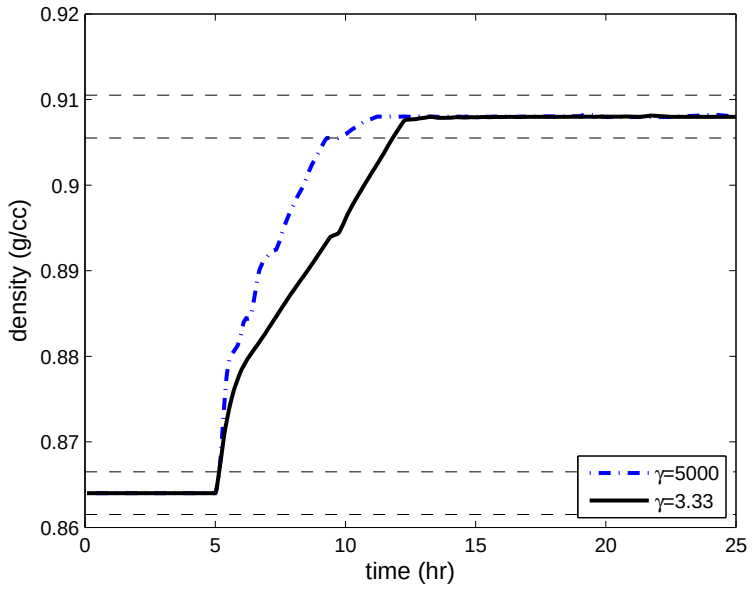

Figure 4.17: B→A: Comparison of density profiles obtained from two candidate solutions

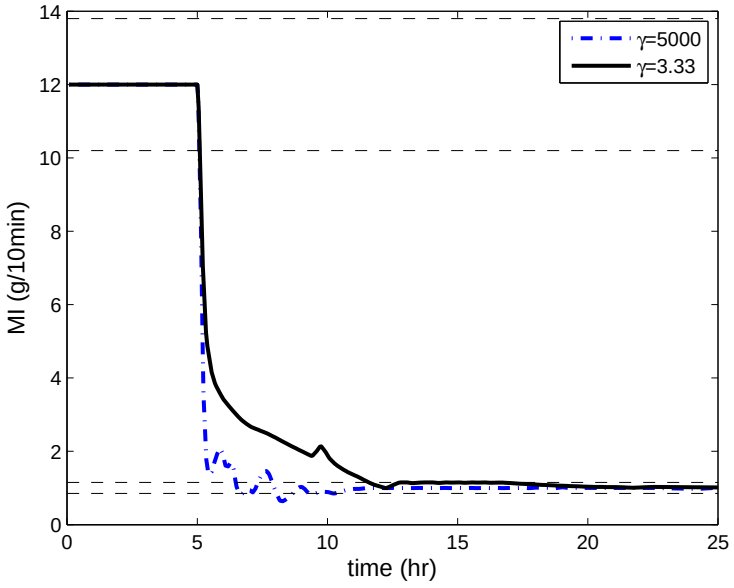

Figure 4.18: B→A: Comparison of MI profiles obtained from two candidate solutions

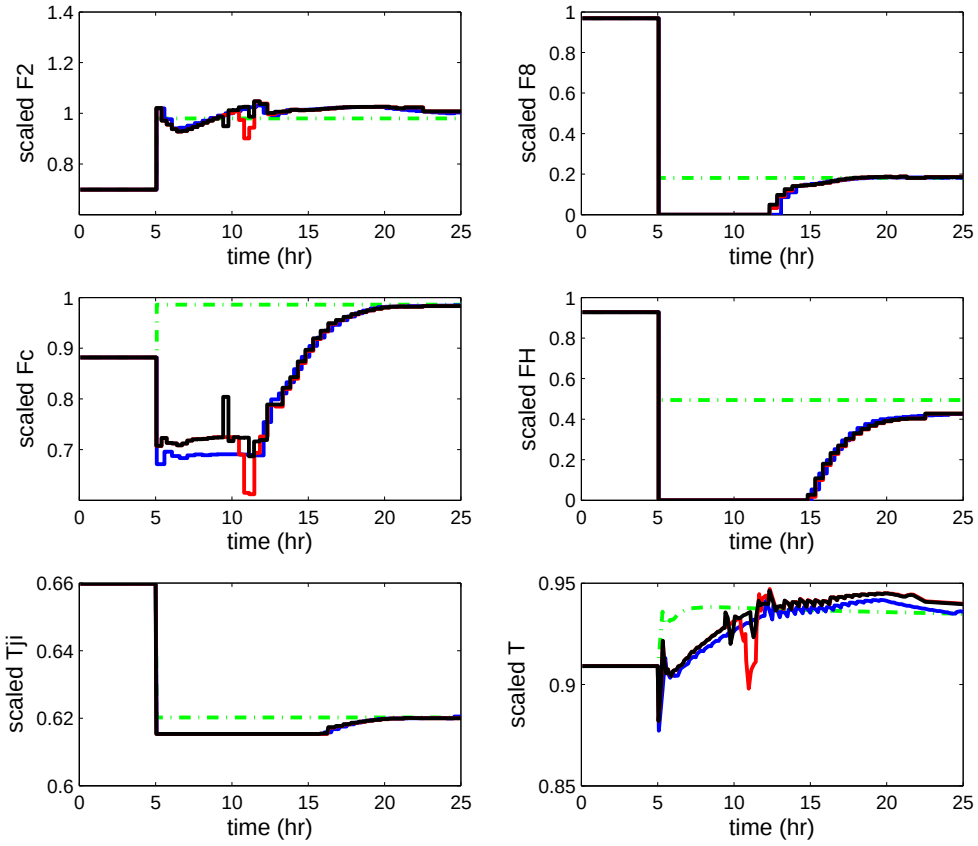

Figure 4.19: B→A: Optimization result of manipulated variables and reactor temperature with a green dashed-dotted curve for step response and solid blue curve for single-stage problem (4.4). The multistage solutions are represented by solid red curves for minimum off-spec production (4.6) and solid black curve for minimum transition time (4.5)

Results and discussion

For the final comparison, we choose $\gamma = 20$ in single-stage formulation and $\gamma = 3.33$ in the multistage objective. A summary of all the weights is presented in Table 4.4. Fig. 4.19 shows the controls and the reactor temperature profiles. While the single-stage policy is smooth and exhibits gradual changes of inputs to their target, more aggressive controls can be found in the input profiles of the multistage solutions.

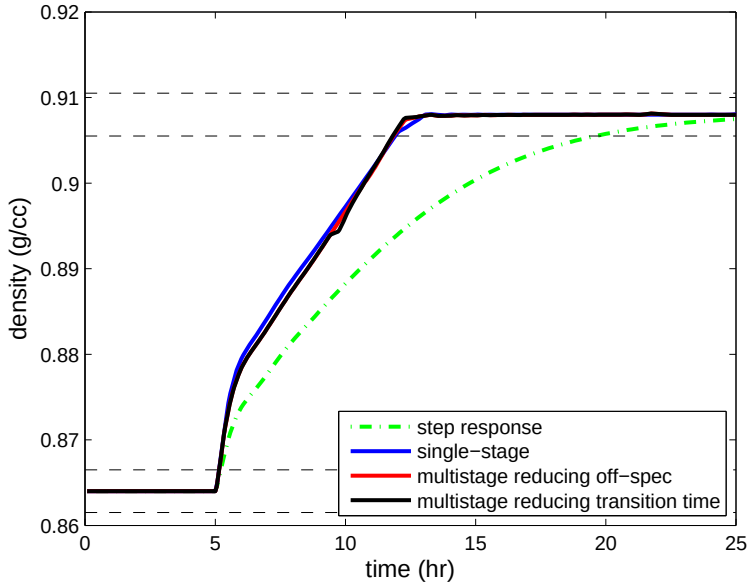

Figure 4.20: B→A: Comparison of density profiles

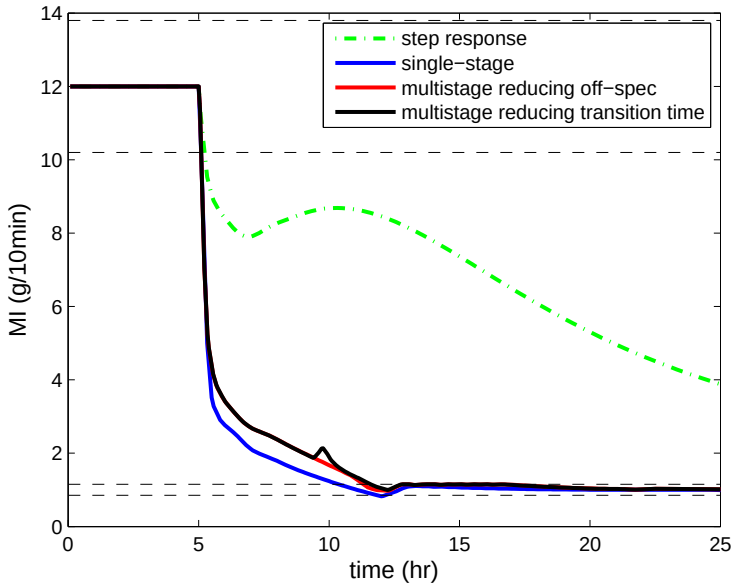

Figure 4.21: B→A: Comparison of MI profiles

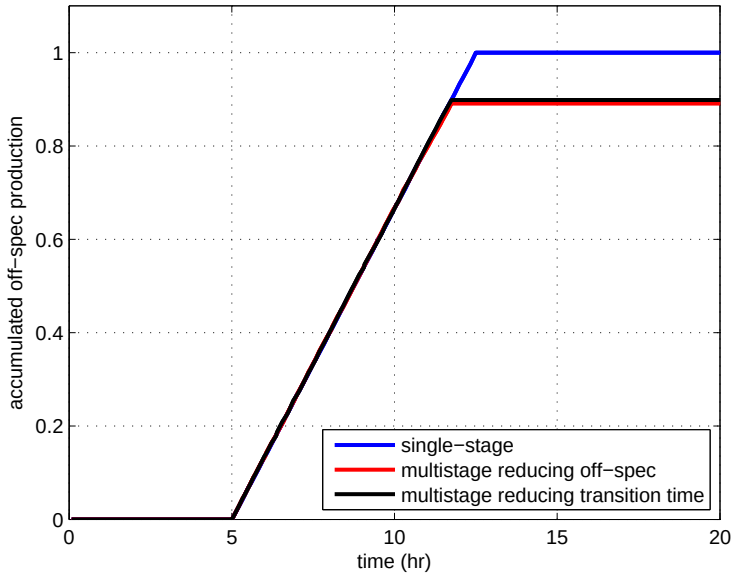

Figure 4.22: B→A: Comparison of accumulated off-spec production

The performance for optimal transition to high density product is shown in Fig. 4.20 and Fig. 4.21, and the transition times, the off-spec production and the durations of Stage 1 and Stage 2 are listed in Table 4.6. The accumulated off-spec production is shown as well in Fig. 4.22. Based on those figures, it can be seen that the single-stage solution greatly reduces the transition time and the amount of off-grade, compared to step response. Moreover, the multistage formulation further reduces the transition time and the off-spec production by about 10%. According to the previous discussion on the selection of γ, it is clear that multistage formulation has the potential to further cut the transition time and off-spec product at the expense of some oscillatory control profiles. We also observe that transitions to a higher density take much more time than transitions to lower density, no matter which formulation is used. This is in accordance with our previous discussion on the presence of comonomers during the transition.

Transition B→A	Transition time (hr)	Stage 1 duration (hr)	Stage 2 duration (hr)	Off-spec production
Step response	>20	0.22	>20	>2.03
Single-stage	7.14	0.14	7.00	1
Min-off-spec	6.84	0.10	6.74	0.89
Min-time	6.82	0.10	6.72	0.89

Table 4.6: B→A: Comparison of step response, single-stage and multistage solutions for transition to high density. Off-spec production is scaled by single-stage solution.

4.4 Concluding Remarks

To minimize transition time and off-spec production, two formulations are considered to deal with single value targets (single-stage formulation) as well as specification bands (multistage formulation). Product specification bands are carefully considered in the proposed multistage formulation within a compact nonlinear programming formulation. This enables the explicit minimization of transition times, off-spec production times and off-spec production. Moreover, this multistage formulation exploits the simultaneous dynamic optimization approach, and provides an efficient formulation that extends from single stage to multistage dynamic optimization problems. The results of two transition case studies demonstrate the effectiveness of the multistage formulation, which has the ability to directly minimize transition time and off-spec product, and achieves a significant improvement over single-stage solutions.

In addition, in both single-stage and multistage objectives, we incorporate the idea of regularization. Given the singular nature of the grade transition problem when the regularization term is removed, systematically tuning the weighting factors is necessary. By changing the regularization factors, a trade-off between short transition time and smooth control profiles to steady state is made. In this study, detailed evaluation of tuning parameters and a thorough numerical comparison are provided for the resulting dynamic optimizations, thus demonstrating significant

improvements of the multistage strategy.

Future work will be devoted to optimization of grade transitions under uncertainties, both for off-line analysis and on-line operation. Moreover, these formulations for pairwise grade transition can easily be extended to production scheduling with multiple grades over a product wheel. For this case, integrated production scheduling can be addressed through the formulation of mixed-integer dynamic optimization (MIDO) problems, the inclusion of binary decision variables, and supported by the solution of MILP subproblems[50, 52, 67, 69].

Chapter 5

Optimization under Uncertainty

The offline dynamic optimization in Chapter 4 is capable of effectively handling grade transition problems, but its performance can deteriorate in the presence of uncertainties. In order to assess the impact of uncertainty and generate transition policies that work in different scenarios, robust optimization strategies for grade transitions need to be considered. In this chapter, we review related optimization strategies and then formulate the optimization problem with back-off constraints obtained from Monte Carlo simulation. A set of case studies is presented to show the effectiveness of the proposed approach.

5.1 Problem Statement

The success of model-based control and optimization strategies highly rely on model accuracy. In order to obtain reliable, realistic solutions, models used in optimization problems need to be accurate and representative of the actual process. In addition, any model mismatch, either structural imperfection, model simplification or parameter uncertainty, may lead to infeasible solutions or unsafe control actions in the actual plant. In our previous work [64], optimal grade transition policies

of a realistic industrial LLDPE process were considered. A large-scale mathematical model that captures the dynamic behaviors of solution polymerization process carried out in a CSTR is developed for optimization purposes. In addition to mass and heat balance equations, the model uses the molecular weight moment model for the prediction of product properties and incorporates a simple, yet accurate, vapor-liquid equilibrium (VLE) model derived from rigorous calculations. The model also includes the recycle loop, whose time delays are modeled through variable transportation delay model.

Two optimization formulations, single stage and multistage, were developed to deal with single-value specification and specification bands of product properties, respectively. The results obtained using simultaneous dynamic optimization demonstrate significant improvement in transition times and off-grade production, compared with the baseline performance. In addition, the multistage formulation is shown to outperform the single stage formulation as the former led to more aggressive control profiles and allowed oscillations within the specification bands.

The previous work on offline dynamic optimization demonstrates the potential in dealing with grade transition problems; however the performance of the optimized transition policy can deteriorate in the presence of uncertainties. Optimal solutions obtained at nominal uncertainty level may become non-optimal, or even infeasible, and the safety constraint might be violated under uncertainty.

Uncertainties come from different sources, such as uncertain model parameters, disturbances, noises, unmeasured variables and measurement errors. Usually, the uncertainty can be classified as time-invariant and time-varying uncertainty. On the other hand, it can also be categorized into two types as in [39]: those that are random and never resolved and those that are resolved at a later time.

Several approaches have been proposed to handle uncertainties in the optimization problem [2, 38, 46, 84]. Depending on whether measurements are utilized, the ap-

proaches can be grouped into two categories: robust optimization and measurement-based optimization [65, 66]. In terms of problem formulation, either compact problem formulations with modifications on the constraint (back-off constraints) or multi-scenario formulation with each scenario corresponding to one discretized uncertainty level is adopted.

In order to assess the impact of uncertainties in the grade transition problem, different transitions under various uncertainty levels are performed and robust optimization strategies for grade transitions are taken into account to obtain optimal policies that can be applied to systems with different uncertainty levels. In this work, back-off constraints calculated from Monte Carlo simulations are incorporated in the optimization problem. The resulting solution is shown to be robust under various uncertainty levels.

5.2 Literature Review

The *traditional robust optimization approach* aims at optimal solutions that give the best performance in the absence of measurement. The performance metric of the robust objective function is usually based on expectation, weighted mean-variance or worst-case scenario. One main factor that distinguishes robust optimization from other strategies is the lack of recourse variables. Typically robust optimization does not take reactive actions into account, and thus makes the optimal solution conservative. A bilevel minmax problem is a typical formulation of robust optimization, in which the lower level problem seeks the worst scenario and the upper level one optimizes over the worst case. Since the worst case usually has a low probability of occurring, the robust solution is often conservative and its performance is largely sacrificed when the nominal or the most probable uncertainty level is realized.

In this approach, identifying and quantifying the worst case is crucial. Researchers

working on this approach seek constraint feasibility despite uncertainty by modifying the original constraints with back-off terms (or margins). These back-off terms tighten the constraint and shrink the feasible region of the optimization problem to such a level that variations of the constraints in the worst case can still be handled and thus the feasibility ensured.

Visser *et al.* considered the end-point optimization of a nonlinear, control affine batch process under parametric uncertainties and disturbances [71]. In order to handle uncertainties, back-off terms are introduced into the original constraints and the size of those back-off terms is determined using the linearization of the constraints and the linear time-varying state space model of the original optimization problem. Diehl *et al.* proposed an approximation technique based on first order derivatives of the constraints in robust nonlinear optimization problem [17]. Similar to the work of Visser *et al.*, the worst case is approximated by linearization of the lower level problem and the resulting dual norms are used to represent the back-off terms (or penalty terms as named in the paper). Besides those analytical solutions to the linearized problem, another iterative procedure is mentioned in [65], where the back-off terms are first initialized using an initial guess, and the optimization problem with the current back-offs is solved. The back-offs are then updated using the probability density function of the states computed at the optimal solution. The back-off strategy is also shown to be effective in model-based experiment design under parametric uncertainty. As discussed in [24], suitable back-offs are calculated from the prediction of system responses for the given parameter distribution, and then these back-offs are used in the experiment design problem to ensure both feasibility and optimality of the planned experiment.

The back-off terms are shown to ensure constraint feasibility despite uncertainty effectively. However, the current derivation of back-off terms can be difficult to implement for large scale optimization problems due to problem complexity. Besides, the derivation relies heavily on the first-order approximation of the optimization

problem. This may result in inaccurate back-offs since only *linearized* worst-case feasibility is guaranteed.

On the other hand, *stochastic programming* assumes that the probability distribution of the uncertain parameter can be estimated and it takes advantage of the probability information to optimize the expected performance. Moreover, measurement is utilized and recourse variables are introduced to increase the flexibility of the optimal trajectory. Once the uncertainty is realized in the first stage, its effect is observed and evaluated such that reactive actions tailored to different uncertainty levels can be applied. The solution of stochastic programming problem is less conservative compared to the robust solution. However, its problem size always increases significantly as the probability distribution or multiple scenarios are needed.

Ruppen *et al.* utilized the discrete probability distribution of the uncertain parameters and formulated the problem using several parallel model descriptions with distinct uncertainty realizations [61]. Over the last couple of years, the idea has been extended to reformulate economic nonlinear model predictive control (economic NMPC) problems. In the work of Lucia *et al.*[43, 44], the evolution of uncertainty is represented as a scenario tree and multi-stage NMPC problem is formulated accordingly. Although those extensions and their applications successfully demonstrate its effectiveness in handling uncertainties, increased problem size and heavy computational burden are always the bottlenecks of this approach to large-scale applications.

In summary, the robust optimization approach typically has a compact problem form and additional variables or equations are not required, while the stochastic programming approach usually considers multiple scenarios and requires advanced computational capability to handle large scale problems. Given that the grade transition problem of polyethylene solution polymerization process is already large scale and complex, it is hard to solve such multi-scenario stochastic

programming problems in reasonable time using available optimizers and processors. Instead, modifying the original constraints with back-offs would be a more practical choice. In our study, we adopt the concept of robust optimization and use Monte Carlo simulation to calculate the size of back-off terms. A detailed description of the procedure and its application is the main focus of this chapter.

5.3 Concept of Back-off Constraints

As we discussed in the first section, there are two strategies to optimize in the presence of uncertainty: stochastic programming and robust optimization. Due to the heavy computational burden, it is more difficult to apply a scenario-based stochastic programming formulation. Instead, we adopt the idea of robust optimization to solve the problem, which takes the worst-case scenario into account.

Consider the original inequality constraint in the problem

$$h(z, y, u, p) \leq 0 \tag{5.1}$$

where z is the differential variable vector, y is the algebraic variable vector, u is the input/manipulated variable vector and p is the uncertain parameter vector. To ensure that the inequality constraint is satisfied in the presence of uncertainties, a back-off term $b_c \geq 0$ is introduced into the constraint at nominal uncertainty level $\bar{p}$.

$$h(z, y, u, \bar{p}) + b_c \leq 0 \tag{5.2}$$

Replacing the original constraints (5.1) with the modified one (5.2), we obtain the updated optimization formulation with back-off constraints, as represented in (5.3):

$$\begin{aligned} min \quad & F(z(t_f)) \\ s.t. \quad & \dot{z} = f(z, y, u, \bar{p}), z(0) = z_0 \\ & g(z, y, u, \bar{p}) = 0 \\ & h(z, y, u, \bar{p}) + b_c \leq 0 \end{aligned} \tag{5.3}$$

The confidence level c of the robust optimization solution is defined as the probability of the constraint being satisfied under uncertainties $c = P[h(z, y, u, p) \leq 0]$. When the confidence level $c = 1$, the constraint can be satisfied under all possible uncertainty levels, i.e. the solution considers the worst-case scenario and represents the robust solution.

The previous section mentions two ways to obtain the back-off terms. Diehl *et al.* [17] uses the linearized problem formulation and the dual norm to derive analytical solutions to the robust optimization problem, while Srinivasan *et al.* [65] iteratively update the back-off terms until the simulation results agree with the required confidence level. The linearization of the first approach may lead to inaccurate back-offs when the system is highly nonlinear, and the approach is expensive to derive for large systems. On the other hand, the second approach, as pointed out in [65], may not guarantee convergence to the solution of (5.3).

Relating Back-off Constrained Formulations with Multi-scenario Optimization

Consider the following optimization problem under uncertainty:

$$\min_x E_{p \in \Pi}[f(x, p)], s.t.\ h(x, p) \leq 0, \forall p \in \Pi \tag{5.4}$$

where x are the decision variables after any state variables and equations (including DAEs) have been eliminated. Note that for optimal control problems, decision variables include control profiles and stage times. A straightforward approach to

find an approximate solution is to discretize the probably distribution function for p as $p_i \in I_\Pi$ and form the following multi-scenario problem:

$$\begin{aligned} \min_x \quad & \sum_{i \in I_\Pi} w_i f(x, p_i) \\ s.t. \quad & h(x, p_i) \leq 0, \forall i \in I_\Pi. \end{aligned} \tag{5.5}$$

The first order KKT conditions for (5.5) are given by:

$$\begin{aligned} \sum_{i \in I_\Pi} (w_i \nabla_x f(x, p_i) + \nabla_x h(x, p_i) \lambda_i) = 0 \\ 0 \leq \lambda_i \perp h(x, p_i) \leq 0, \forall i \in I_\Pi. \end{aligned}$$

Writing the constraints only in terms of critical uncertainty points, $p_{\bar{i}}, \bar{i} \in I_\Pi$ where $h(x, p_{\bar{i}}) = 0$ and all other constraints are inactive, leads to:

$$\begin{aligned} \sum_{i \in I_\Pi} w_i \nabla_x f(x, p_i) + \sum_{\bar{i} \in I_\Pi} (\sum_j \nabla_x h_j(x, p_{\bar{i}}) \lambda_{\bar{i}j}) = 0 \\ 0 \leq \lambda_{\bar{i}j} \perp h_j(x, p_{\bar{i}}) \leq 0, \forall j, \forall \bar{i} \in I_\Pi. \end{aligned} \tag{5.6}$$

We also assume that $\sum_{i \in I_\Pi} w_i = 1$. With backoff constraints we consider the following approximation:

$$\begin{aligned} f(x, p) &\approx f(x, \bar{p}) + F(x, \bar{p})^T (p - \bar{p}) \\ h_j(x, p) &\approx h_j(x, \bar{p}) + H_j(x, \bar{p})^T (p - \bar{p}) \end{aligned}$$

and consequently,

$$\begin{aligned} f(x,p) &\approx f(x,\bar{p}) + F(x,\bar{p})^T(p-\bar{p}) \leq f(x,\bar{p}) + |F(x)^T(p-\bar{p})| \\ &\leq f(x,\bar{p}) + \|F(x)\|_1\|p-\bar{p}\|_\infty \leq 0. \\ h_j(x,p) &\approx h_j(x,\bar{p}) + h_j(x)^T(p-\bar{p}) \leq h_j(x,\bar{p}) + |H_j(x)^T(p-\bar{p})| \\ &\leq h_j(x,\bar{p}) + \|H_j(x)\|_1\|p-\bar{p}\|_\infty \leq 0. \end{aligned}$$

In Diehl et al. (2005), $\|F(x)\|_1$ and $\|H_j(x)\|_1$ are estimated through adjoint sensitivities, which may be expensive to calculate for large systems. They also lead to an inaccurate approximation for nonlinear constraints when $\|p-\bar{p}\|$ is large.

Instead, we approximate the back-off terms $|F(x,\bar{p})^T(p-\bar{p})| \approx \tilde{F}(x;p)$ and $|H_j(x,\bar{p})^T(p-\bar{p})| \approx \tilde{H}_j(x;p)$ through off-line Monte Carlo simulations for a *fixed* value of x. On the other hand, these terms evaluated at nominal conditions may not lead to optimal back-off solutions unless we can show that the back-off term is insensitive to x, i.e.,

$$\|\nabla_x f(x,\bar{p})\| >> \|\nabla_x \tilde{F}(x;p)\| \approx 0, \quad \|\nabla_x h_j(x,\bar{p})\| >> \|\nabla_x \tilde{H}_j(x;p)\| \approx 0. \quad (5.7)$$

Through an iterative approach, where the back-off terms are updated with optimal values of x from (5.8), we can improve this solution as well as the back-off terms.

Under these assumptions the backoff problem is equivalent to the multiscenario problem with optimality conditions (5.6) if (5.7) is satisfied. Replacing the backoff terms with their approximations the problem becomes:

$$\min_x f(x,\bar{p}) + \tilde{F}(x,p),\ s.t.\ h(x,\bar{p}) + \tilde{H}(x,p) \leq 0 \quad (5.8)$$

with the optimality conditions of (5.8) given by:

$$\nabla_x f(x, \bar{p}) + \sum_j \nabla_x h_j(x, \bar{p}) \bar{\lambda}_j = 0 \tag{5.9}$$
$$0 \leq \bar{\lambda}_j \perp h_j(x, \bar{p}) + \tilde{H}_j(p) \leq 0.$$

where we have used $\sum_{i \in I_\Pi} w_i = 1$ and define $\bar{\lambda}_j := \sum_{\tilde{i} \in I_\Pi} \lambda_{\tilde{i}j}$.

Monte Carlo Simulation to Approximate Back-offs

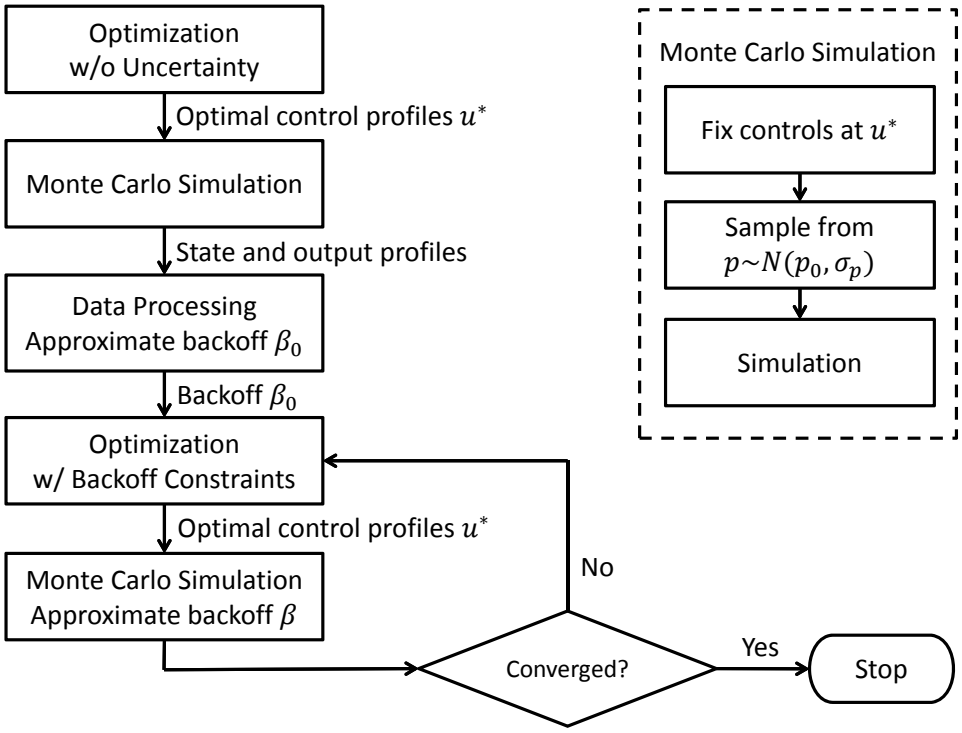

Figure 5.1: Steps to obtaining robust optimal transition strategy

We now consider Monte Carlo simulation to calculate the size of back-off. Monte Carlo simulation is capable of probing the system and providing an idea of how state and output variables changes when the uncertainty level varies. The steps to obtaining a robust and optimal transition strategy are outlined below and the

flowchart is presented in Figure 5.1.

Step 1: Solve the optimization problem (5.3) with at nominal conditions, $p = \bar{p}$ and $b_c = 0$. The optimal solution can be obtained under the assumption that the uncertainty stays at its nominal level and there is no variation with the control profile.

Step 2: Assume the probability distribution of uncertainty is known. At the nominal optimal solution, the whole model is simulated using Monte Carlo simulation and the resulting dynamic profiles reveal the sensitivity information of state and output variables to uncertainties.

Step 3: Calculate the back-off term based on the simulation result from the previous step. The size of back-off is dependent on the sample standard deviation S and a tuning parameter η which influences the confidence level (larger η results in greater confidence level). Here m is the total number of simulation runs, $S^2(t)$ is the sample variance, $h_i(t)$ is the constraint function value at time t when the uncertainty realizes the ith value sampled from its probability density distribution, p_i, in the Monte Carlo simulation. Assume that the uncertain parameter p follows Gaussian distribution, $p \sim N(\bar{p},\ \sigma_p^2)$, then p_i is sampled from Gaussian distribution $N(\bar{p},\ \sigma_p^2)$.

$$b_c(t) = \eta S(t) \tag{5.10}$$

$$S^2(t) = \frac{\sum_{i=1}^{m}(h_i(t) - \bar{h}(t))^2}{m-1} \tag{5.11}$$

$$\bar{h}(t) = \frac{\sum_{i=1}^{m} h_i(t)}{m} \tag{5.12}$$

Based on the formula shown above, two different designs of b_c are implemented and compared. The first way to calculate the back-off b_c is to take the maximum deviation over time as a conservative hedge against constraints infeasibility under uncertainty, while the second one relaxes the

back-off constraint using time-varying back-offs.

- Constant back-off: $b_c = \max_t b_c(t)$
- Time-varying back-off: $b_c(t)$

Step 4: Solve the updated optimization problem (5.3) again with back-off constraints.

Step 5: Perform Monte Carlo simulation to check the performance and update back-off terms based on the updated solution of (5.3).

Step 6: (Optional) Go to Step 4 and solve the optimization problem with updated back-off constraints. Stop when the convergence criterion is satisfied, *i.e.* $\|b_c^{k+1} - b_c^k\| \leq \epsilon$.

The iterative approach presented here may not converge to the optimal solution of Problem (5.3) unless the back-off term b_c is insensitive to the control profile.

More detailed information on this approach, along with the results from each step, will be described with the case study.

5.4 Application to Polyethylene Grade Transitions

In the solution polymerization process, there are various sources of uncertainties, including ambient temperature, fouling factor, and kinetic parameters. Among all these uncertainties, the unknown catalyst deactivation rate is hard to measure and it has a large influence on the system performance [44]. In this work, we focus on developing transition policies that are applicable over a wide range of unknown deactivation rates.

Our current knowledge of the deactivation mechanism as shown in Table 3.1 suggests that the catalyst deactivation is governed by two reactions: thermal deactivation (i.e., spontaneous deactivation) and deactivation by poison. Since there is not enough information to separate the impact of these two reactions, a lumped term

$K_d = K_{dsp} + K_{dx}C_x$ is introduced as an uncertainty parameter. K_d is the overall deactivation rate, K_{dsp} is the spontaneous deactivation rate, K_{dx} is deactivation rate by poison, and C_x is the concentration of the impurity in the reactor (i.e., impurity level).

Different from disturbances which exhibit fast time-varying dynamics, uncertain parameters are usually slow time-varying or time-invariant [65]. In the polyethylene polymerization system considered here, the lumped deactivation rate changes slowly over time and is assumed to be time-invariant in a short period of time. We assume that the lumped term follows the normal distribution with its nominal value as the mean. Detailed settings can be found in Table 5.1.

As outlined in the previous section, the robust optimization approach is realized using back-off constraints calculated from Monte Carlo simulation. We apply this strategy to the same grade transition problem as considered in our previous work; the initial and the target product density and melt index, as well as steady state operating conditions, are shown in Table 5.1. The upper and lower specification bands are illustrative of MI and density specs; actual products will be different depending upon the grade and application.

		Meaning	Grade A	Grade B
Outputs	**MI**	*Melt index (g/10min)*	1.0	12.0
	Density	*Density* (g/cm^3)	0.908	0.864
	$\boldsymbol{\theta}$	*Ethylene conversion rate*	0.825	0.833
Scaled Manipulated Variables	$\mathbf{T_j^0}$	*Inlet cooling water temperature*	0.62	0.66
	$\mathbf{F_1}$	*Ethylene inlet flow*	0.98	0.70
	$\mathbf{F_2}$	*Comonomer inlet flow*	0.18	0.97
	$\mathbf{F_H}$	*Hydrogen inlet flow*	0.50	0.93
	$\mathbf{F_c}$	*Feed catalyst*	0.97	0.88
Uncertain Parameters	$\mathbf{K_d}$	*Catalyst deactivation rate*	$N(7.9 \times 10^3, 1.32 \times 10^2)$	
	$\mathbf{K_{cH}}$	*Chain transfer to hydrogen rate*	$N(4.4 \times 10^6, 2.94 \times 10^4)$	

Table 5.1: Steady states of two grades and uncertain parameters

In this study, we consider a mathematical model capturing the dynamics of the solution polymerization process carried out in a CSTR. Four key components of the

mathematical model are (1) mass and energy balance equations, (2) the moments model to predict product properties, (3) a simple yet accurate vapor-liquid equilibrium (VLE) model derived from rigorous calculations, and (4) a variable time delay model for recycle streams. In the first part, five dynamic mass balances are derived for ethylene, comonomer, empty catalyst site, hydrogen and solvent. Besides, there are two energy balance equations capturing the temperature change inside the reactor and the cooling jacket. The second component featuring the method of moments is built in the model to avoid a set of computationally intractable and inefficient population balance equations. The resulting 12 moments (6 for the living polymer moments up to the second order and 6 for bulk polymer moments up to the second order) can be used to calculate the average distributional properties, such as melt index and product density, which are the key properties considered in grade transitions. The surrogate VLE model in the third part is built with both quadratic regression model and Gaussian correlation model using 250 training points.

The entire model is shown in Chapter 3 and a detailed description of the process and each individual part of the model can be found in [64]. In total, the model contains 59 differential equations, and applying 3-point collocation on 48 finite elements leads to a large-scale nonlinear programming problem with 157,935 variables and 159,683 constraints. The solution approach, simultaneous dynamic optimization, will be discussed in the next section while information on the discretization grid and the resulting NLP problem can be found in [64].

As described in Chapter 4, a simultaneous dynamic optimization approach is applied to solve the grade transition problem without considering uncertainties. Two optimization formulations, single stage and multistage, are developed to deal with single-value specification and specification bands of product properties, respectively. The results show significant improvement in transition times and reduction in off-grade production as compared to the baseline. Additionally, the multistage

formulation designed for problems with specification bands has the ability to minimize transition time and off-grade production directly (in the objective function) and outperforms the single stage formulation as the former one leads to more aggressive control profiles and allows oscillations within the bands. In this section, we will focus on multistage optimization formulation as represented in (5.13).

$$
\begin{aligned}
min \quad & \alpha_t(t_2 - t_1) + \beta_t(t_1 - t_0) + \int_{t_0}^{t_f} ||y(t) - y^*||_Q^2 + \frac{1}{\gamma} ||u(t) - u^*||_R^2 \, dt \\
s.t. \quad & \textit{Reactor model} \\
& \textit{Moment model} \\
& \textit{Product property correlations} \\
& \textit{Surrogate VLE model} \\
& \textit{Recycle variable time delay model} \\
& \textit{Process constraints} \\
& \textit{Property specifications in the first and the last stages} \\
& \quad MI_{A,min} \leq MI \leq MI_{A,max}, \;\; \rho_{A,min} \leq \rho \leq \rho_{A,max}, \;\; t \in [t_0, t_1] \\
& \quad MI_{B,min} \leq MI \leq MI_{B,max}, \;\; \rho_{B,min} \leq \rho \leq \rho_{B,max}, \;\; t \in [t_2, t_f]
\end{aligned}
\tag{5.13}
$$

In problem (5.13), $y(t)$ denotes output (algebraic) variables, $u(t)$ are manipulated variables and t is time. In the objective function, the terms represent the time period of producing off-spec product $(t_2 - t_1)$, initiation to the first transition $(t_1 - t_0)$ and a regularization term that promotes a smooth solution to the target steady state of the second grade, respectively. α_t, β_t, γ, Q and R are weighting factors and matrices which balance these objectives.

$$
Q = \begin{pmatrix} w_{MI}/(MI_0 - MI^*)^2 & 0 \\ 0 & w_\rho/(\rho_0 - \rho^*)^2 \end{pmatrix} \tag{5.14}
$$

$$
R = diag(1/(u_j^0 - u_j^*)^2) \tag{5.15}
$$

As shown in (5.13), the multistage objective function considers the actual economic objective (minimizing transition time and reducing off-grade production) and the regularization term. A key weighting factor γ plays an important role in shaping the control profiles and determining the transition time. The determination of the weighting factors at nominal uncertainty level is discussed and illustrated through a case study in [64]. The scaling matrices Q and R are chosen such that the two key product properties, MI and density, can reach the target at the same time. The weight γ on the regularization term can be used to smooth oscillatory profiles without significant loss of optimality. As γ decreases, more emphasis is put on the regularization term and thus the transition time increases.

5.4.1 Dynamic Optimization with Constant Back-offs

In the first case study, the same setting of weighting factors, $\alpha_t = 30, \beta_t = 15, \gamma = 20, w_{MI} = 10, w_\rho = 100$, is used as suggested in Chapter 4. A more extensive assessment of influence of the weighting factors and other settings will also be discussed.

Following the steps in Figure 5.1:

Step 1: Obtain the optimal transition policy based on the nominal parameter value. The solution of multistage formulation provides optimal transition policies with large reduction of transition time and off-spec product, but the aggressive control strategy is more likely to violate constraints and specification ranges compared to other conservative non-optimal solutions. Therefore, we use the multistage formulation as the focus of our robust optimization study. The optimal solution at nominal parameter values can be in Figures 5.2, 5.3 and 5.4.

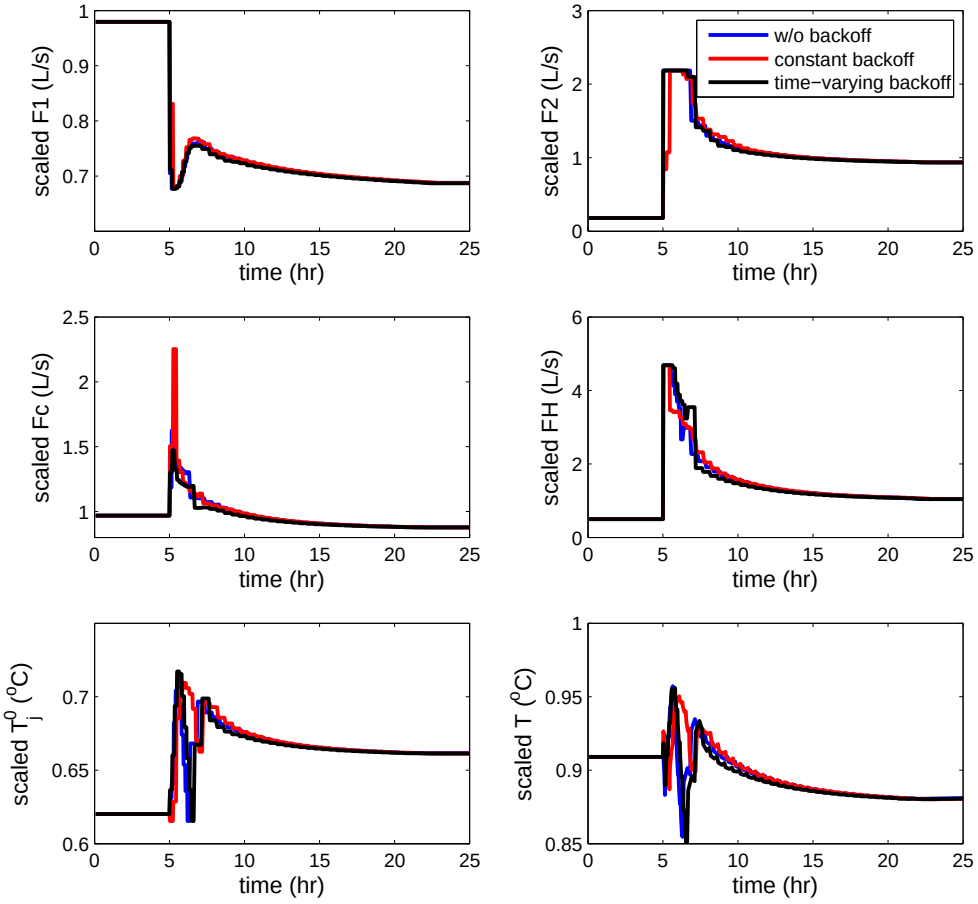

Figure 5.2: Control profiles with nominal parameter values, $\bar{p}$

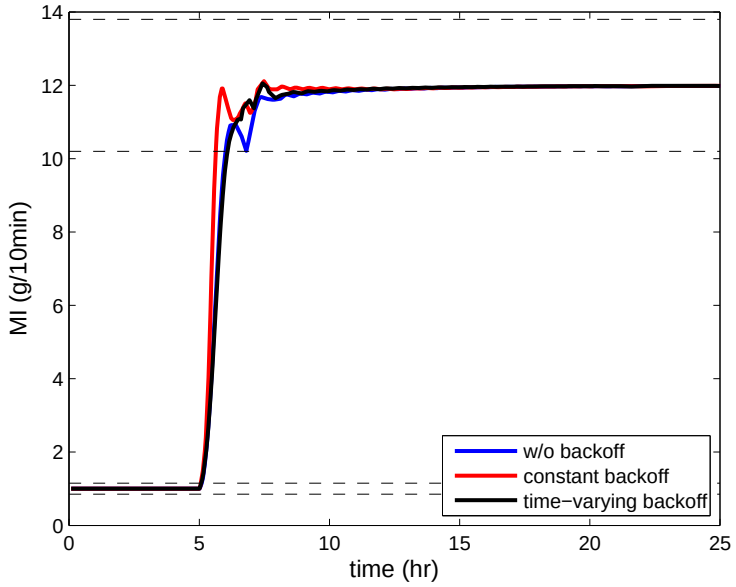

Figure 5.3: MI profiles with nominal parameter values, $\bar{p}$

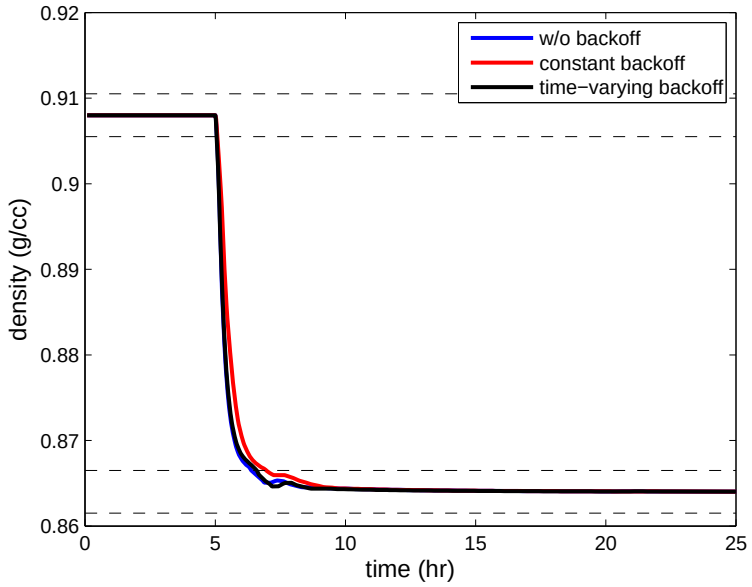

Figure 5.4: Density profiles with nominal parameter values, $\bar{p}$

Step 2: Perform Monte Carlo simulation. Assume that the parameter uncertainty is normally distributed and centered around the nominal parameter value. Sample m values from this distribution to capture a statistically significant range of pa-

rameter values in the system; m should be large enough to adequately capture the range of uncertainty (in our study, we use the setting $m = 200$ and the sampled values are scaled and shown in Figure 5.5).

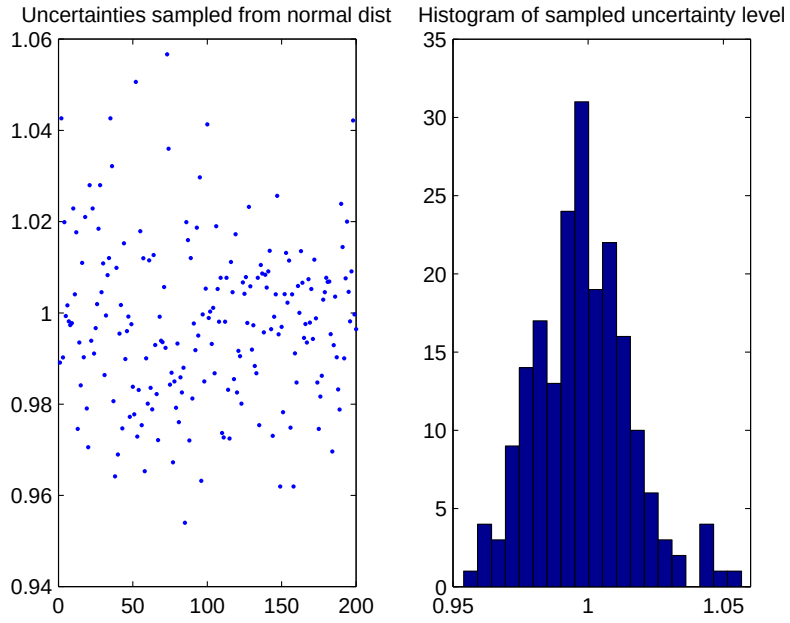

Figure 5.5: Sampled uncertainty level in Monte Carlo simulation, m = 200

For every parameter value, simulate the state and output profiles that would result from implementing the optimal transition strategy obtained in step 1. This helps us visualize the impact that the uncertainty has on our system. Note that melt index is more heavily influenced by the variations in the uncertainty level, catalyst deactivation rate, as compared to density, as illustrated in Figure 5.6 and Figure 5.7.

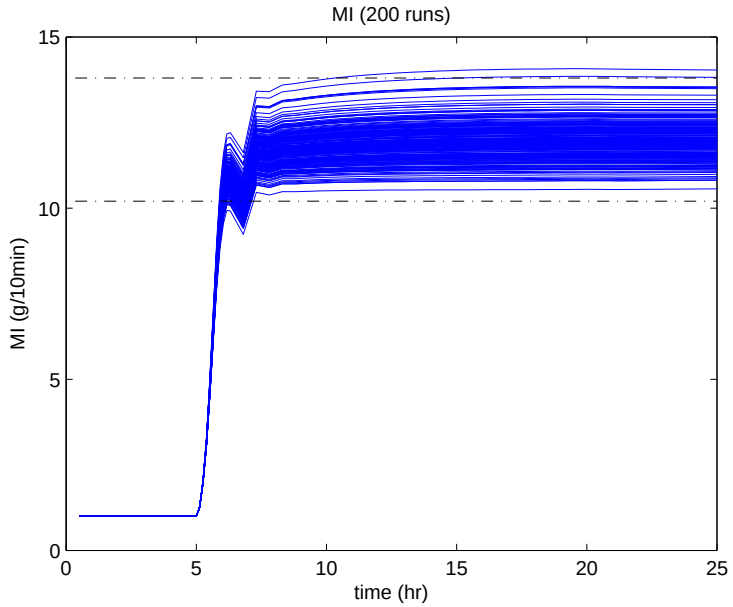

Figure 5.6: Monte Carlo simulations of MI with $m = 200$ at nominal optimal

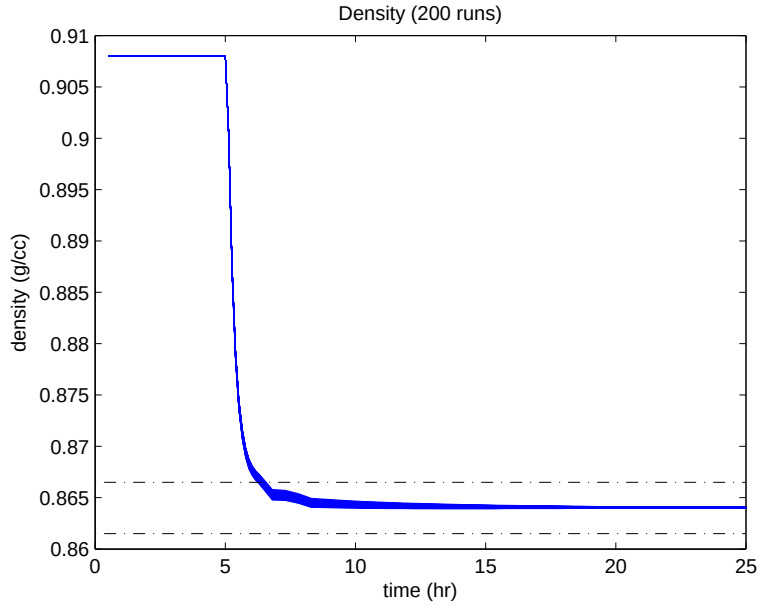

Figure 5.7: Monte Carlo simulations of density with $m = 200$ at nominal optimal

Figure 5.6 shows clearly that there are several constraints violations when the uncertainty level is different from its nominal value. As we can see from Figure 5.6, one of the product properties, MI, is expected to increase quickly to the target spec-

ification band of Grade B ($MI_{B,min} = 10.2\ g/10min$ and $MI_{B,max} = 13.8\ g/10min$), and oscillations are acceptable within the band. However, this aggressive solution deteriorates in the presence of uncertainty resulting in bounds violations and long-time off-spec production.

Step 3: Approximate back-off constraints. At each time point of the entire horizon, the sample standard deviation of inequality constraint h is calculated and the resulting maximum standard deviation is summarized in Table 5.2. Incorporating the back-off terms into the original optimization problem gives us a problem that can be represented as Problem (5.3). η in (5.10) is set to 3 to ensure a confidence level greater than 99.8%.

	Max standard deviation S_{max}	Unit
Melt Index (MI)	0.5634	$g/10min$
Density	1.8349×10^{-4}	g/cm^3
Production rate	10.7583	g/s
Reactor temperature	0.2264	^oC
Ethylene concentration	0.0104	mol/L
Bubble point pressure in reactor	0.0300	MPa
Bubble point pressure in feed	0.0082	Mpa

Table 5.2: Maximum standard deviation calculated from Monte Carlo simulation output profiles

Step 4: Optimization with back-off constraints. Obtain the optimal transition policy based on the nominal parameter values and the multistage formulation that has been modified with back-off constraints. As Figure 5.3 shows, the resulting melt index profile has little to no oscillations as compared to step 1 (this is a desirable outcome of robust optimization).

Step 5: Perform Monte Carlo simulation to check the performance of the robust solution and update the back-offs. As is observed in Figure 5.8 and Figure 5.9, the majority output profiles of the m-sampled uncertainty levels remain within the desired specification range for both melt index and density. However, it is obvious

to see the error propagation over time; as time proceeds, the MI profile diverges from the center value which may lead to lower bound violations for the extreme case.

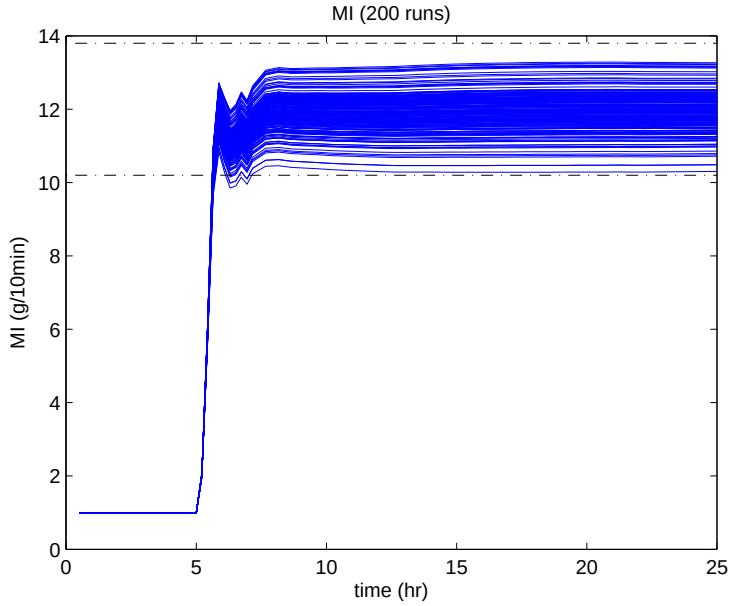

Figure 5.8: Monte Carlo simulations of MI with $m = 200$ (robust optimization with constant back-offs)

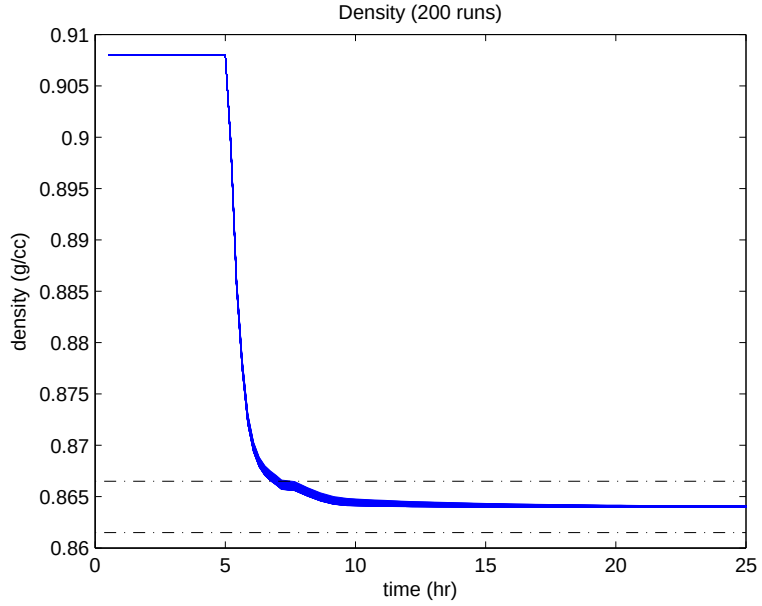

Figure 5.9: Monte Carlo simulations of density with $m = 200$ (robust optimization with constant back-offs)

Step 6: Go to Step 4 and solve the optimization problem with updated back-off constraints. As discussed in Section 3.3, we utilize Monte Carlo simulation to approximate the back-off term under the assumption that the back-off is insensitive to the decision variables. An iterative approach is necessary to update the back-off term with the change of optimal decisions. In the constant back-off case, we observe fast convergence of back-off terms and objective function value. A more rigorous discussion of the iterative approach will be presented for the time-varying back-off case.

5.4.2 Dynamic Optimization with Time-varying Back-off Constraints

In the case study above, constant back-offs b_c are calculated using maximum standard deviation. In reality, back-off b_c is a function of input and state variables and it also varies over time.

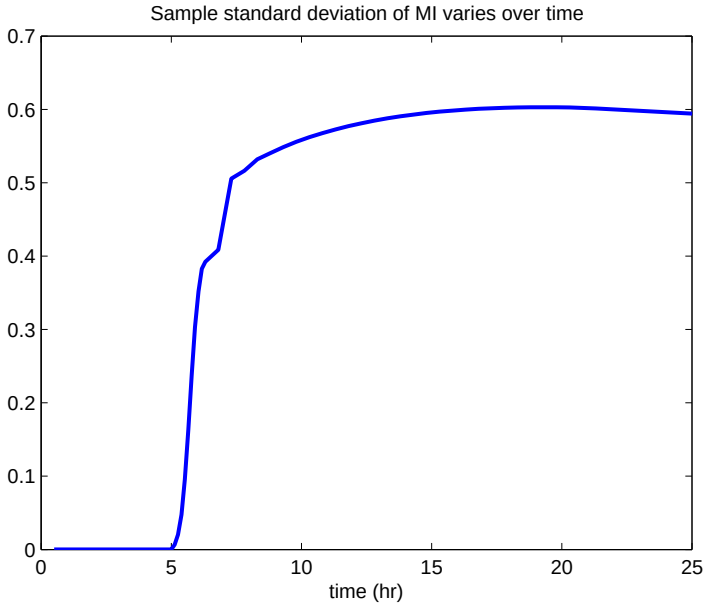

Figure 5.10: Sample standard deviation of MI varies over time

As shown in Figure 5.10, the sample standard deviation of Melt Index increases from zero at the beginning of the horizon to around at the end. If we use the

maximum standard deviation as a constant back-off in the inequalities, the original constraint is tightened too much and the feasible region shrinks at the cost of performance.

Based on the observation from Figure 5.10, we propose using time-varying back-offs $b_c(t)$ instead of constant b_c to formulate the robust optimization problem. The only difference between the current case study and the previous one is the time-varying back-off; all the steps and procedure remain the same, as illustrated in the previous section.

The optimization solutions without back-off, with constant back-off and with time-varying back-off are shown in Figure 5.3 and Figure 5.4. Compared to the solution with constant back-off, the time-varying back-off relaxes inequality constraints and allows oscillations within the specification bands. As seen in the profile of Melt Index, oscillations with smaller peaks occur within the band. However, in contrast to the non-robust multistage optimization solution, the peak in the robust optimization solution never hits the original boundaries and thus leaves a safety margin for uncertainties.

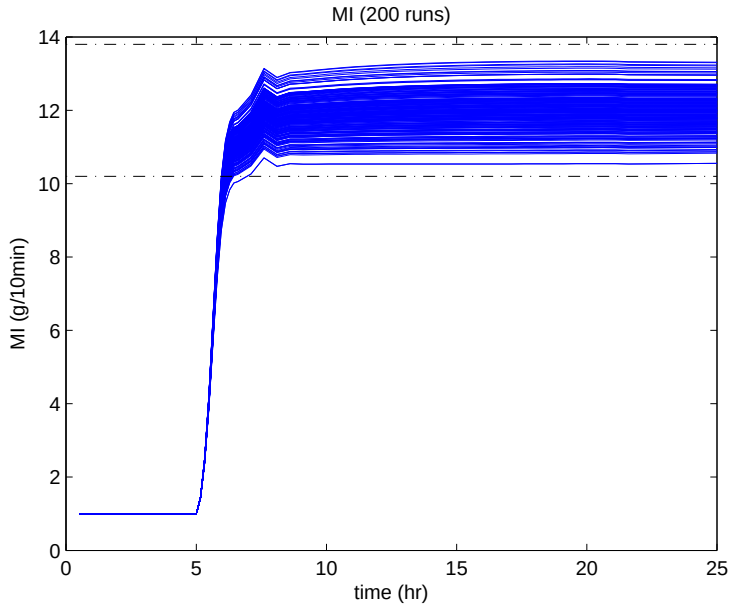

Figure 5.11: Monte Carlo simulations of MI with $m = 200$ (robust optimization with time-varying back-offs)

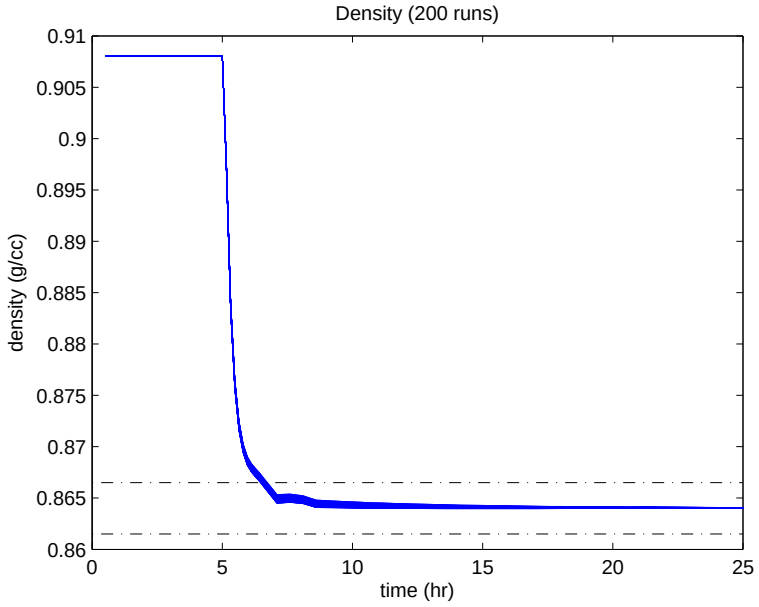

Figure 5.12: Monte Carlo simulations of density with $m = 200$ (robust optimization with time-varying back-offs)

Figure 5.11 and Figure 5.12 show the performance of the robust optimal transition

policy under uncertainties. The control policy is feasible for all 200 realizations of uncertainty, which demonstrates its robustness.

The back-off terms are updated after Step 5. The optimal solution without back-offs is considered as the initial guess, and the approximation from Step 5 is the first iteration result. The evolution of two performance metrics, transition time and objective function value, is plotted in Figure 5.13. It is clear that the solution converges in one iteration; the resulting solution from the first iteration is representative of the following solutions. In Figures 5.14 and 5.15, standard deviation of MI and density for 6 iterations are shown.

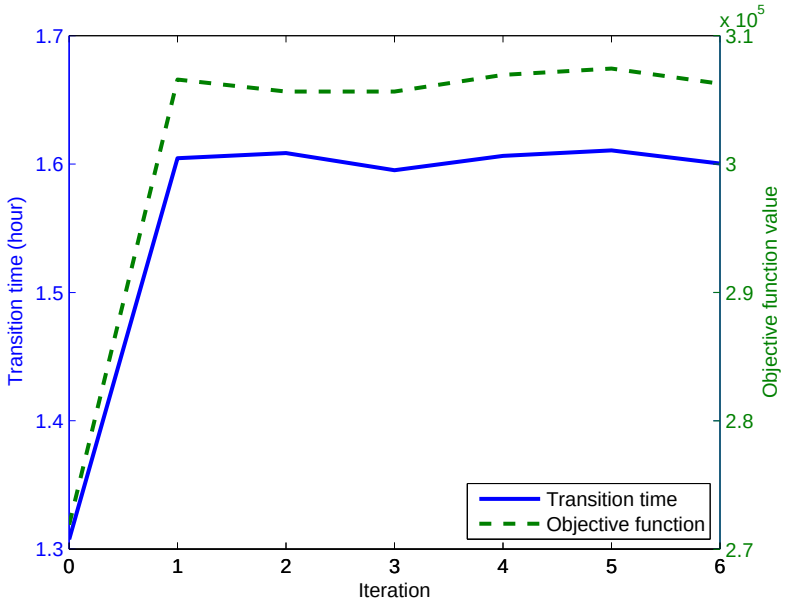

Figure 5.13: Optimal transition time and objective function value in the iterative approach

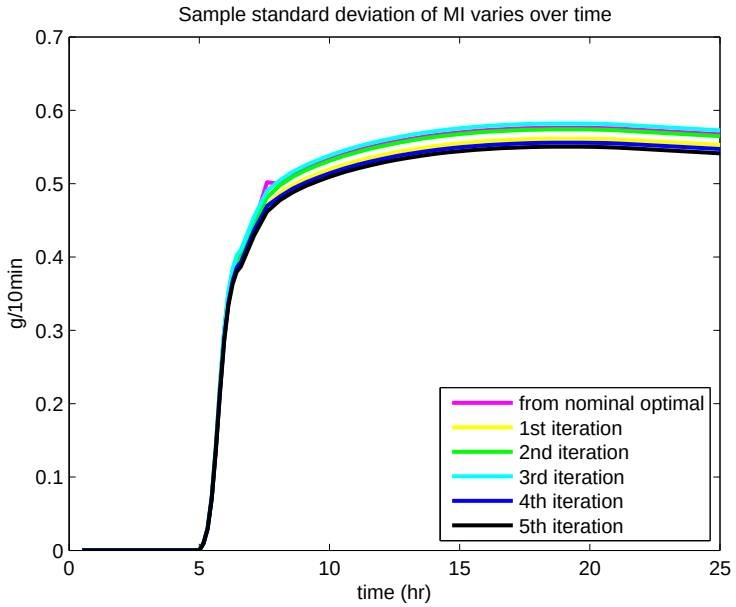

Figure 5.14: Sample standard deviation of MI in the iterative approach

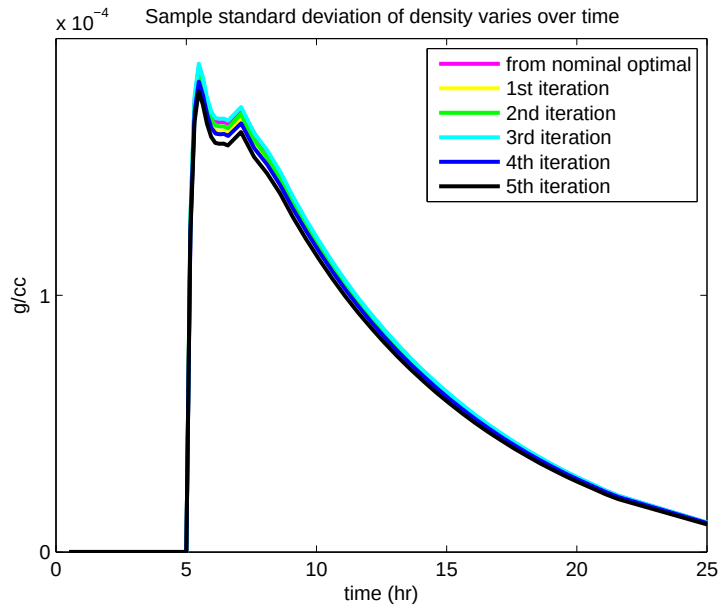

Figure 5.15: Sample standard deviation of density in the iterative approach

Now we compare the performance of the non-robust and the robust solutions at nominal uncertainty level and in the worst-case of the Monte Carlo simulation. As seen in Table 5.3, the loss of the objective due to considering uncertainties is small;

the robust solution has a longer transition time at nominal uncertainty level than that of the non-robust case. However the gain of considering back-off constraints is large; the worst-case transition time is reduced from infinity to 1.95 hours. On the other hand, by using time-varying back-offs, the conservatism of robust optimization and the back-off constrained formulation is reduced to some extent.

	Transition Time (hour)		Optimization	Monte Carlo
	with $p = \bar{p}$	worst case, p	CPU time (s)	CPU time (hr)
w/o backoff	1.31	infinite	169.0	$\sim$1
constant b_c	1.96	2.10	121.1	$\sim$1
time-varying b_c	1.59	1.95	47.7	$\sim$1

Table 5.3: Comparison among non-robust, robust solution with constant back-offs and with time-varying back-offs

5.4.3 Influence of Weighting Factors

The influence of weighting factors in the objective function of Problem (5.13) is assessed in Chapter 4 without consideration of uncertainty. In this section, we present a case study focusing on the influence of the weights on grade transitions under uncertainty. Besides the previous case with $\alpha_t = 30, \beta_t = 15, \gamma = 20, w_{MI} = 10, w_\rho = 100$, another two cases with either smaller or larger regularization are performed here.

Large Regularization

To obtain a representative case with relatively larger regularization, the weight in the objective function is set to $\alpha_t = 30, \beta_t = 15, \gamma = 2, w_{MI} = 10, w_\rho = 100$. The weight on the regularization term, $1/\gamma$, is ten times as much as the original setting.

First, the optimization problem under nominal uncertainty level is solved and followed by Monte Carlo simulation. The resulting profiles can be found in Figure

5.16 and 5.17. Similar to the previous case with $\gamma = 20$, the worst case in Monte Carlo simulation leads to infinite transition time since its MI profile goes off the specification band gradually. On the other hand, the difference from the solution to the last case study is obvious; the overall transition time is much longer since more emphasis is put on regularization and thus relatively small weight is on the actual objective.

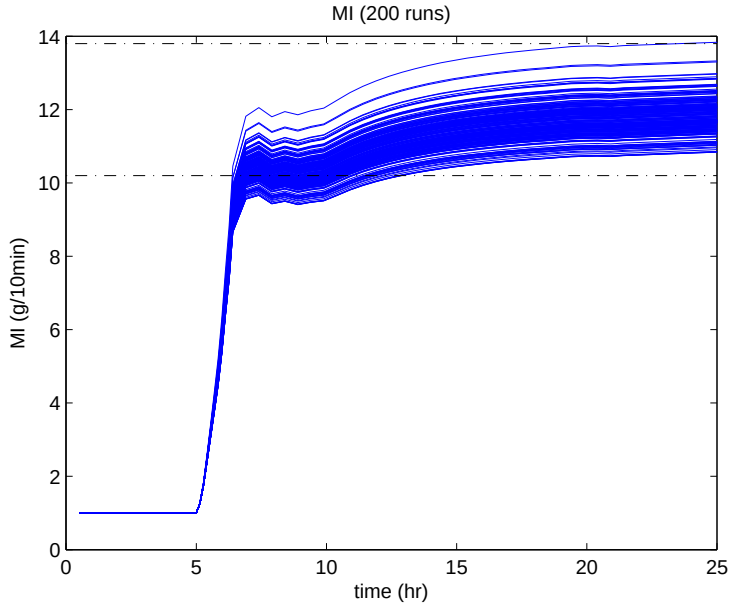

Figure 5.16: Monte Carlo simulations of MI with $m = 200$ (nominal optimal and large regularization)

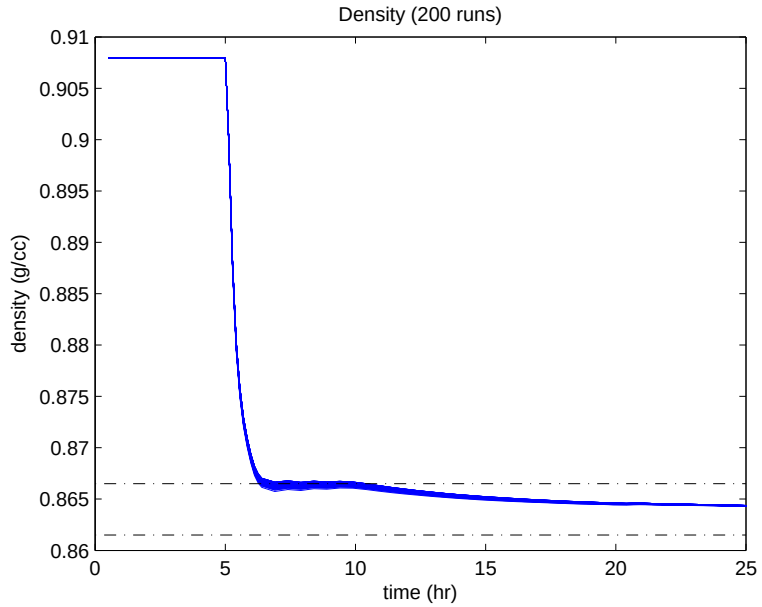

Figure 5.17: Monte Carlo simulations of density with $m = 200$ (nominal optimal and large regularization)

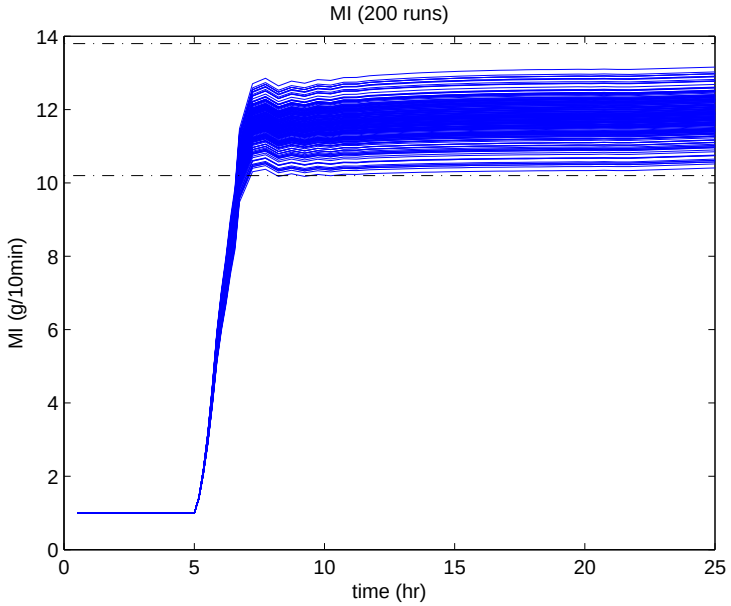

Figure 5.18: Monte Carlo simulations of MI with $m = 200$ (time-varying back-offs and large regularization)

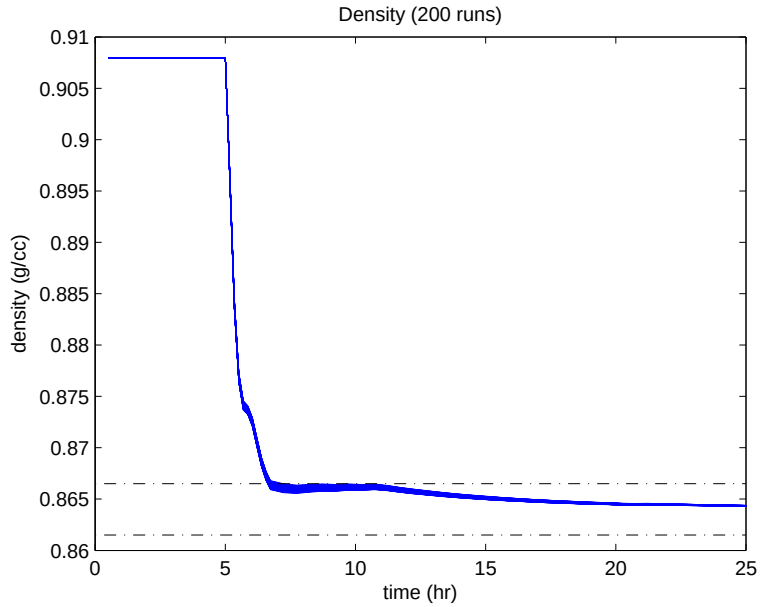

Figure 5.19: Monte Carlo simulations of density with $m = 200$ (time-varying back-offs and large regularization)

Then, the time-varying back-off is calculated and incorporated into the inequality constraints. The optimization with back-off constraints is solved. In Figure 5.18 and 5.19, the Monte Carlo simulation result with time-varying back-offs is shown. Both MI and density profiles are shifted into the specification band in the time segment where constraint violations were observable in non-robust solution. This adjustment results in much shorter transition time (5.29 hours), which demonstrates the effectiveness of the back-off constraints.

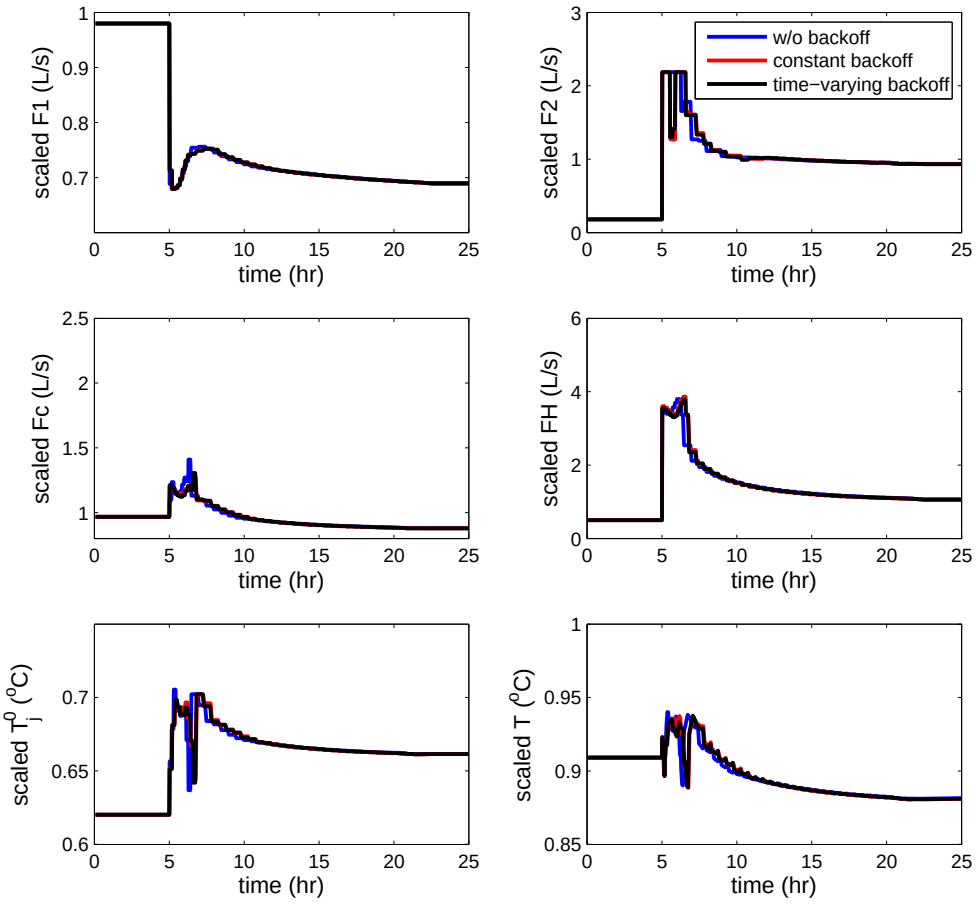

Figure 5.20: Control and temperature profiles with nominal parameter values and large regularization

Figures 5.20 to 5.22 show the optimal solutions obtained from both non-robust problem and the one with back-offs. Because a larger weight is placed on the regularization term, the control profiles are smoother and have fewer oscillations. From the one without back-offs to those with back-offs, the differences in the control actions are moderate; only small adjustments are observed to compensate for the influence of uncertainty.

The change of transition policy is clear in Figure 5.21. As our objective is to minimize the transition time/off-grade production time, the non-robust MI profile stays

above the lower specification bound for a longer time. However, this type of behavior is more sensitive under uncertainty. Therefore, the profiles are pushed deep inside the band after applying back-off constraints so that a safety margin is guaranteed.

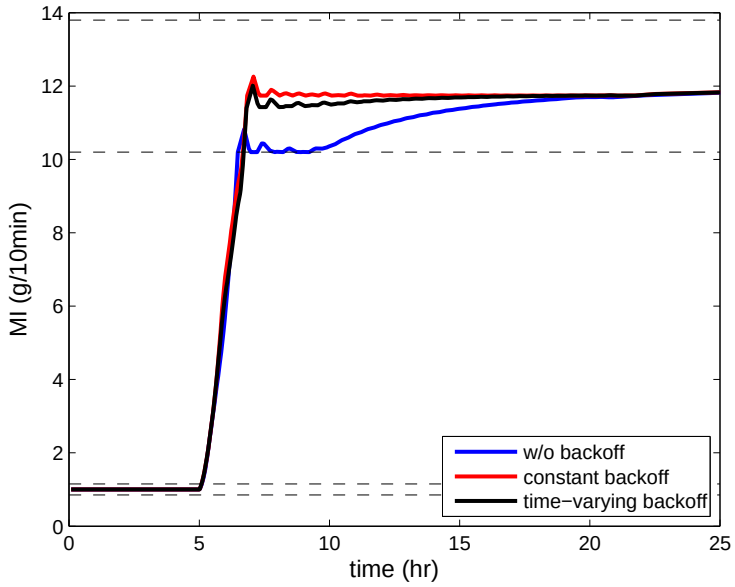

Figure 5.21: MI profiles with nominal parameter values and large regularization

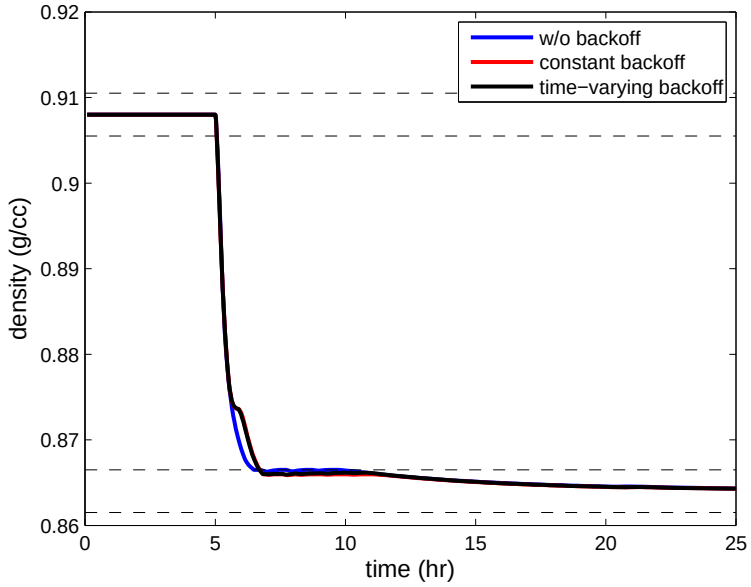

Figure 5.22: Density profiles with nominal parameter values and large regularization

Small Regularization

To complete the case study on regularization, another case with smaller regularization is performed. In the objective function, we keep $\alpha_t, \beta_t, w_{MI}$ and w_ρ the same as the previous cases and increase γ from 2 to 200. In this way, the actual weight $1/\gamma$ on the regularization term is now one tenth of the original one.

Here we present the solutions obtained from two Monte Carlo simulations: one without back-offs and the other one with time-varying back-offs. This particular case gives us a different perspective on the back-off constraint. In the previous two cases, the control policies obtained without back-off constraints fail in the Monte Carlo simulation as constraints violations are observed. However, the non-robust control policy in this case does lead to good performance when the uncertainty level varies. A small violation can be seen in Figure 5.23, but it does not greatly affect overall transition time. When back-off constraints are incorporated in the optimization problem, the transition time is sacrificed in order to get rid of that

violation.

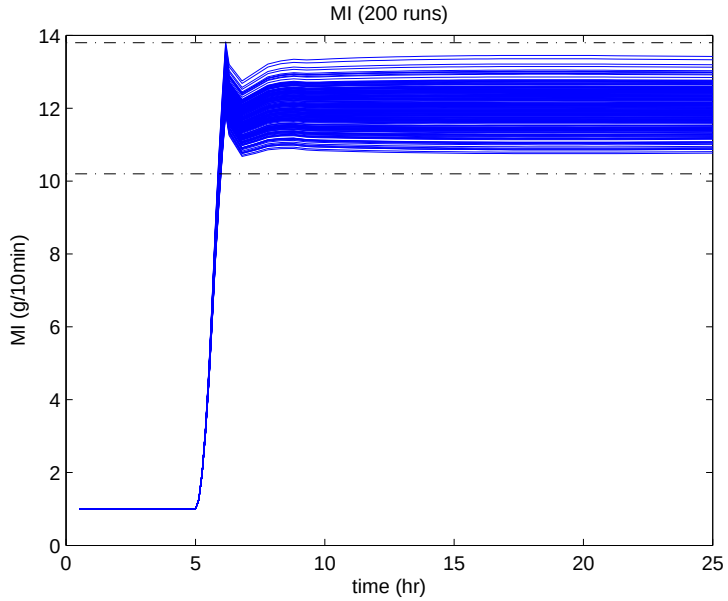

Figure 5.23: Monte Carlo simulations of MI with $m = 200$ (nominal optimal and small regularization)

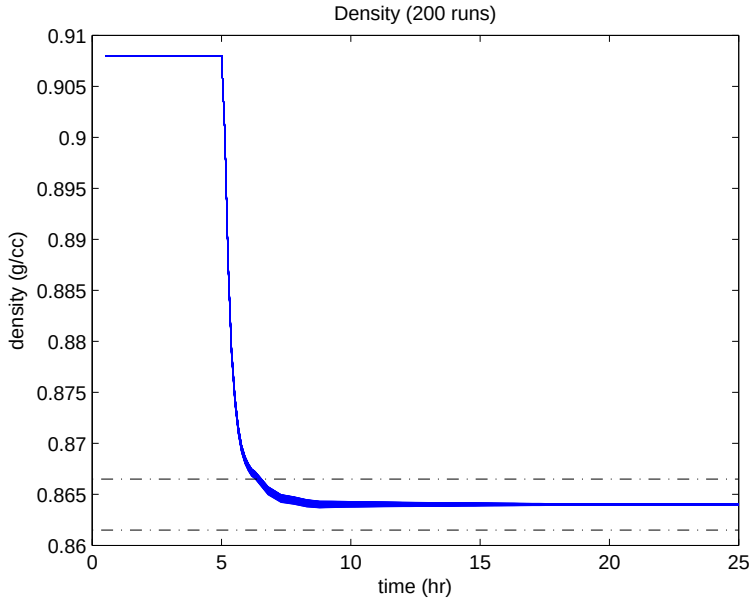

Figure 5.24: Monte Carlo simulations of density with $m = 200$ (nominal optimal and small regularization)

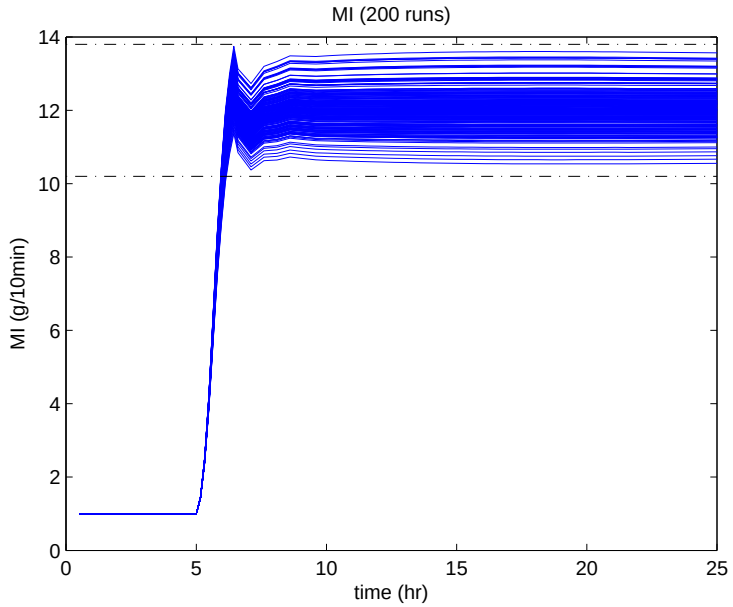

Figure 5.25: Monte Carlo simulations of MI with $m = 200$ (time-varying back-offs and small regularization)

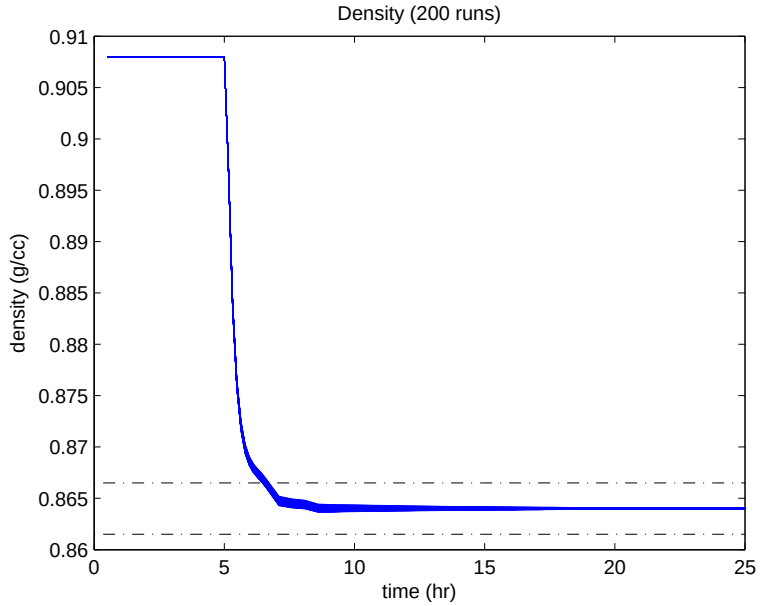

Figure 5.26: Monte Carlo simulations of density with $m = 200$ (time-varying back-offs and small regularization)

A valuable lesson gained from this case study is that the performance check under

uncertainty is of great importance and should be conducted before a robust optimization strategy is applied to the problem. In the case where uncertainty is small enough or the system is insensitive enough not to trigger any constraint violation, the original control policy may suffice.

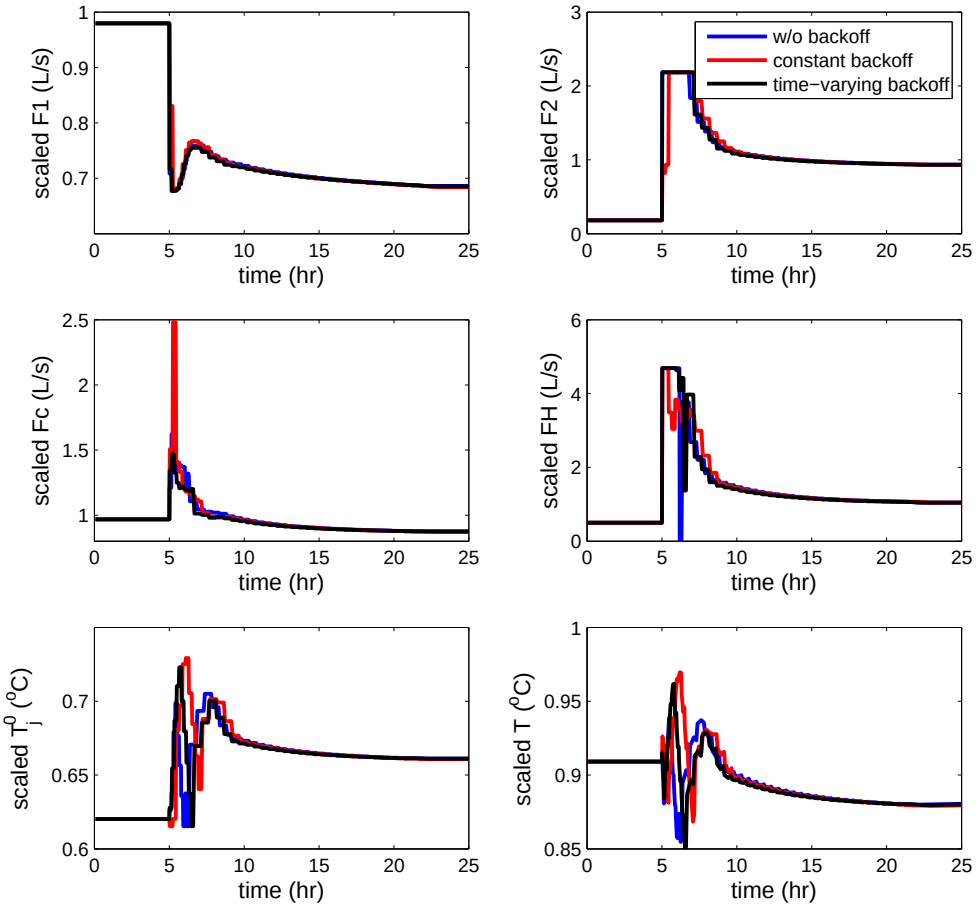

Figure 5.27: Control and temperature profiles with nominal parameter values and small regularization

Back to the topic of this section, the influence of the regularization term can be revealed by comparing the solutions of the previous two cases with Figures 5.27 to 5.29. The manipulated variables in Figure 5.27 show more oscillatory behavior. But the transition time becomes much shorter because relatively larger weight is

placed on minimizing transition time. Detailed information of these different case studies can be found in the table below.

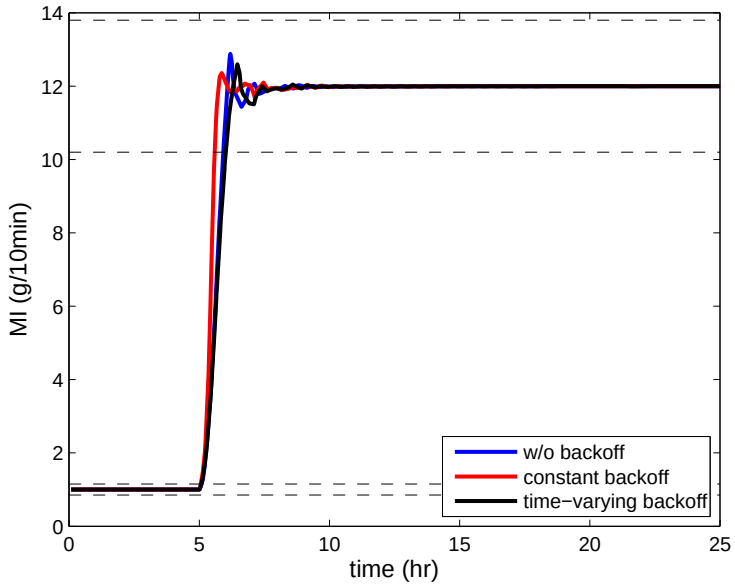

Figure 5.28: MI profiles with nominal parameter values and small regularization

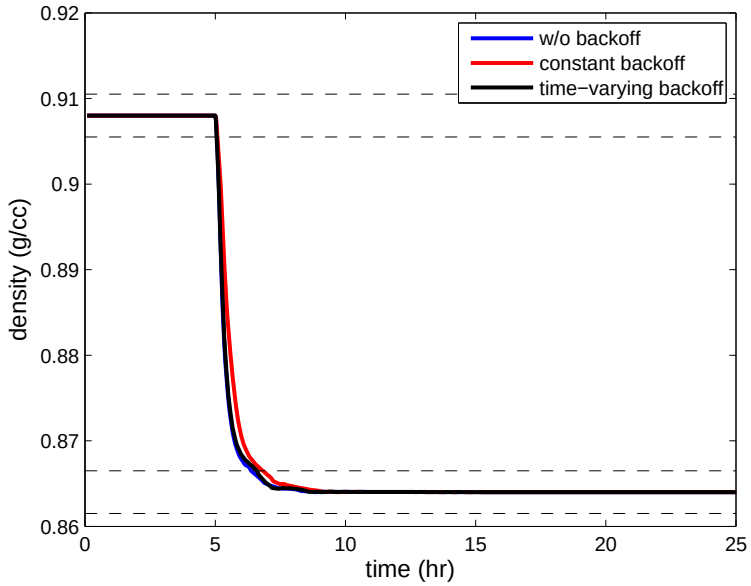

Figure 5.29: Density profiles with nominal parameter values and small regularization

5.4.4 Influence of Output Tracking

Another interesting point which draws our attention is the influence of output tracking term in the objective function. Recall the objective function

$$min\ \alpha_t(t_2 - t_1) + \beta_t(t_1 - t_0) + \int_{t_0}^{t_f} ||y(t) - y^*||_Q^2 + \frac{1}{\gamma} ||u(t) - u^*||_R^2\, dt.$$

We keep one term for output tracking $\int_{t_0}^{t_f} ||y(t) - y^*||_Q^2\, dt$ whose weight is determined by matrix Q.

$$Q = \begin{pmatrix} w_{MI}/(MI_0 - MI^*)^2 & 0 \\ 0 & w_\rho/(\rho_0 - \rho^*)^2 \end{pmatrix} \tag{5.16}$$

In the cases considered above, non-zero weights are placed on the output tracking term, $w_{MI} = 10, w_\rho = 100$. Now we remove the output tracking term by setting $w_{MI} = w_\rho = 0$ and follow the same procedure shown in Figure 5.1.

From Figures 5.30 to 5.32, the influence of output tracking is clear. The nominal case without back-offs results in density and MI profiles that stay at the boundary of the target specification band in the third stage. This phenomenon can be well explained as there is no driving force to push the outputs to the center of the band.

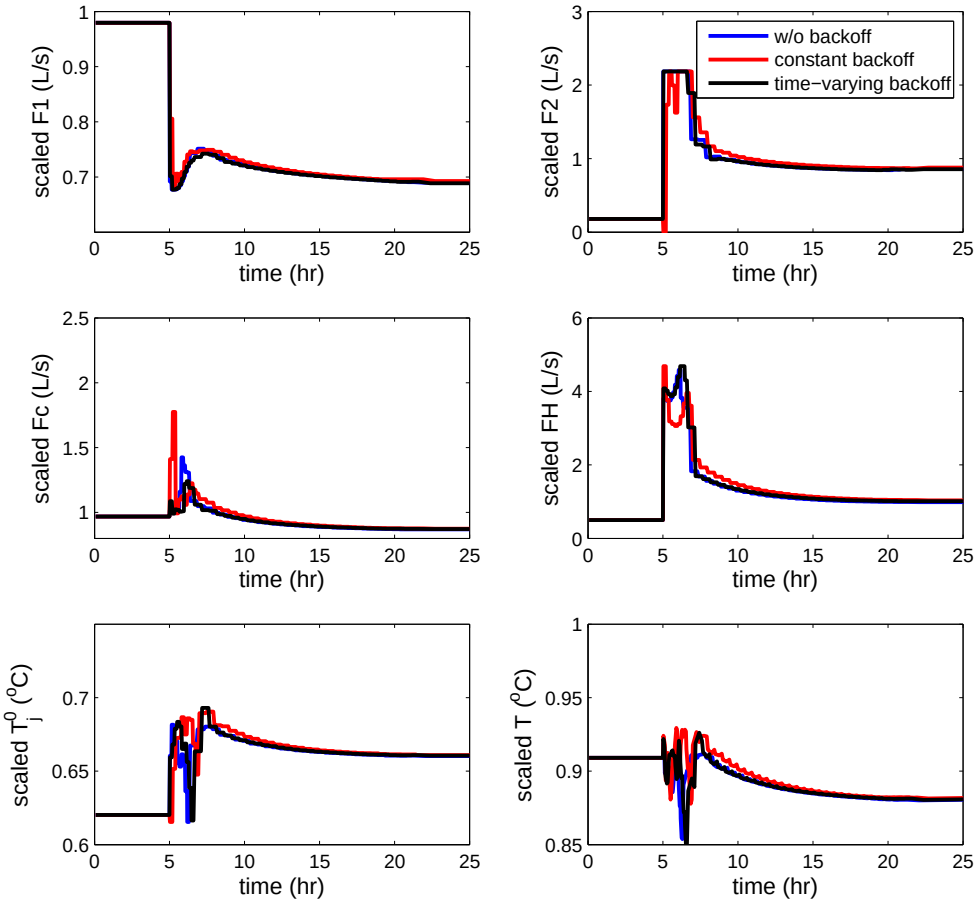

Figure 5.30: Control and temperature profiles with nominal parameter values and no output tracking

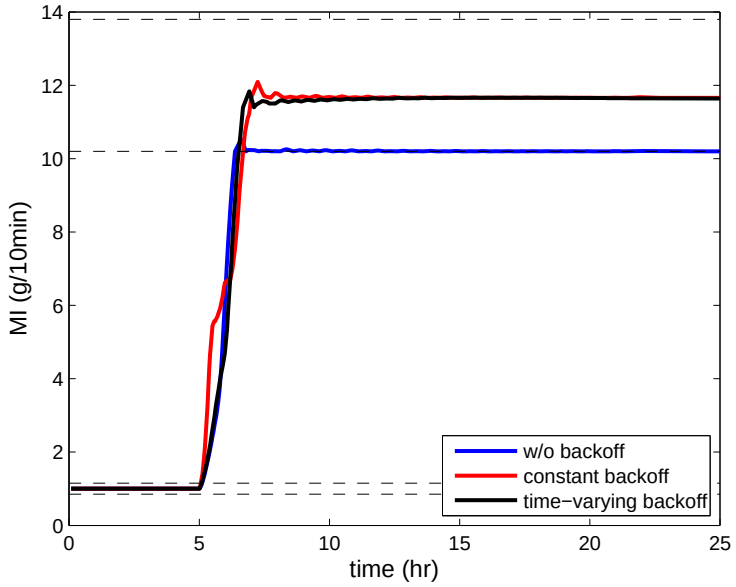

Figure 5.31: MI profiles with nominal parameter values and no output tracking

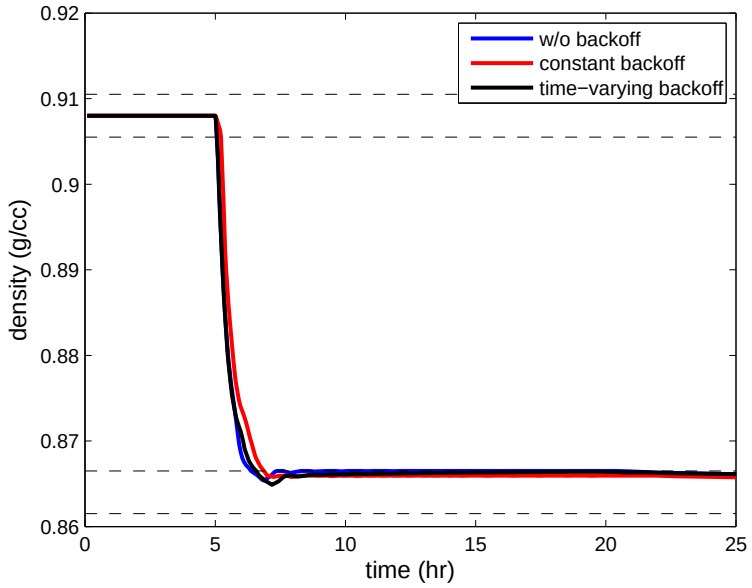

Figure 5.32: Density profiles with nominal parameter values and no output tracking

Monte Carlo simulations are performed with those three control policies shown in Figure 5.30. As mentioned above, without output tracking the nominal solution

stays at the boundary and leaves no safety margin. Therefore, it leads to trouble if uncertainties or disturbances exist. Figures 5.33 and 5.34 show severe constraint violations in about half of the simulation runs.

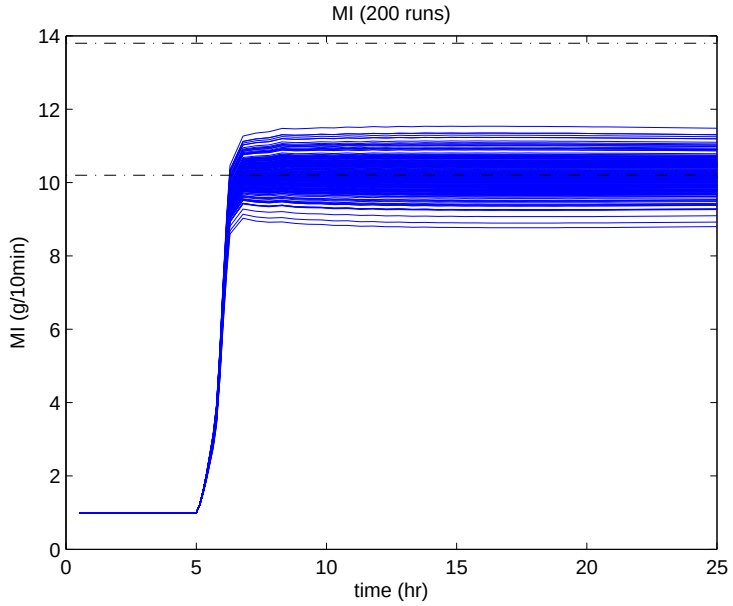

Figure 5.33: Monte Carlo simulations of MI with $m = 200$ (nominal optimal and no output tracking)

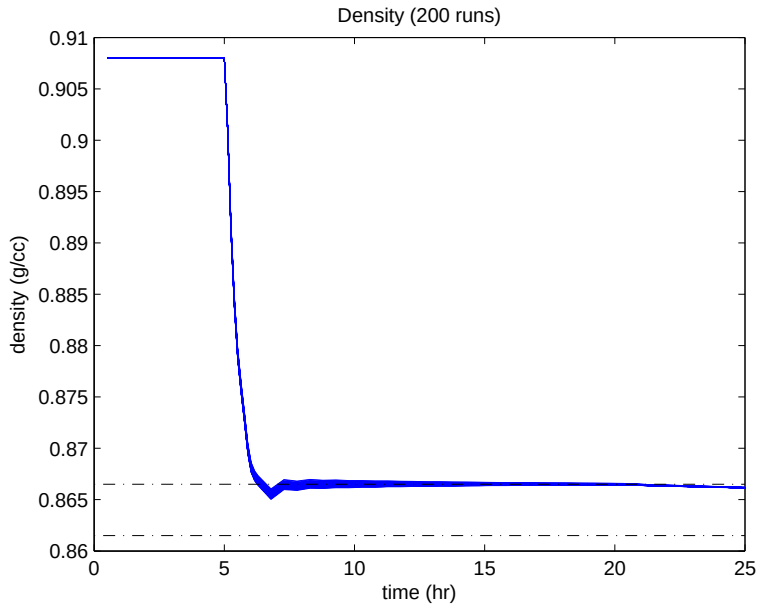

Figure 5.34: Monte Carlo simulations of density with $m = 200$ (nominal optimal and no output tracking)

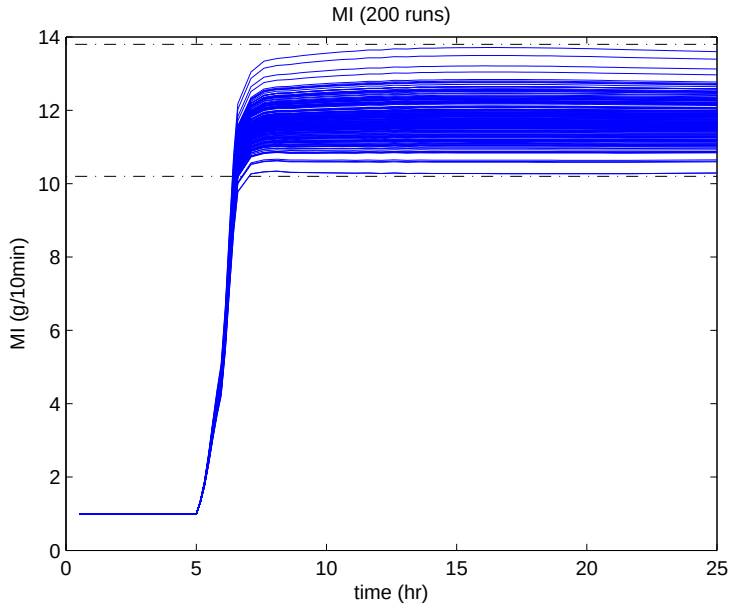

Figure 5.35: Monte Carlo simulations of MI with $m = 200$ (time-varying back-offs and no output tracking)

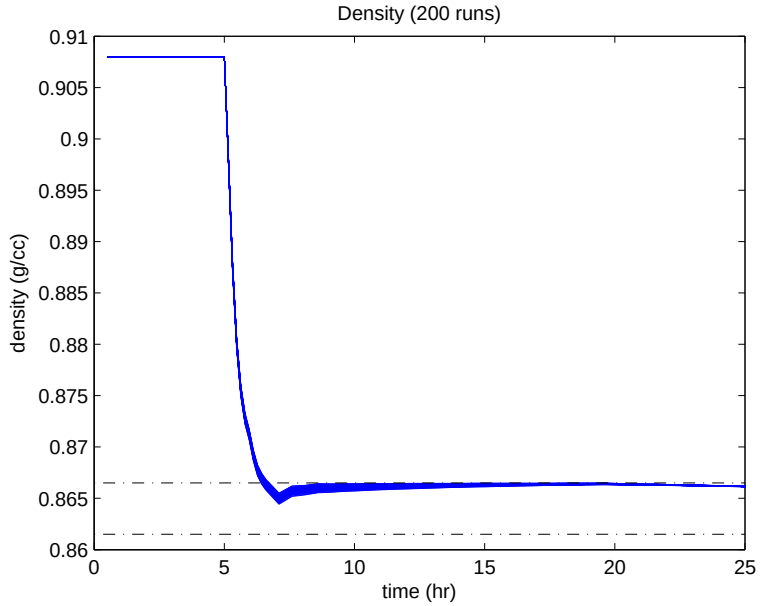

Figure 5.36: Monte Carlo simulations of density with $m = 200$(time-varying back-offs and no output tracking)

With time-varying (or constant) back-offs incorporated in the optimization prob-

lem, the disadvantages of neglecting the output tracking term are greatly compensated. As shown in Figure 5.35 and 5.36, all uncertainty scenarios can finish transition and enter the specification band at 2.03 hours.

From another point of view, the output tracking term is not only useful for driving the output profiles to the center of the spec, but also beneficial to the process robustness.

5.4.5 Handling Multiple Uncertainties

The number of uncertain parameters in the system is always a challenge to optimization under uncertainty. Instead of adding extra equations or sensitivity calculations in the optimization model, our current approach can be easily extended to cases with multiple uncertainties. In order to obtain a certain approximation accuracy of the probabilistic distribution of the response, the Monte Carlo simulation requires a larger number of runs in the cases with multiple uncertainties. Fortunately, the proposed flowchart is still valid and easy to follow; the only change happens in the Monte Carlo simulation during which random samples are drawn from either correlated or uncorrelated probabilistic density functions.

To demonstrate the effectiveness, a case study with two uncorrelated uncertain parameters is performed. Beside the uncertain catalyst deactivation rate, the chain transfer rate to hydrogen (K_{cH}) is also considered as uncertain parameters in this case. Following the procedure in Figure 5.1, we obtain the figures below.

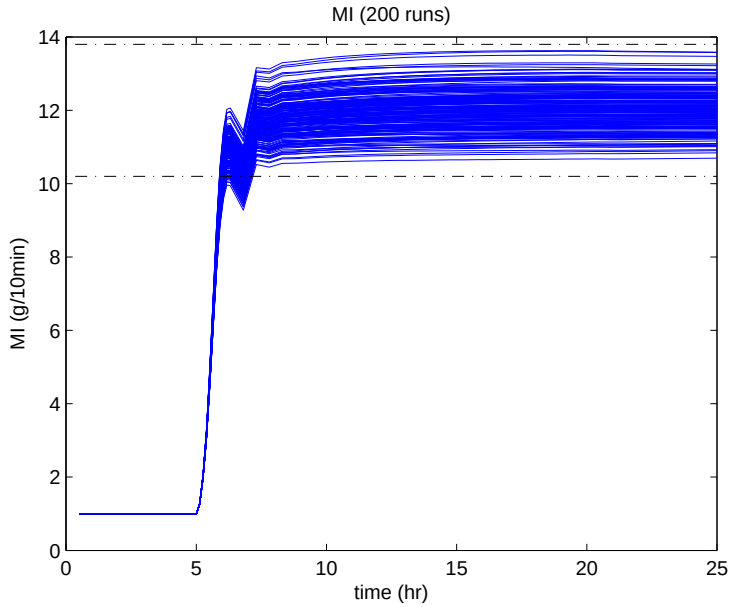

Figure 5.37: Monte Carlo simulations of MI with $m = 200$ (nominal optimal and multiple uncertain parameters)

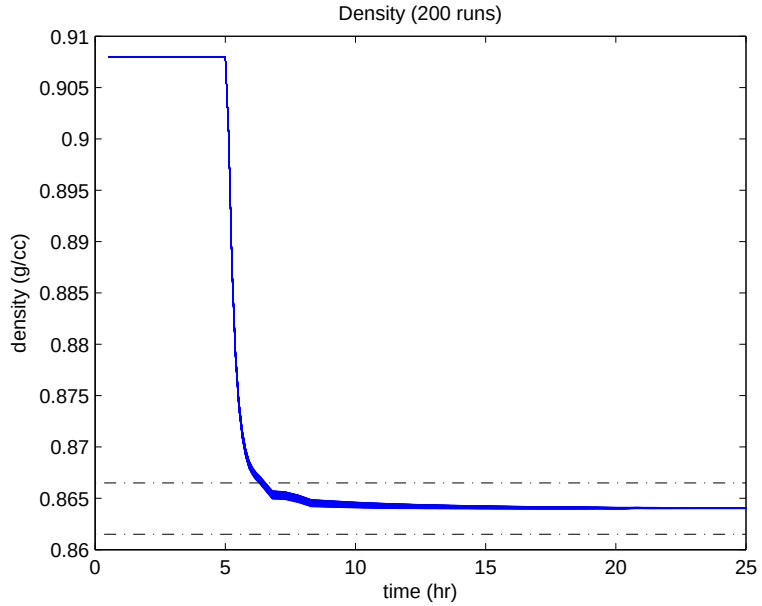

Figure 5.38: Monte Carlo simulations of density with $m = 200$ (nominal optimal and multiple uncertain parameters)

As additional uncertain parameters are considered in the process, the standard

deviation calculated from Monte Carlo simulation increases and thus the back-off terms become larger. Other than this point, it is hard to distinguish between the multiple uncertainty case and the single uncertainty case based on the Monte Carlo simulation results; the resulting back-offs are similar in both cases.

The simulation results with time-varying back-offs are shown in Figure 5.39 and 5.40.

Note that we still use 200 runs in the Monte Carlo simulation, $m = 200$, as it is sufficient to capture the probabilistic distribution of the output variables. For more detailed analysis on the required number of sampling in Monte Carlo simulation, please refer to [24].

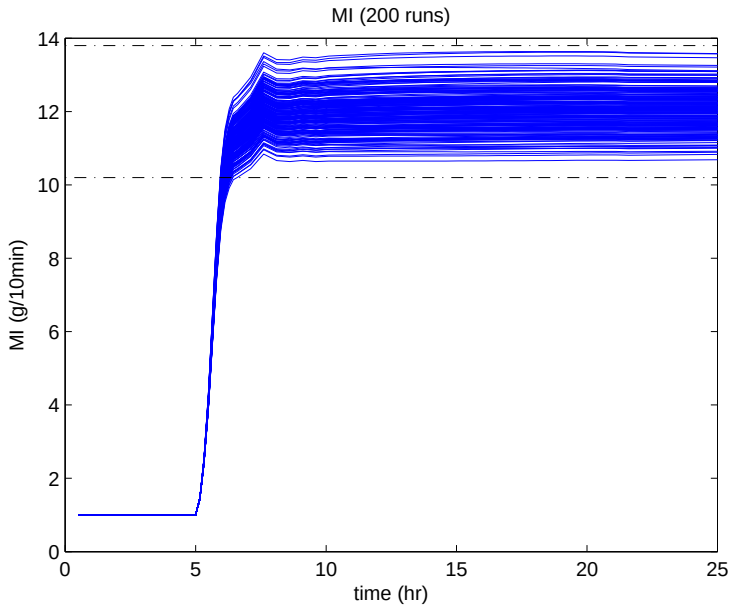

Figure 5.39: Monte Carlo simulations of MI with $m = 200$ (time-varying back-offs and multiple uncertain parameters)

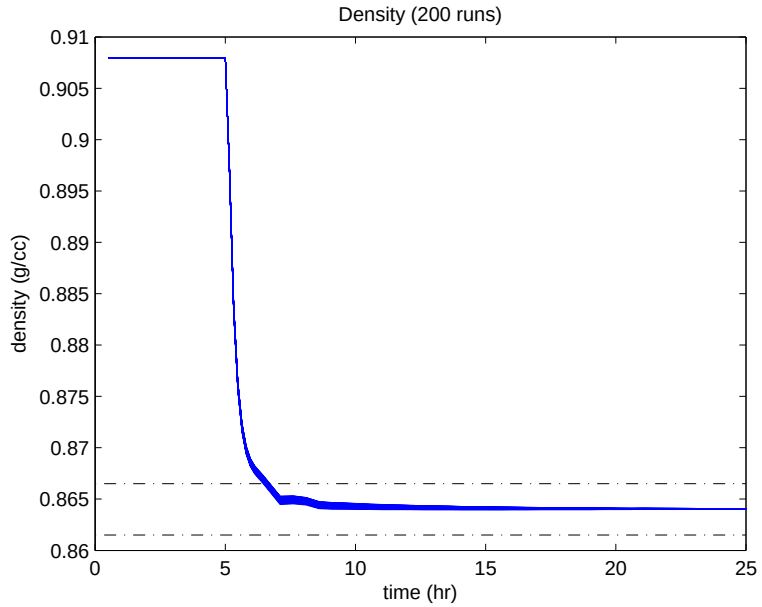

Figure 5.40: Monte Carlo simulations of density with $m = 200$ (time-varying backoffs and multiple uncertain parameters)

Optimal solution and performance obtained from all the case studies are summarized in Table 6.2.

Case	Setting	Transition Time (hour)			
		w/o backoff		Time-varying b_c	
		N	W	N	W
Original	$\gamma = 20$	1.39	infinite	1.59	1.95
Large regularization	$\gamma = 2$	1.49	infinite	1.71	2.15
Small regularizaiion	$\gamma = 200$	1.38	1.56	1.60	1.72
No output tracking	$w_{MI} = w_\rho = 0$	1.37	infinite	1.57	2.18
Multiple uncertainty	$2\%K_{cH}, 5\%K_d$	1.39	2.18	1.59	1.71

Table 5.4: Summary of the optimal solution and performance under uncertainty in all case studies. N: nominal uncertainty level, W: worst-case scenario in Monte Carlo simulation.

5.5 Concluding Remarks

System uncertainties have a huge impact on the process performance; control policies generated without considering this issue may deteriorate in the presence of uncertainty. Stochastic programming and robust optimization are two candidate methods for tackling optimization problems under uncertainty. Although a great number of studies have been conducted to better solve this type of problem, they suffer from either intricate derivation or heavy computational burdens. This issue becomes a bottleneck for the large-scale optimization problem, which is challenging itself even when only nominal uncertainty level is considered. The concept of back-off is preferred here because it can maintain the problem size at an acceptable level.

In this study, Monte Carlo simulation is applied and the robust solutions with constant back-offs and time-varying back-offs are evaluated. The effectiveness and the robustness of this formulation are demonstrated using an industrial example. In addition, we reported the computational performance and the transition time. As mentioned in the previous discussion, four key points should be re-emphasized: 1) the use of back-off constraints results in slightly longer transition time at nominal uncertainty level, but it effectively avoids violating constraints under uncertainty; 2) since the back-off constraints do not change the size of the model, the computational burden when considering uncertainties is well-maintained at an acceptable level; 3) the relaxed formulation with time-varying back-offs is proposed based on the change of standard deviation over time, which also reflects sensitivity at different status; 4) the iterative approach applied to back-off terms in the case study shows fast convergence.

In addition, three complementary studies are conducted to assess the influence of regularization, output tracking and multiple uncertainties. The first two cases provide valuable information and guidance on the choice of objective function and

the determination of weighting factors in future applications. The last one demonstrates the effectiveness of the proposed approach when more than one uncertain parameter is present in the system.

In addition to advantages mentioned above, another key point should also be discussed. The first column in Table 5.3 shows the increase of transition time when back-off constraints are used. Although the time-varying back-off provides a shorter transition time, the loss due to the incorporation of conservative back-offs and the lack of measurement is still not negligible.

The back-off constraint is relatively conservative compared to other measurement-based schemes. Therefore for future work, we will extend the current offline work to online implementation with measurements and other disturbances considered. For the polyethylene solution polymerization process considered in this chapter, there are several measurements and model predictions in place which can reflect the system status. Those valuable measurements might be further utilized to better approximate the back-off terms. Moreover, state and parameter estimation will be taken into account such that the system status, as well as the parameters, can get updated online.

Another research direction which is out of the scope of this project but of interest to many researchers is the sampling technique. When several uncertainty sources are taken into account in the Monte Carlo simulation, fast and efficient sampling techniques are of great importance and should be treated with care.

Chapter 6

Online Optimization and Control

From Chapter 3 to Chapter 5, our model-based optimization framework of grade transitions is extended with more features and advanced optimization strategies. In Chapter 4, the offline optimization formulations are developed for different specifications. The multistage optimization formulation is more advantageous in the sense that it effectively deals with product specification bands and leads to relatively more aggressive control policies. Then in Chapter 5, the aggressive control profiles are hedged by introducing back-off constraints in the optimization problem. The resulting output profiles show smaller oscillations and thus leave a safety margin in case uncertainties ruin the control performance. Taken together, these features comprise the real-time optimization layer in the decision-making hierarchy, and thus lay a solid foundation for the development of the advanced control layer.

In this chapter, we take one step closer to the process and concentrate on the model predictive control layer (or advanced control layer). We extend the off-line framework described above to include online state estimation and optimal control of the large-scale grade transition problem. In addition, the multistage optimization formulation enables the consideration of a good economic objective and is adopted to

extend the normal setpoint-tracking NMPC to economic NMPC. The control performance of both NMPC designs with full state measurement will be discussed. The design of state estimator is also mentioned to deal with partial state feedback, and will be further considered as future work in Chapter 7.

It should be noted that some notation changes are made that differ from the previous chapters.

6.1 Background Information

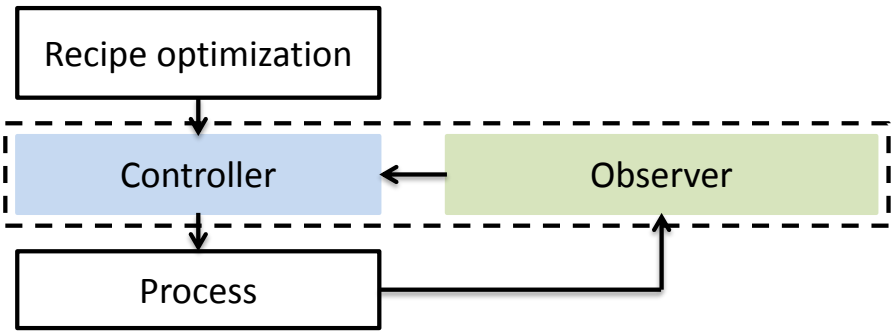

Figure 6.1: Classic control diagram

Figure 6.1 depicts the classic control framework, which consists of two main building blocks: the observer and the controller, as seen in the middle layer.

The top layer is the recipe optimization and its function is to generate optimal operational decisions given tactical decisions made in the scheduling and planning layer. The task is usually performed offline to maximize the profit or the product quality, and various constraints considered at this level involve product schedule, production rate, product quality satisfaction, safety issues, etc. The development of recipe optimization is often considered in the real-time optimization layer and the detailed discussion on this block is presented in Chapter 4 and 5.

Next, the setpoint or the optimal trajectory calculated in recipe optimization is sent

to the middle layer, which interacts directly with the process of interest. The selection of the controller and the observer is determined mainly by the characteristics of the process. Nonlinear Model Predictive Control (NMPC) and Moving Horizon Estimator (MHE) are two advanced control and estimation strategies which are suitable for highly-nonlinear processes with coupled controls and various constraints in the form of path constraints, end-point constraints and variable bounds.

6.1.1 Nonlinear Model Predictive Control and Economic NMPC

In recent years, more and more applications adopt model predictive control and benefit from it [81]. (N)MPC uses a dynamic model of the process to predict the future dynamic behavior over a time horizon and make optimal control actions. It is advantageous in the following three aspects compared to classical controllers:

1. It handles multi-input-multi-output systems without decoupling, which might be difficult to perform when the number of controls and outputs becomes large or when the process itself is complex and has highly coupled variables.
2. It imposes constraints and variable bounds.
3. NMPC based on the first-principle dynamic model reflects the behavior of highly nonlinear processes and deals with frequent transitions or other transient behaviors.

Meanwhile, the development of NMPC drives the need for detailed, accurate nonlinear dynamic models and efficient optimization strategies to handle computational complexities. Research directions for enabling fast, efficient execution of NMPC can be categorized as:

1. Simplify or reduce the first-principle model;
2. Improve nonlinear programming solvers for large-scale problems;
3. Develop fast NMPC strategies which utilize sensitivity information or paral-

lel computing to reduce the heavy computational burden for solving nonlinear dynamic optimization problems [32, 76, 79, 83].

Advances in these directions efficiently address the obstacles of applying NMPC online in different areas and promote its adoption in large-scale, highly-nonlinear processes.

On the other hand, economic objectives and process disturbances are isolated in two layers in the classical control framework; the economical consideration is usually managed solely in the real-time optimization layer while NMPC tries to track the trajectory and reject disturbances. Such a framework has a few drawbacks. First, the optimal setpoints/trajectories generated in the RTO layer can not guarantee economical optimality in the presence of disturbances. Also, model inconsistency between the steady-state model in RTO layer and the dynamic model in NMPC layer may lead to infeasible solutions. In recent decades, economic NMPC has attracted many researchers' attention as it integrates these two layers and optimizes economic objectives with the influence of process disturbances considered. The economic NMPC scheme can be illustrated in Figure. 6.2.

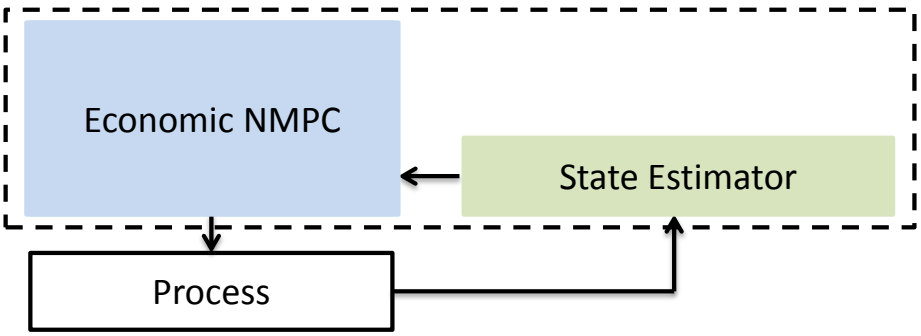

Figure 6.2: Economic control diagram

To solve the dynamic optimization problem considered in NMPC, dynamic optimization strategies mentioned in Chapter 2 are applied. The dynamics of the plant

can be described as

$$x(k+1) = f(x(k), u(k), p) \tag{6.1}$$

where $x(k)$ is the plant state at time t_k, $u(k)$ is the control input at time t_k and p are the uncertain parameters in the system with nominal value $\bar{p}$. Here we consider the NLP problem for NMPC converted from the dynamic optimization problem at time t_k as

$$\begin{aligned} \min_{z_l, v_l} \quad & J \\ s.t. \quad & z_{l+1} = f(z_l, v_l, \bar{p}),\ l = 0, ..., N-1 \\ & y_l = g(z_l, v_l, \bar{p}),\ l = 0, ..., N \\ & h(z_l, v_l, \bar{p}) \leq 0,\ l = 0, ..., N \\ & z_0 = x(k),\ z_N \in \mathbb{X} \\ & z_l \in \mathbb{X},\ y_l \in \mathbb{Y},\ v_l \in \mathbb{U}, \end{aligned} \tag{6.2}$$

where z_l are predicted values of the states $x(k+1)$, v_l are predicted values of control inputs $u(k+1)$, y_l are predicted outputs, and N is the horizon length.

The objective function J represents either the setpoint tracking or the economic objective in terms of z_l and v_l. In the standard setpoint tracking NMPC, terminal cost Ψ and the stage cost ψ are included in the objective function as follows:

$$J = \Psi(z_N) + \sum_{l=0}^{N-1} \psi(z_l, v_l). \tag{6.3}$$

On the other hand, the economic NMPC directly minimizes the economic cost and may lead to unstable performance. One way to stabilize is adding a setpoint tracking term in the economic objective function [32]. The weight on the setpoint tracking term is carefully selected such that both the economic objective and the stability are adequately addressed.

6.1.2 State Estimation and Moving Horizon Estimation

The controller can not stand alone without the support of observers or state estimators; without accurate measurements of process status, the control action is not solid nor convincing. In the framework we consider, NMPC makes optimal control decisions based on the current status of the process. However, not all the states can be measured. Even for these measured states, such as temperature or concentration that have a sensor in place, the measurement obtained from a certain sensor might be colored with measurement noise or may also be delayed. In order to provide accurate estimates of the unmeasured states, state estimation is required. The goal of state estimation is to recover/estimate the state of the process based on limited input and output information [57, 80].

Some commonly used state estimators are Extended Kalman Filter (EKF), Unscented Kalman Filter (UKF), and Moving Horizon Estimation (MHE). Compared to other state estimators, MHE can be formulated directly as an NLP problem and thus it is capable of handling variable bounds efficiently.

Typically, MHE problem is formulated as

$$\begin{aligned} \min_{z_{k-N},\ldots,z_k} \quad & \Phi(z_{k-N}) + \sum_{l=k-N}^{k-1} w_l^T Q_l^{-1} w_l + \sum_{l=k-N}^{k} v_l^T R_l^{-1} v_l \\ s.t. \quad & z_{l+1} = f(z_l, u_l, \bar{p}) + w_l \\ & y_l = g(z_l, u_l, \bar{p})) + v_l \\ & z_l \in \mathbb{X}, l = k-N, \ldots, k \end{aligned} \tag{6.4}$$

where z_l are the state estimates, y_l are the outputs, v_l represent measurement noises and w_l for state disturbances. The objective function includes the arrival cost Φ, minimization of process noise and measurement noise. Q_l is the covariance matrix of the unknown disturbances and R_l is the covariance matrix of the measurement noise. An important assumption made in the formulation is that both w_l and v_l are white noise; they have zero means and follow Gaussian distribution.

6.2 Model-based Online Optimization Framework for Grade Transitions

For batch processes or grade transitions in a continuous process, the entire time horizon considered in the control problem has a finite time window. Based on this setting, Jung *et al.* propose an online optimization framework with shrinking horizon nonlinear model predictive control (*sh*-NMPC) and expanding horizon least squares estimation (*eh*-LSE). The framework is tested on a semi-batch polymerization process; efficient computational statistics and good control performance are shown in the presence of measurement noise. In this section, we discuss the framework in detail using the grade transition problem in polyethylene solution polymerization processes as an example and extend it to consider large parametric uncertainties. Figure 6.3 illustrates the online framework with estimation horizon equal to 2 and control horizon equal to 3 at time step $k = 2$.

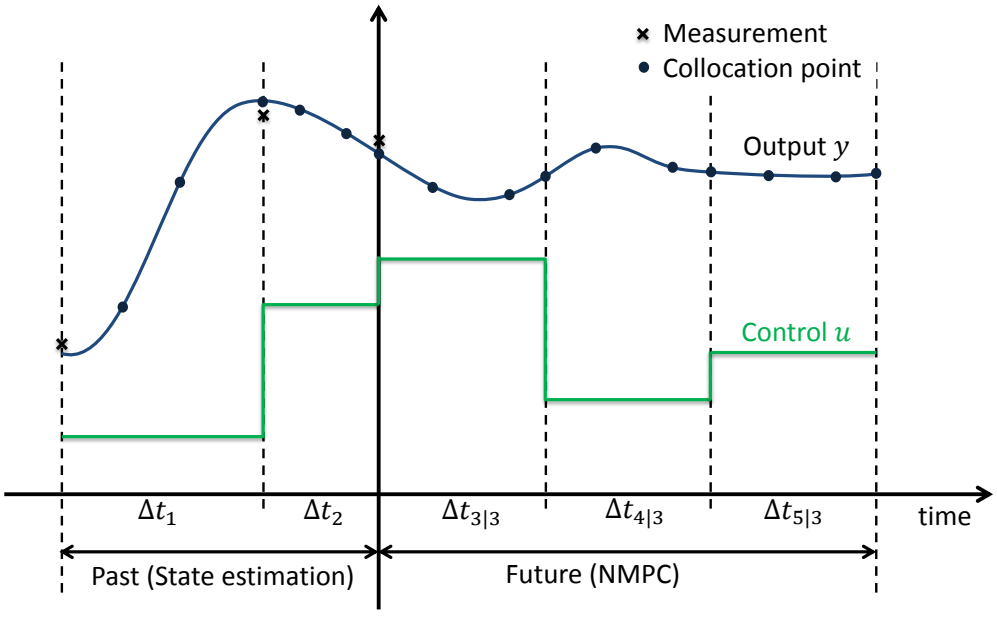

Figure 6.3: Online framework with shrinking horizon NMPC and expanding horizon LSE

Two key components of the framework are state estimator and model predictive controller; both components incorporate the rigorous dynamic model we developed in our previous work and rely on efficient NLP solvers to solve. First, *sh*-NMPC is applied to minimize transition time and off-grade product, and to refine the control schemes. As time proceeds, the control horizon shrinks, fewer finite elements and thus fewer control decisions are considered in the controller. Next, *eh*-LSE is designed to provide state estimates based on measurements in the past. The expanding horizon scheme minimizes the information loss by considering all the measurement data in the past. As a result, the estimation horizon increases and the state estimate is expected to be more accurate with adequate information revealing the system status.

In this chapter, we mainly focus on the design of NMPC. Several modifications are made based on the standard NMPC problem (6.2):

1. To ensure more stable and less oscillatory control behavior, a regularization term is incorporated in the multistage objective, as discussed in Chapter 4.

2. To handle parametric uncertainties, we adopt the back-off constraint in the NMPC problem.

3. To ensure feasibility of the online problem, relaxation of the inequality constraints is introduced and a penalty term is minimized in the objective function.

4. To minimize the grade transition time using multistage formulation, length of each stage is also treated as a decision variable. As the number of finite element in each stage is fixed and the elements are evenly distributed in the stage, variable element length h is equivalent to variable stage length in the following case study.

The resulting NMPC formulation after modification is represented as

$$\begin{aligned} \min_{z_l, v_l} \quad & J + \mu P \\ s.t. \quad & z_{l+1} = f(z_l, v_l, \bar{p}),\ l = 0, ..., N-1 \\ & y_l = g(z_l, v_l, \bar{p}),\ l = 0, ..., N \\ & h(z_l, v_l, \bar{p}) + b_c \leq P,\ l = 0, ..., N \\ & z_0 = x(k),\ z_N \in \mathbb{X} \\ & z_l \in \mathbb{X},\ y_l \in \mathbb{Y},\ v_l \in \mathbb{U} \end{aligned} \tag{6.5}$$

where b_c is the back-off term, P is a vector of slack variables and μ is an adjustable constant weighting factor on the penalty term. The construction of economic objective function J can be found in Problem (4.5) and the penalty term is added to ensure solutions of Problem (6.2).

In short, the proposed online optimization framework solves two slightly different NLP problems repeatedly. At each time step, process measurements obtained from the beginning of the transition to the current time are obtained and used in *eh*-LSE optimization problem. The resulting state estimates serve as the initial value of an updated NMPC problem, which is then solved to reduce the overall transition time and the off-grade product. The resulting control scheme is also applied to the system at each time step so that new measurements are added. The effectiveness of the framework is demonstrated by case studies in which uncertainties, measurement errors and disturbances are taken into account.

6.3 Case Study

In this section, we apply the proposed framework on online optimization and control of the polyethylene solution polymerization process as discussed in the previous chapter. In addition to the controller and the state estimator, the actual process is also represented by the dynamic process model as developed in Chapter

3, with slight modifications to include parametric uncertainties, disturbances and measurement noise in the process simulation.

6.3.1 Problem Settings

The two grades of polyethylene and their corresponding operation conditions are summarized in Table 4.1. The setting of the weighting factors in the objective function and discretization grid can be found in Section 4.3.

In addition, random disturbances are added to all the states which directly reflect physical states of the process. This includes concentrations of all species in the reactor, reactor temperature, jacket temperature, as well as the $0th$ moments. The $1st$ and the $2nd$ moments are excluded since the influence of disturbances on polymer chains is reflected in the $0th$ moments and thus is passed to the higher order moments. The concentration in the recycle streams is not subject to disturbances because they are fictional states used to approximate the actual state with long time delay. The random disturbance is assumed to be white noise, which takes samples from Gaussian distribution with zero mean. Its magnitude is bounded within 1% of the nominal state value (3% in the last case which tests the control performance in the presence of greater disturbances).

For the parametric uncertainty, similar setting as presented in Chapter 5 is used; the lumped rate constant for chain deactivation is considered as uncertain and it is assumed to vary within 5% of the nominal value.

At current stage, we assume all the states are perfectly known (i.e. they can be measured accurately with no time delay) and focus on the development of different types of control schemes: 1) standard setpoint-tracking NMPC which utilizes the single stage formulation as shown in Problem (4.4), 2) economic NMPC based on the multistage optimization formulation without back-off constraints as seen in Problem (5.13), and 3) economic NMPC with back-off constraints. The single stage

formulation minimizes the time-integral of the squared deviation of current states and outputs from their setpoints, while the multistage formulation has variable finite elements and is capable of directly minimizing the economic objective, *i.e.* transition time in the current grade transition problem. The economic objective can also be extended to minimization of off-grade production or economic cost as demonstrated in Chapter 4.

All computations for the subsequent case studies are performed using NLP solver CONOPT in GAMS 24.0.2, on a desktop with Intel® Core^{TM} i7 CPU @ 2.80 GHZ and 9.00 GB memory.

6.3.2 Adjustable Back-off Constraints

In the previous section, we discussed several modifications aiming at improving either the economic objective or the computational performance of the standard NMPC. In short, there are two modifications applied to ensure the feasibility and the convergence of the NLP problem: 1) non-negative slack variables are introduced to convert original constraints to soft constraints, and the penalty of relaxing the constraint is minimized in the objective function [6]; 2) variable stage length in the NLP problem helps ensure constraint satisfaction and optimizes the objective [33].

However, artificial lower and upper bounds should be assigned for variable stage lengths. The determination of both upper and lower bounds strongly influences control performance. In Figures 6.4 and 6.5, we test the control performance of economic NMPC with back-off constraints and three different upper bounds for variable finite elements h (unit in second): $h \leq 7200$, $h \leq 3600$ and $h \leq 1900$. The initial guess of all the elements is $h = 1800$. 1% state disturbances and 5% parametric uncertainty are assumed. The interval between two markers in the same curve in both plots represents the resulting stage length. Here, the resulting element length

always hits its upper bound, and larger deviation of MI from the center target is observed in the case with longer stages. This is in accordance with our expectation that less frequent control actions degrade the overall control performance.

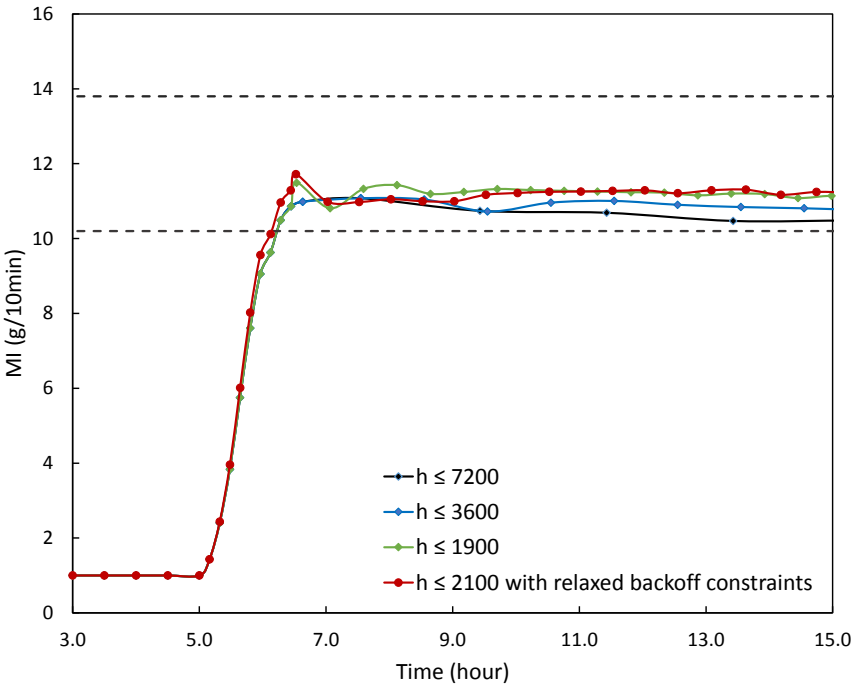

Figure 6.4: MI performance with different upper bound for finite element length, 1% disturbance and 5% parametric uncertainty

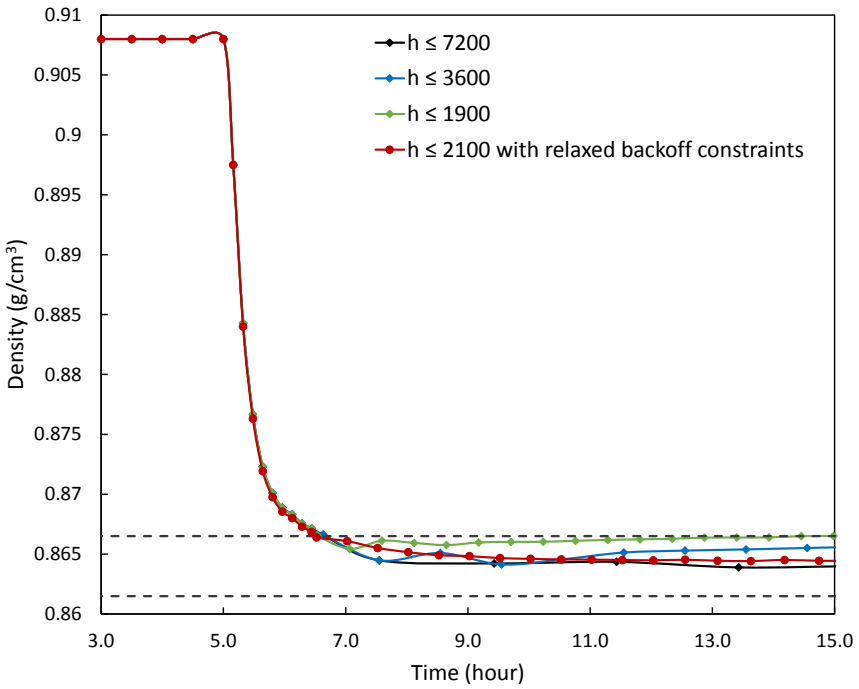

Figure 6.5: Density performance with different upper bound for finite element length, 1% disturbance and 5% parametric uncertainty

The phenomena that stage lengths reach the upper bound is not accidental. In the multistage formulation, the transition time is defined as the duration of the first two stages which are minimized. When the controller proceeds to the third stage, the minimization of time is no longer addressed directly in the objective function. Instead, the program tries to reduce the penalty for soft constraints, which results in the need for longer stage lengths, especially in cases with back-off constraints. To conclude, the idea of variable stage length guarantees constraint feasibility at the cost of control performance.

Another issue is nonzero slacks related to the soft constraints. Although soft constraints help the convergence of the NLP problem, the existence of positive slacks in the solution may result in infeasible solutions of the original problem. As can be seen in Figure 6.5, the solution of the case $h \leq 1900$ is close to the upper bound of the specification band, and the corresponding slack variables are nonzero. For the

case which enforces tight back-off constraints, the presence of nonzero slacks can easily cancel out the effect of back-offs and generate solutions that are vulnerable to uncertainty and disturbances.

Based on these observations, an adjustable relaxation of the back-off constraint is proposed to avoid long stage lengths and nonzero slacks while maintaining problem feasibility. During the online execution of economic NMPC with back-offs, the model prediction from the previous run and the new measurement are compared. If the difference between the prediction and the measurement is large, relaxation of back-offs in the next NLP problem is activated. For this particular NLP problem, the back-off constraint in the first finite element is relaxed; η is reduced from 3 to 1 in Eqn. (5.10). Meanwhile, the size of the back-off term remains at the designed level in the subsequent finite elements.

Two output profiles obtained from the proposed scheme are presented in Figure 6.4 and 6.5. Clearly, better control performance is achieved as both curves go deeper inside the specification band. The upper bound of the element length is set to 2100, but it is never reached. Moreover, all the resulting slack variables are zero. Detailed computational statistics can be found in Table 6.1. All these cases have the same number of constraints and variables, and the computational time is comparable. The relaxation of back-offs produces the best control performance among these cases within the least CPU time.

	Problem size: Const.(Var.)		CPU time (s)	
	Largest	Smallest	Average	Worst
$h \leq 7200$	159,713 (159,181)	29,963 (29,847)	41.84	317.46
$h \leq 3600$	159,713 (159,181)	29,963 (29,847)	41.85	151.84
$h \leq 1900$	159,713 (159,181)	29,963 (29,847)	53.27	290.33
$h \leq 2100^*$	159,713 (159,181)	29,963 (29,847)	36.02	133.35

Table 6.1: Influence of upper bound of element length and relaxed back-off constraints on computational time (*last case with relaxed back-off constraints)

As explained above, the back-off constraint tightens the feasible region and calls for longer stages. At the same time, the stage length is not minimized directly in the objective function. The combined action produces long stages together with poor control performance. The proposed modification is especially useful in the multistage formulation with back-off constraints. In the following case studies, this modification is adopted to facilitate the solution of economic NMPC with back-offs.

6.3.3 Case Study with No Parametric Uncertainty

Enhanced by the proposed modification, the economic NMPC with back-off constraints is compared with the other two control designs, *i.e.* setpoint-tracking NMPC and economic NMPC without back-off constraints. In this section, we assume that only state disturbances exist in the actual system and the model is representing the process with no model mismatch or parametric uncertainty.

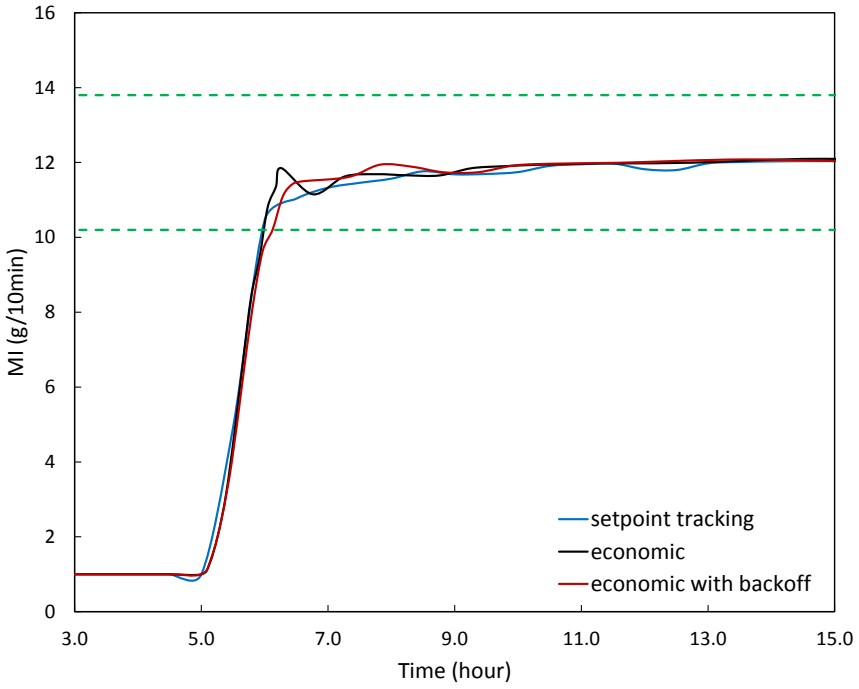

Figure 6.6: MI online performance with 1% disturbance and no parametric uncertainty

The comparison of three control designs is shown in Figures 6.6 and 6.7. In both figures, three curves obtained from setpoint-tracking NMPC, economic NMPC and robust economic NMPC are plotted. Both MI and density profiles reach the center of the specification band no matter which controller is applied, which indicates that the process with only small state disturbances can be well controlled.

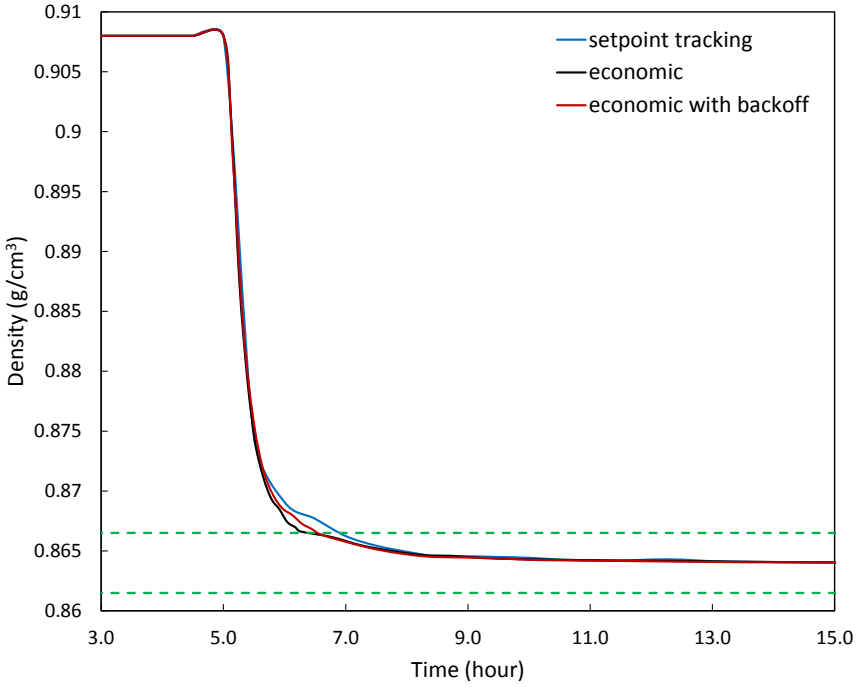

Figure 6.7: Density online performance with 1% disturbance and no parametric uncertainty

As seen in Table 6.2, both economic NMPC and robust economic NMPC lead to shorter transition time (1.40 hr and 1.56 hr) compared to setpoint-tracking NMPC (1.91 hr). The setpoint-tracking NMPC minimizes the deviation from the setpoint/trajectory only and it is not capable of handling economic objectives. Because of this, it loses the ability to explore the entire domain of decision variables or the power of taking advantage of specification bands. On the contrary, economic NMPC fully exploits the degree of freedom in the problem and results in oscillatory profiles that yield better economic benefits.

In addition, since there is no parametric uncertainty in the system, the addition of back-off constraints offers no benefit. It slows down the transition as tightened constraints are considered in the problem.

	Case with 1% disturbance, no parametric uncertainty				
	Transition	Problem size: Const.(Var.)		CPU time(s)	
	time(hr)	Largest	Smallest	Average	Worst
Tracking	1.91	158,881(158,833)	29,791(29,782)	18.35	130.81
Economic w/o b_c	1.40	159,713(159,181)	29,963(29,847)	19.42	86.36
Economic w/ b_c	1.56	159,713(159,181)	29,963(29,847)	26.21	123.93
	Case with 1% disturbance, 5% parametric uncertainty				
	Transition	Problem size: Const.(Var.)		CPU time(s)	
	time(hr)	Largest	Smallest	Average	Worst
Tracking	2.14	158,881(158,833)	29,791(29,782)	109.25	475.26
Economic w/o b_c	1.81	159,713(159,181)	29,963(29,847)	109.12	806.06
Economic w/ b_c	1.50	159,713(159,181)	29,963(29,847)	36.02	133.35
	Case with 3% disturbance, 5% parametric uncertainty				
	Transition	Problem size: Const.(Var.)		CPU time(s)	
	time(hr)	Largest	Smallest	Average	Worst
Tracking	2.15	158,881(158,833)	29,791(29,782)	100.41	521.245
Economic w/o b_c	2.73	159,713(159,181)	29,963(29,847)	46.29	377.76
Economic w/ b_c	1.51	159,713(159,181)	29,963(29,847)	53.86	585.425

Table 6.2: Summary of online implementation results. Tracking in first column stands for setpoint-tracking NMPC, Economic w/o b_c for economic NMPC without back-off constraints, and Economic w/ b_c for economic NMPC with back-off constraints.

6.3.4 Case Study with Parametric Uncertainty

Now we take parametric uncertainty into consideration. Assume the actual deactivation rate is 1.05 times of its nominal value. The three controllers are again applied to control the same transition, and the resulting MI and density profiles are presented in Figures 6.8 and 6.9.

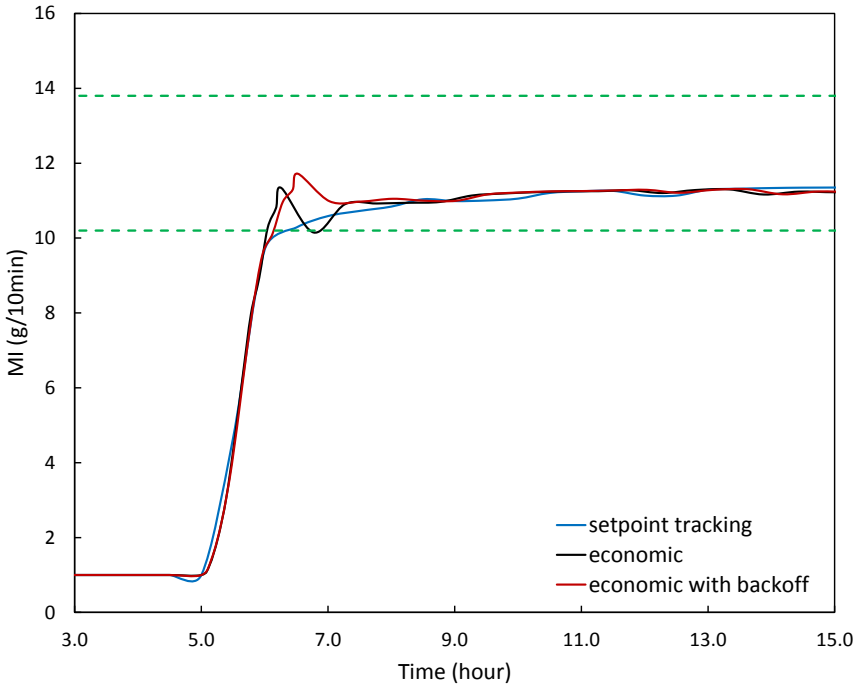

Figure 6.8: MI online performance with 1% disturbance and 5% parametric uncertainty

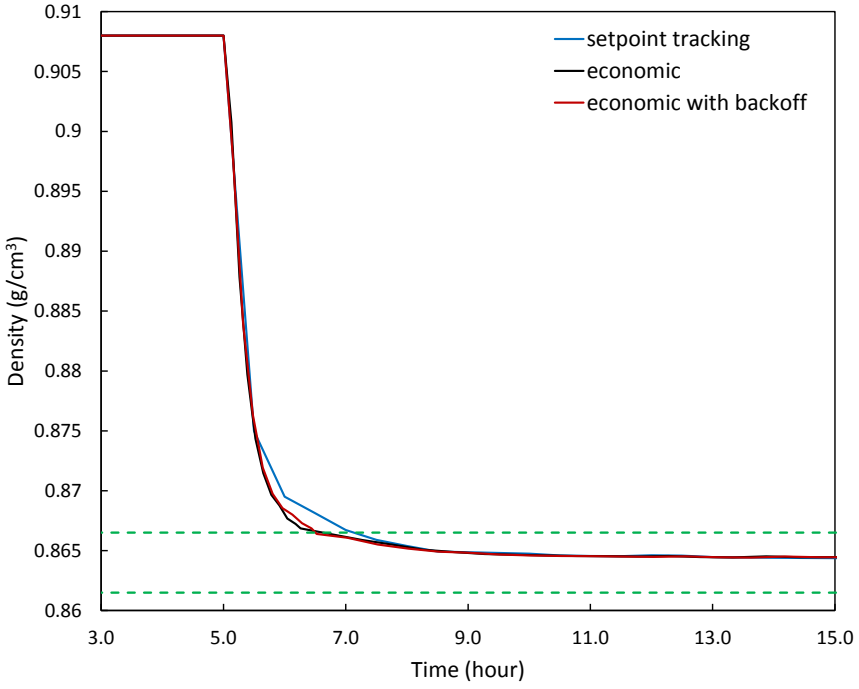

Figure 6.9: Density online performance with 1% disturbance and 5% parametric uncertainty

As shown in these figures, the robust economic NMPC formulation with back-off constraints is able to handle large uncertainties in the system. The MI profile obtained from economic NMPC hits the lower bound when it oscillates inside the specification band. This is caused by the combined influence of an uncertain parameter and process disturbances, and it is not desired as off-grade production as well as the transition time would increase due to the bound violation. After incorporating back-off constraints in the economic NMPC, the magnitude of those oscillations is reduced to leave a safety margin, and the overall curve is pushed deep inside the specification band. Although the transition time may get slightly longer under some uncertainty realizations, the constraint violation is effectively prevented. As a result, the whole system becomes more tolerant of uncertainties.

Different from the previous case with no parametric uncertainty, all the curves in this setting are off the center of the specification band. Parameter estimation or output correction would be required to close the gap between the current model prediction and the actual measurement, which is out of the scope of this work.

6.3.5 Case Study with Increased Disturbance Level

In the last case study, we test the control performance with increased disturbance levels. The influence of state disturbances can be revealed from the oscillatory profiles in Figures 6.10 and 6.11.

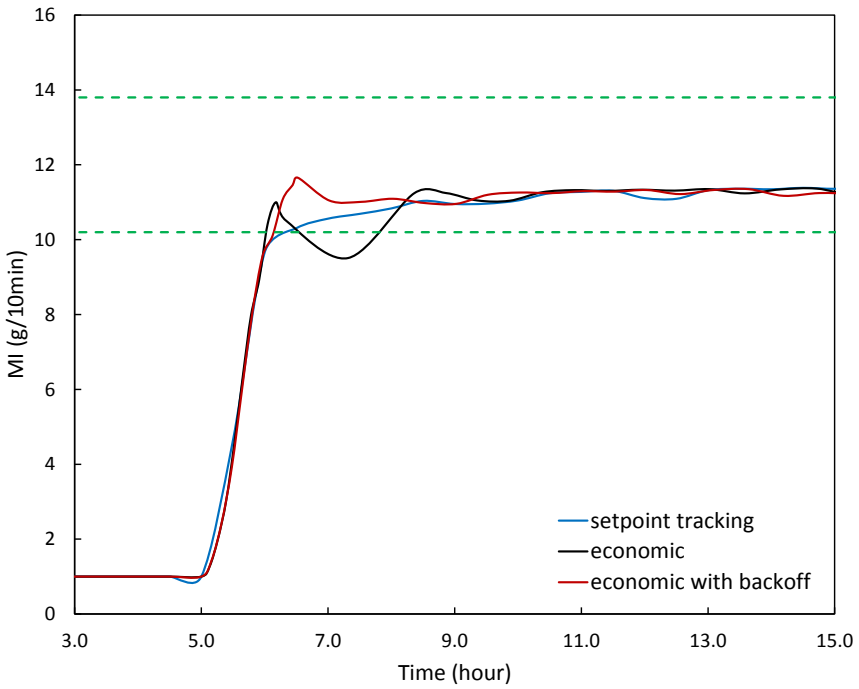

Figure 6.10: MI online performance with 3% disturbance and 5% parametric uncertainty

Similar to previous observations, the resulting profiles are off the center due to the parametric uncertainty. Because the model used in NMPC is different from the actual process, the gap between the output and the center line of its specification band exists and persists.

The nonrobustness of economic NMPC is disclosed in Figure 6.10. A large oscillation violating the lower bound of the specification band is observed and thus the transition time is prolonged. Moreover, the transition time of economic NMPC, as summarized in Table 6.2, is longer than that of the setpoint-tracking case.

The performance of robust economic NMPC is slightly affected by the increased disturbance level, and it results in the best control performance among the three controllers.

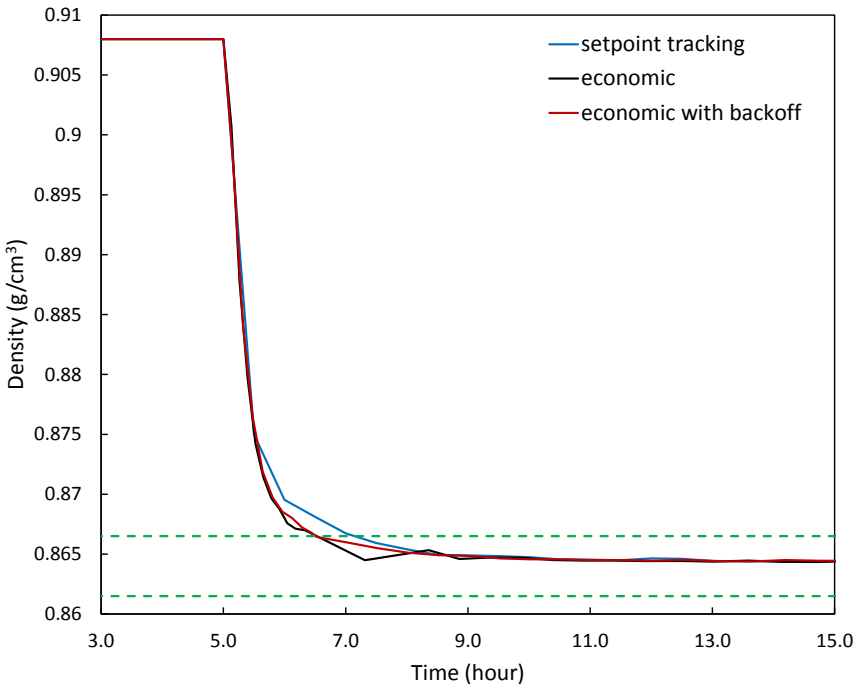

Figure 6.11: Density online performance with 3% disturbance and 5% parametric uncertainty

6.4 Concluding Remarks

In summary, this chapter gives a brief overview of the classic control diagram and discusses model-based online optimization framework and its modifications. The proposed framework features shrinking horizon NMPC and expanding horizon LSE, and three different designs of NMPC are compared. The effectiveness of robust economic NMPC is demonstrated through several case studies of grade transitions in a polyethylene polymerization process.

Some highlights are listed below:

- One highlight of this chapter is the demonstrated effectiveness of economic NMPC. By merging the RTO layer with the advanced control layer, economic NMPC is capable of pursuing the economic objective and maintaining feasible control actions simultaneously in the presence of disturbances.

- Another highlight is the adoption of back-offs empowering the previously aggressive economic NMPC to avoid constraint violations under uncertainties.
- The proposed modification, a relaxation of back-off constraints in the first element, greatly facilitates the solution of NLP problems and yields better control performance without sacrificing computational performance.
- The use of shrinking horizon scheme reduces the size of subsequent NMPC problems and relieves the computational burden to some extent.
- Lastly, we should mention that computationally tractable solutions of these NLP problems are obtained in these case study with the aid of well-initialized NLP problems offline.

For future work, there are several interesting topics that are worth investigating.

First, this chapter deals only with shrinking horizon NMPC and does not include state estimation. In future, an observability analysis should be conducted and then the proposed expanding horizon state estimation needs to be included.

Second, although the NLP problems can be solved quickly, the computational time is not negligible. The delay in state estimation and optimization may give rise to system instability and degrade the control performance. Advanced step NMPC and MHE use sensitivity information to update the control and the estimates, respectively. Therefore, the advanced step strategy should be considered if the proposed framework is applied to the real plant where computational time can not be ignored.

We also note that applying *sh*-NMPC and *eh*-LSE in continuous processes requires switching of controllers once the grade transition is finished. To maintain the process in steady state production mode is easier compared to fast grade transitions, and could be operated with a simplified control and estimation scheme.

Lastly, seeking less conservative robust solutions to the control problem needs to be considered. The current back-off terms are calculated offline using Monte Carlo simulation, and online update of those terms would be an interesting research direction.

Chapter 7

Conclusions

Model-based control and optimization is a well-known strategy for process optimization and control, and an increasing number of applications appear in different disciplines. Although simplified or linearized process models help reduce the required computational resource, the nonlinear dynamic process model is of great importance as it captures detailed dynamic behavior that occurs in the process and provides much more accurate model predictions, especially when the process is highly nonlinear. In this dissertation, we consider grade transitions in polyethylene solution polymerization processes and aim at developing suitable optimization and control strategies for the process. With the support of the advanced dynamic optimization methods, we construct the dynamic process model, propose the multistage optimization formulation, introduce back-off constraints into the optimal control problem and set up the online control and optimization framework at the end. In this chapter, we summarize the result in each chapter and propose some future directions that would be worth investigating.

7.1 Thesis Summary and Contributions

Chapter 1 briefly introduces the decision-making hierarchy and narrows the scope of the dissertation to the two operational decision-making layers: real-time optimization and advanced control. Then the motivating industrial polyethylene polymerization process is described and the current issue with grade transitions is brought up. All the subsequent chapters explain the elements introduced in this chapter in detail. As we can see from the entire dissertation, the methodology developed in this work is inspired and motivated by the industrial application, but is not limited to this single application. Batch or continuous processes with similar needs can also be considered under this framework.

Chapter 2 discusses the most important supporting tool throughout the entire thesis: dynamic optimization approaches. Simultaneous dynamic optimization is explained and the following section provides several methods that solve the resulting nonlinear programming problem. The singular control problem is also addressed in this chapter.

Chapter 3 presents a rigorous mathematical model for the entire flowsheet of the solution polymerization process in a loop reactor, which contains mass and heat balances for depicting the dynamic behavior of the system, moment model to predict product properties, a data-driven surrogate VLE model for monitoring the bubble point pressure, and variable time delay model for modeling variable time delay in the recycle loop. The resulting model is capable of capturing the detailed dynamics of the system. Three novel features of this chapter are:

- A detailed reactor model has been created that includes a moment model that allows product quality to be incorporated directly into the optimization problem. Moreover, this model has been formulated using a simultaneous collocation approach that allows for detailed representation of state and control profiles.

- The solution polymerization process that we consider requires the operating pressure to always remain above the bubble point pressure. This is enforced in our model through non-ideal VLE constraints (with monomers and co-monomers, solvents and polymers) at all points in time. These constraints are facilitated through the development and integration of a surrogate model for non-ideal VLE.

- The grade transition problem considers not just the individual reactor, but the dynamic optimization of the entire plant with liquid and vapor recycles. This also requires consideration of longer time horizons for the grade transition. Moreover, to approximate the transport delay in the recycle streams, a variable time delay must be built into the model. Successful application of such a variable time delay model achieves satisfactory approximation accuracy and appropriate level of detail for the model.

Chapter 4 develops an optimal grade transition approach that incorporates detailed kinetic polymerization models to reflect product properties and specifications as well as process constraints. Two optimization formulations, the traditional single-stage formulation for single-value product property targets and the proposed multistage formulation that deals with specification bands, are applied to grade transition problems in the polyethylene solution polymerization process developed in Chapter 3. We demonstrate the effectiveness of multistage formulation through two transition problems. The major contributions in this chapter are:

- We propose the multistage optimization formulation that considers product specification bands carefully within a compact nonlinear programming formulation. This enables the explicit minimization of transition times, off-spec production times as well as direct minimization of off-spec product. The multistage formulation also exploits the simultaneous dynamic optimization approach, and provides an efficient formulation that extends from single stage to multistage dynamic optimization problems.

- For both single-stage and multistage objectives, we incorporate the idea of regularization. Given the singular nature of the grade transition problem when the regularization term is removed, systematic tuning of the weighting factors is necessary. By changing the weighting factors of the real objective and the regularization term, a trade-off between short transition time and smooth control profiles to steady state is made. In this chapter, we provide detailed evaluation of tuning parameters and a thorough numerical comparison of the resulting dynamic optimization problems, which can serve as a guideline for the determination of weighting factors.

Chapter 5 deals with system uncertainties. Although a number of studies have been conducted to solve this type of problem, they suffer from either intricate derivation or heavy computational burden. In this chapter, the concept of back-off is applied to the large-scale dynamic optimization problem. Both robust solutions with constant back-offs and time-varying back-offs are evaluated. The use of back-off constraints results in slightly longer transition time at nominal parameter level, but it effectively avoids the chance of violating constraints under uncertainty. Moreover, several case studies are performed to help better understand the optimization formulation and the effect of weighting factors in the objective function. The key contributions in this chapter are:

- We adopt the concept of back-off and calculate the back-off terms from Monte Carlo such that the computational burden of dealing with uncertainties is well-maintained at an acceptable level. Compared to constant back-offs, the proposed calculation of time-varying back-offs effectively makes the solution less conservative. In addition, an iterative approach is applied to update the back-off terms. Fast convergence of this approach is observed in the case study.

- We conduct a rigorous study to assess the influence of regularization, output tracking and multiple uncertainties. With the first two studies, we give in-

sight into the choice of objective function and the determination of weighting factors. The case study with multiple uncertainties shows the potential of the Monte Carlo simulation-based back-off scheme for handling several distinct uncertainties in the process.

Chapter 6 addresses online optimization and control framework with *sh*-NMPC and *eh*-LSE and compares three different designs of NMPC: setpoint-tracking NMPC, economic NMPC and economic NMPC with back-off constraints. Different from setpoint-tracking NMPC which tracks the predetermined setpoint, the merged layer for dynamic real-time optimization or economic NMPC considers both economic objective and control requirements at the same time, and is able to generate more economic benefit given the same process status. Also, the introduction of back-offs in the inequality constraints ensures constraint satisfaction under uncertainties. In this way, it effectively handles parametric uncertainties that appear in the process model of polyethylene polymerization. The case studies in this chapter demonstrate the superiority of robust economic NMPC over the other two forms through the grade transition example.

The major highlights in this chapter are listed below:

- We develop and evaluate several modifications in the NMPC formulation that improve either the economic objective or the computational performance. In addition, a relaxation of back-off constraints in the first element is proposed to facilitate the solution of NLP problems in robust economic NMPC without sacrificing the control performance under parametric uncertainties.
- We achieve computationally tractable solutions of these large-scale NLP problems by using the shrinking horizon scheme. Initialization based on the offline dynamic optimization problem also helps shorten the computational time.

7.2 Recommendations for Future Work

As mentioned in the concluding remarks in each chapter, there are several interesting research topics that are worth investigating as future work. We would like to point out some of them in the last section to conclude the dissertation.

7.2.1 Model Development of Polyethylene Solution Polymerization

The rigorous dynamic model developed in Chapter 3 is able to provide accurate model calculations and it maintains a great balance between model size and model performance. However, in order to make it representative of the actual process, there are several tasks that should be considered.

1. Model validation and parameter estimation need to be performed to make the model be representative of the actual plant. Some small modifications are expected depending on slightly different reactor configurations.

2. The grade transitions considered in the current work only involve changes of flowrate and temperature. More complex transitions with comonomer change or catalyst change can also be considered.

3. The loop reactor is modeled as a continuous stirred tank reactor under the assumption that the process is operated at a high recycle ratio, in which region the loop reactor and the CSTR behave similarly. However, future research can include the spatial distribution in the loop reactor and build partial differential equations for mass and heat balances such that the resulting model can be utilized over a wider range of recycle ratios.

7.2.2 Alternative Approaches for Optimization under Uncertainty

As we point out in Chapter 5, the back-off strategy is the most conservative approach to handling uncertainties because it always considers the worst-case scenario. On the contrary, multi-scenario approach increases the problem size dramatically [30]. Generating less conservative, yet computationally tractable approaches is a great direction for future work. The main resource we could utilize from the engineering point of view is the online measurement, which could be probably analyzed to reveal the uncertainty level to some extent and to relax the back-off constraints. On the other hand, algorithms need to be developed to solve multi-scenario problems more efficiently. This would enable us to apply the multi-stage NMPC problem proposed in [43, 44] to large-scale applications.

7.2.3 State Estimation with Multi-rate Measurements

The successful execution of the online optimization and control framework relies heavily on two components: the controller and the state estimator. The design of the shrinking horizon NMPC is discussed in detail in Chapter 6, and its performance is demonstrated in the grade transition problem with perfectly known states. However, the assumption that all the states can be measured perfectly with no time delay does not always hold in practice. In most cases, only some of the states are measured and thus state estimation approaches are needed to infer the unmeasured ones.

In addition, available measurements may come at different frequency/sampling rate. For instance, in the polyethylene processes, temperatures and flowrates can be measured quickly while product properties like MI and density need longer time and thus introduce measurement delays. A moving horizon estimator designed for processes with multi-rate measurements are proposed in [41] and the idea can be adopted to solve grade transition problems.

7.2.4 Computational Complexity for Online Implementation

In Chapter 6 we discuss the online optimization and control framework without considering the computational delay. However, the control performance could deteriorate if non-negligible period of time is required to solve either state estimation or model predictive control problem online. Various studies on fast NMPC strategies have been developed and could be possibly used in the large-scale grade transition problem. Related work on advanced step NMPC, advanced-multi-step NMPC and advanced step MHE could be found in [6, 47, 76, 79, 83].

7.2.5 Integration of Scheduling and Real-time Optimization

Similar to the integration of RTO and NMPC, the integration of scheduling with real-time optimization has the potential to generate considerable economic benefits. The formulations proposed in Chapter 4 for pairwise grade transition can easily be extended to production scheduling with multiple grades over a product wheel. For this case, integrated production scheduling can be addressed through the formulation of mixed-integer dynamic optimization (MIDO) problems, and the inclusion of binary decision variables, supported by the solution of MILP subproblems [48, 50, 52, 67, 69].

Bibliography

[1] B.W. Bequette. Nonlinear control of chemical processes: A review. *Industrial & Engineering Chemistry Research*, 30(7):1391–1413, 1991.

[2] T.K. Bhatia and L.T. Biegler. Dynamic optimization for batch design and scheduling with process model uncertainty. *Industrial & engineering chemistry research*, 36(9):3708–3717, 1997.

[3] L.T. Biegler. An overview of simultaneous strategies for dynamic optimization. *Chemical Engineering and Processing: Process Intensification*, 46(11):1043–1053, 2007.

[4] L.T. Biegler. *Nonlinear programming: concepts, algorithms, and applications to chemical processes*. Society for Industrial and Applied Mathematics, 2010.

[5] L.T. Biegler, A.M. Cervantes, and A. Wächter. Advances in simultaneous strategies for dynamic process optimization. *Chemical Engineering Science*, 57(4):575–593, 2002.

[6] L.T. Biegler, X. Yang, and G.A.G. Fischer. Advances in sensitivity-based nonlinear model predictive control and dynamic real-time optimization. *Journal of Process Control*, 30:104–116, 2015.

[7] H.G. Bock, M. Diehl, D.B. Leineweber, and J.P. Schlöder. A direct multiple shooting method for real-time optimization of nonlinear dae processes. In *Nonlinear model predictive control*, pages 245–267. Springer, 2000.

[8] D. Bonvin, L. Bodizs, and B. Srinivasan. Optimal grade transition for polyethylene reactors via nco tracking. *Chemical Engineering Research and Design*, 83(6):692–697, 2005.

[9] A. Brooke, D. Kendrick, A. Meeraus, R. Raman, and R.E. Rosenthal. Gams a user's guide (gams development corporation, washington dc), 1998.

[10] A.M. Cervantes, S. Tonelli, A. Brandolin, J.A. Bandoni, and L.T. Biegler. Large-scale dynamic optimization for grade transitions in a low density polyethylene plant. *Computers & chemical engineering*, 26(2):227–237, 2002.

[11] C. Chatzidoukas, J.D. Perkins, E.N. Pistikopoulos, and C. Kiparissides. Optimal grade transition and selection of closed-loop controllers in a gas-phase olefin polymerization fluidized bed reactor. *Chemical engineering science*, 58(16):3643–3658, 2003.

[12] W. Chen and L.T. Biegler. Nested direct transcription optimization for singular optimal control problems. *AIChE Journal*, In press, 2016.

[13] W. Chen, Z. Shao, and L.T. Biegler. A bilevel nlp sensitivity-based decomposition for dynamic optimization with moving finite elements. *AIChE Journal*, 60(3):966–979, 2014.

[14] J.E. Cuthrell and L.T. Biegler. On the optimization of differential-algebraic process systems. *AIChE Journal*, 33(8):1257–1270, 1987.

[15] J.E. Cuthrell and L.T. Biegler. Simultaneous optimization and solution methods for batch reactor control profiles. *Computers & Chemical Engineering*, 13(1):49–62, 1989.

[16] J.A. Debling, G.C. Han, F. Kuijpers, J. VerBurg, J. Zacca, and W.H. Ray. Dynamic modeling of product grade transitions for olefin polymerization processes. *AIChE journal*, 40(3):506–520, 1994.

[17] M. Diehl, H.G. Bock, and E. Kostina. An approximation technique for robust nonlinear optimization. *Mathematical Programming*, 107(1-2):213–230, 2006.

[18] A.S. Drud. Conopt - a large-scale grg code. *ORSA Journal on Computing*, 6(2):207–216, 1994.

[19] M. Embiruçu, E.L. Lima, and J.C. Pinto. Continuous soluble ziegler-natta ethylene polymerizations in reactor trains. i. mathematical modeling. *Journal of applied polymer science*, 77(7):1574–1590, 2000.

[20] M. Embiruçu, D.M. Prata, E.L. Lima, and J.C. Pinto. Continuous soluble ziegler-natta ethylene polymerizations in reactor trains, 2–estimation of kinetic parameters from industrial data. *Macromolecular Reaction Engineering*, 2(2):142–160, 2008.

[21] W.F. Feehery and P.I. Barton. Dynamic optimization with state variable path constraints. *Computers & chemical engineering*, 22(9):1241–1256, 1998.

[22] A. Flores-Tlacuahuac, L.T. Biegler, and E. Saldívar-Guerra. Dynamic optimization of hips open-loop unstable polymerization reactors. *Industrial & engineering chemistry research*, 44(8):2659–2674, 2005.

[23] A. Forrester, A. Sobester, and A. Keane. *Engineering design via surrogate modelling: a practical guide*. John Wiley & Sons, 2008.

[24] F. Galvanin, M. Barolo, F. Bezzo, and S. Macchietto. A backoff strategy for model-based experiment design under parametric uncertainty. *AIChE journal*, 56(8):2088–2102, 2010.

[25] C.E. Garcia, D.M. Prett, and M. Morari. Model predictive control: theory and practice—a survey. *Automatica*, 25(3):335–348, 1989.

[26] A. Gisnas, B. Srinivasan, and D. Bonvin. Optimal grade transitions for polyethylene reactors. *Computer Aided Chemical Engineering*, 15:463–468, 2003.

[27] J.D. Guzmán, D.J. Arriola, T. Karjala, J. Gaubert, and B.W.S. Kolthammer. Simple model to predict gel formation in olefin-diene copolymerizations catalyzed by constrained-geometry complexes. *AIChE Journal*, 56(5):1325–1333, 2010.

[28] M.A. Henson. Nonlinear model predictive control: current status and future directions. *Computers and Chemical Engineering*, 23(2):187–202, 1998.

[29] A. Hosseini, M. Oshaghi, and S. Engell. Mid-course control of particle size distribution in emulsion polymerization using a hybrid model. In *Control Applications (CCA), 2013 IEEE International Conference on*, pages 728–733. IEEE, 2013.

[30] R. Huang, S.C. Patwardhan, and L.T. Biegler. Multi-scenario-based robust nonlinear model predictive control with first principle models. *Computer Aided Chemical Engineering*, 27:1293–1298, 2009.

[31] D.H. Jacobson, S.B. Gershwin, and M.L. Lele. Computation of optimal singular controls. *Automatic Control, IEEE Transactions on*, 15(1):67–73, 1970.

[32] J. Jäschke, X. Yang, and L.T. Biegler. Fast economic model predictive control based on nlp-sensitivities. *Journal of Process Control*, 24(8):1260–1272, 2014.

[33] T.Y. Jung, Y. Nie, J.H. Lee, and L.T. Biegler. Model-based on-line optimization framework for semi-batch polymerization reactors. *IFAC-PapersOnLine*, 48(8):164–169, 2015.

[34] S. Kameswaran and L.T. Biegler. Simultaneous dynamic optimization strategies: Recent advances and challenges. *Computers & Chemical Engineering*, 30(10):1560–1575, 2006.

[35] C.I. Kao, R.B. Combs, G.A. Camp, D.A. Eversdyk, P. Jain, G.A. Winter, and J.H. Stultz. Non-adiabatic olefin solution polymerization, November 2 1999. US Patent 5,977,251.

[36] T.W. Karjala, H. Meerdink, and B.C. Dems. Real-time estimation of polymer properties in an industrial polyethylene reactor. In *American Control Conference, 1997. Proceedings of the 1997*, volume 5, pages 3063–3067. IEEE, 1997.

[37] C. Kiparissides, P. Seferlis, G. Mourikas, and A.J. Morris. Online optimizing control of molecular weight properties in batch free-radical polymerization reactors. *Industrial & engineering chemistry research*, 41(24):6120–6131, 2002.

[38] S. Körkel, E. Kostina, H.G. Bock, and J.P. Schlöder. Numerical methods for optimal control problems in design of robust optimal experiments for nonlinear dynamic processes. *Optimization Methods and Software*, 19(3-4):327–338, 2004.

[39] A. Krasławski. Review of applications of various types of uncertainty in chemical engineering. *Chemical Engineering and Processing: Process Intensification*, 26(3):185–191, 1989.

[40] D.B. Leineweber, I. Bauer, H.G. Bock, and J.P. Schlöder. An efficient multiple shooting based reduced sqp strategy for large-scale dynamic process optimization. part 1: theoretical aspects. *Computers & Chemical Engineering*, 27(2):157–166, 2003.

[41] R. López-Negrete and L.T. Biegler. A moving horizon estimator for processes with multi-rate measurements: A nonlinear programming sensitivity approach. *Journal of Process Control*, 22(4):677–688, 2012.

[42] S.N. Lophaven, H.B. Nielsen, and J. Søndergaard. Dace-a matlab kriging toolbox, version 2.0. Technical report, 2002.

[43] S. Lucia, J.A.E. Andersson, H. Brandt, M. Diehl, and S. Engell. Handling uncertainty in economic nonlinear model predictive control: A comparative case study. *Journal of Process Control*, 24(8):1247–1259, 2014.

[44] S. Lucia, T. Finkler, and S. Engell. Multi-stage nonlinear model predictive con-

trol applied to a semi-batch polymerization reactor under uncertainty. *Journal of Process Control*, 23(9):1306–1319, 2013.

[45] M. Morari and J.H. Lee. Model predictive control: past, present and future. *Computers & Chemical Engineering*, 23(4):667–682, 1999.

[46] Z.K. Nagy and R.D. Braatz. Open-loop and closed-loop robust optimal control of batch processes using distributional and worst-case analysis. *Journal of process control*, 14(4):411–422, 2004.

[47] B. Nicholson, R. López-Negrete, and L.T. Biegler. On-line state estimation of nonlinear dynamic systems with gross errors. *Computers & Chemical Engineering*, 2013.

[48] Y. Nie, L.T. Biegler, and J.M. Wassick. Integrated scheduling and dynamic optimization of batch processes using state equipment networks. *AIChE Journal*, 58(11):3416–3432, 2012.

[49] Jorge Nocedal and Stephen Wright. *Numerical optimization*. Springer Science & Business Media, 2006.

[50] R.H. Nyström, R. Franke, I. Harjunkoski, and A. Kroll. Production campaign planning including grade transition sequencing and dynamic optimization. *Computers & chemical engineering*, 29(10):2163–2179, 2005.

[51] A.J. Peacock. *Handbook of polyethylene: structures, properties, and applications*, volume 57. CRC Press, 2000.

[52] A. Prata, J. Oldenburg, A. Kroll, and W. Marquardt. Integrated scheduling and dynamic optimization of grade transitions for a continuous polymerization reactor. *Computers & Chemical Engineering*, 32(3):463–476, 2008.

[53] S. Qin and T.A. Badgwell. A survey of industrial model predictive control technology. *Control engineering practice*, 11(7):733–764, 2003.

[54] S.J. Qin and T.A. Badgwell. An overview of nonlinear model predictive control applications. In *Nonlinear model predictive control*, pages 369–392. Springer, 2000.

[55] M.R. Rahimpour, J. Fathikalajahi, B. Moghtaderi, and A.N. Farahani. A grade transition strategy for the prevention of melting and agglomeration of particles in an ethylene polymerization reactor. *Chemical engineering & technology*, 28(7):831–841, 2005.

[56] J.B. Rawlings. Tutorial overview of model predictive control. *Control Systems, IEEE*, 20(3):38–52, 2000.

[57] J.B. Rawlings and B.R. Bakshi. Particle filtering and moving horizon estimation. *Computers & chemical engineering*, 30(10):1529–1541, 2006.

[58] W.H. Ray. On the mathematical modeling of polymerization reactors. *Journal of Macromolecular Science—Reviews in Macromolecular Chemistry*, 8(1):1–56, 1972.

[59] A.S. Reginato, J.J. Zacca, and A.R. Secchi. Modeling and simulation of propylene polymerization in nonideal loop reactors. *AIChE journal*, 49(10):2642–2654, 2003.

[60] J.R. Richards and J.P. Congalidis. Measurement and control of polymerization reactors. *Computers & chemical engineering*, 30(10):1447–1463, 2006.

[61] D. Ruppen, C. Benthack, and D. Bonvin. Optimization of batch reactor operation under parametric uncertainty - computational aspects. *Journal of Process Control*, 5(4):235–240, 1995.

[62] M. Schlegel, K. Stockmann, T. Binder, and W. Marquardt. Dynamic optimization using adaptive control vector parameterization. *Computers & Chemical Engineering*, 29(8):1731–1751, 2005.

[63] K.C. Seavey, Y.A. Liu, N.P. Khare, T. Bremner, and C.C. Chen. Quantifying

relationships among the molecular weight distribution, non-newtonian shear viscosity, and melt index for linear polymers. *Industrial & engineering chemistry research*, 42(21):5354–5362, 2003.

[64] J. Shi, L.T. Biegler, and I. Hamdan. Optimization of grade transitions in polyethylene solution polymerization processes. *AIChE Journal*, 2015.

[65] B. Srinivasan, D. Bonvin, E. Visser, and S. Palanki. Dynamic optimization of batch processes: Ii. role of measurements in handling uncertainty. *Computers & chemical engineering*, 27(1):27–44, 2003.

[66] B. Srinivasan, S. Palanki, and D. Bonvin. Dynamic optimization of batch processes: I. characterization of the nominal solution. *Computers & Chemical Engineering*, 27(1):1–26, 2003.

[67] M. Takeda and W.H. Ray. Optimal-grade transition strategies for multistage polyolefin reactors. *AIChE Journal*, 45(8):1776–1793, 1999.

[68] V. Touloupides, V. Kanellopoulos, P. Pladis, C. Kiparissides, D. Mignon, and P. Van-Grambezen. Modeling and simulation of an industrial slurry-phase catalytic olefin polymerization reactor series. *Chemical Engineering Science*, 65(10):3208–3222, 2010.

[69] R.L. Tousain. *Dynamic optimization in business-wide process control*. TU Delft, Delft University of Technology, 2002.

[70] V.S. Vassiliadis, R.W.H. Sargent, and C.C. Pantelides. Solution of a class of multistage dynamic optimization problems. 1. problems without path constraints. *Industrial & Engineering Chemistry Research*, 33(9):2111–2122, 1994.

[71] E. Visser, B. Srinivasan, S. Palanki, and D. Bonvin. A feedback-based implementation scheme for batch process optimization. *Journal of Process Control*, 10(5):399–410, 2000.

[72] A. Wächter and L.T. Biegler. On the implementation of an interior-point filter

line-search algorithm for large-scale nonlinear programming. *Mathematical programming*, 106(1):25–57, 2006.

[73] Y. Wang, H. Seki, S. Ohyama, M. Ogawa, and M. Ohshima. Optimal grade transition control for polymerization reactors. *Computers & Chemical Engineering*, 24(2-7):1555–1561, 2000.

[74] L. Würth, R. Hannemann, and W. Marquardt. Neighboring-extremal updates for nonlinear model-predictive control and dynamic real-time optimization. *Journal of Process Control*, 19(8):1277–1288, 2009.

[75] X. Yang and L.T. Biegler. Advanced-multi-step nonlinear model predictive control. In *Advanced Control of Chemical Processes*, volume 8, pages 426–431, 2012.

[76] X. Yang and L.T. Biegler. Advanced-multi-step nonlinear model predictive control. *Journal of Process Control*, 23(8):1116–1128, 2013.

[77] W.J. Yoon, Y.S. Kim, I.S. Kim, and K.Y. Choi. Recent advances in polymer reaction engineering: modeling and control of polymer properties. *Korean Journal of Chemical Engineering*, 21(1):147–167, 2004.

[78] J.J. Zacca and W.H. Ray. Modelling of the liquid phase polymerization of olefins in loop reactors. *Chemical Engineering Science*, 48(22):3743–3765, 1993.

[79] V.M. Zavala and L.T. Biegler. The advanced-step nmpc controller: Optimality, stability and robustness. *Automatica*, 45(1):86–93, 2009.

[80] V.M. Zavala and L.T. Biegler. Nonlinear programming strategies for state estimation and model predictive control. In *Nonlinear model predictive control*, pages 419–432. Springer, 2009.

[81] V.M. Zavala and L.T. Biegler. Optimization-based strategies for the operation of low-density polyethylene tubular reactors: nonlinear model predictive control. *Computers & Chemical Engineering*, 33(10):1735–1746, 2009.

[82] V.M. Zavala, A. Flores-Tlacuahuac, and E. Vivaldo-Lima. Dynamic optimization of a semi-batch reactor for polyurethane production. *Chemical Engineering Science*, 60(11):3061–3079, 2005.

[83] V.M. Zavala, C.D. Laird, and L.T. Biegler. A fast moving horizon estimation algorithm based on nonlinear programming sensitivity. *Journal of Process Control*, 18(9):876–884, 2008.

[84] Y. Zhang, D. Monder, and J.F. Forbes. Real-time optimization under parametric uncertainty: a probability constrained approach. *Journal of Process control*, 12(3):373–389, 2002.

Nomenclature

α_p	Weighting factor on the term of off-grade production
α_t	Weighting factor on the term of off-grade production time
$M\bar{W}$	Molecular weight of the repeating units
β_t	Weighting factor on the term of duration of Stage 1 in multistage formulation
ΔH	Reaction heat
γ	Weighting factor on regularization
$\lambda_{k,i}$	kth moment of bulk (live and dead) polymer with end-group M_i
$\mu_{k,i}$	kth moment of growing polymer with end-group M_i
ω	Branch content of comonomer in the polymer chains
ρ	Product density
ρ_j	Density of the cooling media in the cooling jacket
ρ_s	Density of the mixture in the reactor
θ	Ethylene conversion rate
A	Cocatalyst
a_1	Coefficient in the melt index correlation
a_2	Coefficient in the melt index correlation
b_1	Coefficient in the density correlation
b_2	Coefficient in the density correlation
b_c	Back-off term in robust optimization
C_d	Dead catalyst site

C_{pj} Heat capacity of the cooling media in the cooling jacket

C_{ps} Heat capacity of the mixture in the reactor

$D_{n,i}$ Dead polymer of chain length n and end-group M_i

F_1 Inlet flowrate of fresh ethylene

F_1r Flowrate of recycled ethylene stream

F_2 Inlet flowrate of fresh comonomer

F_2r Flowrate of recycled comonomer stream

F_C Catalyst feed flowrate

F_H Fresh hydrogen flowrate

F_{Hr} Recycled hydrogen flowrate

H_2^0 Concentration of hydrogen in the fresh hydrogen feed

H_{2r} Concentration of hydrogen in the recycled hydrogen stream

k_p Rate constant for chain initialization

k_{cA} Rate constant for chain transfer to cocatalyst

k_{cH} Rate constant for chain transfer to hydrogen

k_{cm} Rate constant for chain transfer to monomer

k_{csp} Rate constant for spontaneous chain transfer

k_{cS} Rate constant for chain transfer to solvent

k_{cT} Rate constant for chain transfer to transfer agent

k_{dsp} Rate constant for spontaneous chain deactivation

k_{dx} Rate constant for chain deactivation by poison

$k_{p,i,j}$ Rate constant for chain propagation with end-group i in the growing chain and monomer j adding to the chain

KC Lumped term in the moment model that combines several reaction rates

M_1^0 Concentration of ethylene in the fresh ethylene feed

M_2^0 Concentration of comonomer in the fresh comonomer feed

M_i Monomer or comonomer, $i = 1$ for ethylene and $i = 2$ for comonomer

M_n Number average molecular weight

M_w Weight average molecular weight

M_{1r} Concentration of ethylene in the recycled ethylene stream

M_{2r} Concentration of comonomer in the recycled comonomer stream

MI Melt index

$MW1$ Molecular weight of ethylene

$MW2$ Molecular weight of comonomer

P_0 Empty catalyst site

P_b Bubble point pressure of the mixture in the reactor

$P_{f,b}$ Bubble point pressure of the feed to the reactor

$P_{n,j}$ Growing polymer of chain length n and end-group M_i

Q Scaling matrix

R Scaling matrix

r_1 Reactivity ratio

r_2 Reactivity ratio

S Solvent

T Reactor temperature

T Transfer agent

T^0 Temperature of the reactor feed flow

T_j Jacket temperature

T_j^0 Inlet temperature of cooling media

U Heat transfer coefficient

V Reactor volume

V_j Cooling jacket volume

w_ρ Weighting factor on density term

w_{MI} Weighting factor on MI term

X Poison